National Library of Canada
Bibliothèque nationale du Canada

Canadian Theses Service
Service des thèses canadiennes

Ottawa, Canada
K1A 0N4

NOTICE

The quality of this microform is heavily dependent upon the quality of the original thesis submitted for microfilming. Every effort has been made to ensure the highest quality of reproduction possible.

If pages are missing, contact the university which granted the degree.

Some pages may have indistinct print especially if the original pages were typed with a poor typewriter ribbon or if the university sent us an inferior photocopy.

Previously copyrighted materials (journal articles, published tests, etc.) are not filmed.

Reproduction in full or in part of this microform is governed by the Canadian Copyright Act, R.S.C. 1970, c. C-30.

AVIS

La qualité de cette microforme dépend grandement de la qualité de la thèse soumise au microfilmage. Nous avons tout fait pour assurer une qualité supérieure de reproduction.

S'il manque des pages, veuillez communiquer avec l'université qui a conféré le grade.

La qualité d'impression de certaines pages peut laisser à désirer, surtout si les pages originales ont été dactylographiées à l'aide d'un ruban usé ou si l'université nous a fait parvenir une photocopie de qualité inférieure.

Les documents qui font déjà l'objet d'un droit d'auteur (articles de revue, tests publiés, etc.) ne sont pas microfilmés.

La reproduction, même partielle, de cette microforme est soumise à la Loi canadienne sur le droit d'auteur, SRC 1970, c. C-30.

NL-339 (r. 88/04)

Canada

THE UNIVERSITY OF ALBERTA

LINEWIDTH REDUCTION AND FREQUENCY MODULATION OF A 1.3 MICRON SEMICONDUCTOR LASER WITH STRONG FREQUENCY SELECTIVE OPTICAL FEEDBACK

by

AZMINA SOMANI

A THESIS

SUBMITTED TO THE FACULTY OF GRADUATE STUDIES AND RESEARCH

IN PARTIAL FULFILMENT OF THE REQUIREMENTS FOR THE DEGREE

OF MASTER OF SCIENCE

DEPARTMENT OF ELECTRICAL ENGINEERING

EDMONTON, ALBERTA

SPRING 1988

Permission has been granted to the National Library of Canada to microfilm this thesis and to lend or sell copies of the film.

The author (copyright owner) has reserved other publication rights, and neither the thesis nor extensive extracts from it may be printed or otherwise reproduced without his/her written permission.

L'autorisation a été accordée à la Bibliothèque nationale du Canada de microfilmer cette thèse et de prêter ou de vendre des exemplaires du film.

L'auteur (titulaire du droit d'auteur) se réserve les autres droits de publication; ni la thèse ni de longs extraits de celle-ci ne doivent être imprimés ou autrement reproduits sans son autorisation écrite.

ISBN 0-315-42820-1

THE UNIVERSITY OF ALBERTA

RELEASE FORM

NAME OF AUTHOR AZMINA SOMANI

TITLE OF THESIS LINEWIDTH REDUCTION AND FREQUENCY MODULATION OF A 1.3 MICRON SEMICONDUCTOR LASER WITH STRONG FREQUENCY SELECTIVE OPTICAL FEEDBACK

DEGREE FOR WHICH THESIS WAS PRESENTED: MASTER OF SCIENCE

YEAR THIS DEGREE GRANTED: SPRING 1988

Permission is hereby granted to THE UNIVERSITY OF ALBERTA LIBRARY to reproduce single copies of this thesis and to lend or sell such copies for private, scholarly or scientific research purposes only.

The author reserves other publication rights, and neither the thesis nor extensive extracts from it may be printed or otherwise reproduced without the author's written permission.

(SIGNED) Assomani

PERMANENT ADDRESS:

#206 15508 - 84 Avenue

Edmonton, Alberta

T5R 3L6

DATED April 6 1988

THE UNIVERSITY OF ALBERTA

FACULTY OF GRADUATE STUDIES AND RESEARCH

The undersigned certify that they have read, and recommend to the Faculty of Graduate Studies and Research, for acceptance, a thesis entitled LINEWIDTH REDUCTION AND FREQUENCY M0DULATION OF A 1.3 MICRON SEMICONDUCTOR LASER WITH STRONG FREQUENCY SELECTIVE OPTICAL FEEDBACK submitted by AZMINA SOMANI in partial fulfilment of the requirements for the degree of MASTER of SCIENCE.

Paul A. Bond

Co-supervisor

Colin G. Englefield.

Co-supervisor

Frank R. Greene

Robert Tedoseyeva

Date 6th April 1988

ABSTRACT

In this thesis, strong optical feedback is used to reduce the linewidth and stabilize the frequency of a semiconductor laser diode. In order to reach the regime of strong optical feedback, the laser facet through which the feedback occurs has to be anti-reflection coated. Simple transmission line theory cannot be applied to laser diodes because a large portion of the electric field exists outside the active region and therefore the influence of the cladding must be included in the design of a reflectionless coating. It was for this reason, as well as the precision with which the refractive index of the coating needs to be controlled, that it was essential to develop a method of actively monitoring the facet reflectivity while the anti-reflection coating was being deposited. This scheme permitted very low reflectivities, in the order of 8×10^{-4}, to be readily and reproducibly obtained. The laser diode thus obtained was used in a strong feedback configuration. Light emitted from the coated facet was collimated and fed back into the laser cavity after being reflected off a diffraction grating. The diffraction grating provides frequency selectivity, which is a desirable feature for obtaining a stable single longitudinal mode laser. The laser in this configuration oscillated in a single mode with a greater than 30dB side mode suppression ratio and a wide tuning range of 43nm (7000 GHz). A linewidth of about 9kHz ± 3kHz was obtained over a wide range of frequencies. However, along with the reduction in linewidth, the frequency modulation capability of the external cavity laser is reduced from several Gigahertz per milliamp to about 2.75 MHz/mA.

ACKNOWLEDGEMENTS

I would like to thank Dr. P. A Goud and Dr. C. G. Englefield for their constant encouragement, advice and support throughout this project. In addition, I would like to extend my gratitude to the following:

-The members of the examining committee for reviewing this work.

-Dr. Brian Kawasaki and the Optical Devices Group of Northern Telecom, for the use of their equipment and premise for conducting part of this research.

-Mr. Jann Binder and Fred Chan for many stimulating discussions and for the use of some of their previous work.

-Dr. Cormack for his support during the project and for the loan of equipment

-Mr. Yan Loke for programming assistance.

-All the staff members of the Alberta Telecommunications Research Center.

-Mr. Keith Wilcox and David Johnson for their competent technical assistance.

-Alberta Telecommunications Research Center for the award of a post-graduate scholarship.

-The Electrical Engineering Department at the U of A for the award of a teaching assistantship.

-Dr. M.Brett and Mr. C.Kelly for assistance in coating the LD and for the use of the evaporator

I would also like to express my sincere thanks to Ms. Joanne Whalen for typing this thesis and to my family and friends for their support during this project. My appreciation is also extended to all the teachers who have made it possible to complete the work reported in this thesis.

TABLE OF CONTENTS

CHAPTER			PAGE
1.	INTRODUCTION		1
	1.1	OVERVIEW OF COHERENT FIBER OPTIC COMMUNICATIONS	1
	1.2	SOURCES FOR COHERENT SYSTEMS	6
	1.3	MODULATION/DEMODULATION SCHEMES	8
	1.4	THESIS OBJECTIVES AND ORGANIZATION	12
		1.4.1 Objectives	12
		1.4.2 Organization	13
2.	FABRICATION OF ANITREFLECTION COATING ON LASER-DIODE FACET		15
	2.1	REAL-TIME FACET REFLECTIVITY MONITORING SYSTEM	16
		2.1.1 Experimental Set-Up	17
		2.1.2 Experimental Results	21
	2.2	MODAL REFLECTIVITY MEASUREMENT	24
	2.3	SUMMARY	29
3.	CONFIGURATION OF THE GRATING LOADED EXTERNAL CAVITY LASER		31
	3.1	DESCRIPTION OF EACH OF THE COMPONENTS CONSTITUTING THE EXTERNAL CAVITY LASER	31
		3.1.1 Diffraction Grating	31
		3.1.2 Collimating Lens	35
		3.1.3 Semiconductor Laser Diode	35
		3.1.4 Optical Isolator	40

3.2 MEASURING/MONITORING EQUIPMENT 42

3.2.1 Scanning Monochromator and Fabry-Perot Interferometer 42

3.2.2 Self-Heterodyne Set-Up 45

3.3 SUMMARY 48

4. SINGLE MODE EXTERNAL CAVITY LASER 49

4.1 THE DIFFRACTION GRATING (FILTER) RESPONSE 49

4.2 THRESHOLD CONDITION 54

4.3 DISCUSSION OF SINGLE MODE OSCILLATION 59

4.4 EXPERIMENTAL RESULTS FOR SINGLE MODE OSCILLATION AND TUNING RANGE 62

4.4.1 Side Mode Suppression Ratio 62

4.4.2 Tuning Range Measurements 66

4.5 SUMMARY 68

5. SPECTRAL LINEWIDTH OF EXTERNAL CAVITY CONTROLLED LASER 70

5.1 SPECTRAL LINEWIDTH DISCUSSION 70

5.2 THEORETICAL CALCULATION OF LINEWIDTH 75

5.3 EXPERIMENTAL RESULTS 81

5.4 SUMMARY 92

6. MODULATION OF EXTERNAL CAVITY LASER 94

6.1 DEGRADATION OF FREQUENCY MODULATION CAPABILITY OF LD IN AN EXTERNAL CAVITY 95

6.2 EXPERIMENTAL RESULTS OF MODULATION CAPABILITY OF LD IN AN EXTERNAL CAVITY 97

6.3 SUMMARY 106

7. SUMMARY AND CONCLUSIONS 107

REFERENCES 110

APPENDIX A: DERIVATION CONFINEMENT FACTOR FOR TE AND TM POLARISATION 116

APPENDIX B: CIRCUIT DIAGRAMS 120

APPENDIX C: COMPUTER PROGRAM 125

LIST OF FIGURES

FIGURE		PAGE
1.1	Basic configuration of a Coherent Long-Haul Optical Fiber Transmission System	3
1.2	A Star Network Configuration suitable for Interoffice Application	5
2.1	Experimental Set-Up for monitoring I D Facet Reflectivity	18
2.2	Dependence of LD Optical Power on Coating Thickness	22
2.3	CW Lasing Characteristics at the Points indicated in Fig. 2.2	23
2.4	Experimental Set-Up for measuring TE and TM Power Spectral Density	26
2.5	Power Spectral Density of the Guided Amplified Spontaneous Emission for TE Polarization; I_{bias} = 16 mA	27
2.6	Power Spectral Density of the Guided Amplified Spontaneous Emission for TM Polarization; I_{bias} = 16 mA	28
3.1	Block diagram of the Experimental Set-Up of a LD with External Grating Feedback	32
3.2	Diagram Showing How The Grating is Mounted With Respect to the LD. The Grooves Are Perpendicular to the Electric Field Vector That is Parallel To the Junction Plane	34
3.3	Optical Power versus Current of the Fujitsu LD at T = 17°C	38
3.4	Output Spectrum of a LD with One Facet Coated for Minimum Reflectivity; $I_{bias} = 2.0\ I_{th}$	39
3.5	Output Power Spectrum without an Optical Isolator. The "Noise Spikes" resulting from Spurious Reflections are marked by B, B , C and C	41
3.6	Monochromator Set-Up for Direct Wavelength and Spectral Measurement	43
3.7	Fabry-Perot Set-Up for High Resolution Spectral Measurement	44

3.8 The Self-Heterodyne Set-Up for measuring Narrow Linewidth. Resolution of this Set-Up is about 250 kHz 46

4.1 Angular Placement of the Grating 52

4.2 Geometry for determining the Spot Size of the Beam incident on the Grating 52

4.3 Geometry for Grating Loaded External Cavity Laser 55

4.4 Optical Power versus Current Plot with and without Feedback measured from a Fiber Coupled to the Uncoated Facet. T = 17°C and λ = 1284 nm 58

4.5 Depiction of Homogeneous Saturation of Gain 60

4.6 Spectral Output of External Cavity Laser (Two Spectral Orders are displayed over One Ramp Period)
(a) $I_{bias} = 1.5\ I_{th}$,
(b) $I_{bias} = 2.3\ I_{th}$ 63

4.7 Spectral Output of External Cavity Laser with $I_{bias} = 2.3\ I_{th}$. Two Spectral Orders are shown over One Ramp Period, enlarged 100 times, as compared to Fig. 4.6 64

4.8 Spectral Output of External Cavity Laser with $I_{bias} = 2.3\ I_{th}$. Two Spectral Orders are shown over Two Ramp Periods, enlarged 1000 times as compared to Fig. 4.6
(a) slightly misaligned cavity to show where a side mode may develop
(b) aligned cavity; side mode non-existent 65

4.9 Wavelength Tuning of Laser Modes obtained by rotation of the Grating 67

5.1 Theoretical calculation (Equation 5.9) of linewidth of the external cavity LD at various wavelengths. Average linewidth ~ 3 kHz 79

5.2 Theoretical Calculation of Linewidth when the Oscillating Frequency is detuned from the Internal Cavity Mode; λ = 1298 nm 80

5.3 Optical Power Spectrum for Linewidth Measurement Using Delayed Self-Heterodyne Technique λ = 1289 nm, $I_{bias} = 2.3\ I_{th}$ 82

5.4 Best Fit Curve for Experimental Results of Fig. 5.3. Fitting Parameters: τ_{fit} = 3.8 μsec, Fitting Range: 78.8 - 79.8 MHz. Linewidth ($\Delta\nu$ = 4 kHz) 83

5.5 Results of Linewidth Measurement and Best Fit Curve at λ = 1292 nm, Ibias = 2.3 I_{th}, Fitting Parameters: τ_{fit} = 3.8 μsec, Fitting Range: 79.0 - 79.9 MHz. Linewidth ($\Delta\nu$ = 7 kHz) 85

5.6 Results of Linewidth Measurement and Best Fit Curve at λ = 1296 nm, Ibias = 2.3 I_{th}, Fitting Parameters: τ_{fit} = 3.8 μsec, Fitting Range: 79.0 - 79.9 MHz. Linewidth ($\Delta\nu$ = 9 kHz) 86

5.7 Results of Linewidth Measurement and Best fit curve at λ = 1302 nm, Ibias = 2.3 I_{th}, Fitting Parameters: τ_{fit} = 3.8 μsec, Fitting Range: 79.0 - 79.9 MHz. Linewidth ($\Delta\nu$ = 13 kHz) 87

5.8 Results of Linewidth Measurement and Best fit curve at λ = 1303 nm, Ibias = 2.3 I_{th}, Fitting Parameters: τ_{fit} = 3.8 μsec, Fitting Range: 79.0 - 79.9 MHz. Linewidth ($\Delta\nu$ = 7.7 kHz) 88

5.9 Results of Linewidth Measurement and Best Fit Curve at λ = 1308 nm, Ibias = 2.3 I_{th}, Fitting Parameters: τ_{fit} = 3.8 μsec, Fitting Range: 79.0 - 79.9 MHz. Linewidth ($\Delta\nu$ = 10 kHz) 89

5.10 Results of Linewidth Measurement and Best Fit Curve at λ = 1312 nm, Ibias = 2.3 I_{th}, Fitting Parameters: τ_{fit} = 3.8 μsec, Fitting Range: 79.0 - 79.9 MHz. Linewidth ($\Delta\nu$ = 30 kHz) 90

5.11 The Linewidth Measurements at Various Wavelengths obtained using Best Fit Curve Analysis 91

6.1 Circuit diagram of laser driver for high bit rate modulation 98

6.2 Modulation Response of Solitary LD modulated at 320 Mbit/sec. The Diagram shows Characteristics of the Driver Circuit of Fig. 6.1
(a)Pulse Response of a Sample Solitary LD
(b)Eye Diagram 99

6.3 Power Spectrum of Frequency Modulated LD at 230 kHz Sinewave, Ibias = 2.3 I_{th} and ΔI = 1 mA pp
(a) Optimally Narrowed Linewidth; Δf = 2.75 MHz
(b) ~ 14 times Wider Linewidth; Δf = 10.5 MHz 101

6.4 Power Spectrum of Frequency Modulated LD at 230 KHz Sinewave, Ibias = 2.3 I_{th} and Optimally Narrowed Linewidth:
(a) ΔI = 2 mA pp; Δf = 3.25 MHz
(b) ΔI = 3.2 mA pp; Δf = 5.75 MHz 103

6.5 Power Spectrum of LD under 50 MHz Sinewave Modulation, Ibias = 2.3 I_{th} and ΔI = 4.0 mA pp 104

B.1 Thermistor Temperature Calibration 121
B.2 Laser Temperature Control Circuit 122
B.3 Laser CW Bias Circuit 123
B.4 Manufacturer's Data Sheet 124

LIST OF TABLES

TABLE		PAGE
1.	Laser Linewidth Requirements for Different Types of Modulation [3]	7
2.	Linewidth Obtained With Various Feedback Configurations	9
3.	Physical Properties of the Buried Heterostructure Lasers Used in this Work	19
4.	Physical Properties of the Stripe Geometry Double Heterostructure Laser Used in the External Cavity Configuration [Figure 3.1]	37

CHAPTER 1

INTRODUCTION

In recent years, significant advances have been achieved in all areas of lightwave communication technology. These advances have particularly focussed on achieving higher data rates and/or longer repeaterless transmission distances. A further most significant advance in the past several years has been that coherent lightwave communications has begun to show promise of competing with the established direct-detection method. These systems improve not only the detection sensitivity, thus permitting longer unrepeatered transmission spans, but they also have the potential advantage of allowing the frequency multiplexing of a large number of optical channels with a narrow frequency separation between channels. This makes possible the use of the nearly 50,000 GHz of bandwidth in the 1.25 to 1.6 μm low-loss silica fiber window. The ability to transmit a large number of channels in a single fiber, coupled with the possibility of accessing any particular channel by tuning a local oscillator, broadens the capabilities and networking architectures of high capacity multi-terminal local networks.

1.1 OVERVIEW OF COHERENT FIBER OPTIC COMMUNICATION

The term "coherent", as used in the literature, refers to a technique employing non-linear mixing between two optical waves at the receiver. The small amplitude information signal (attenuated due to transmission through the

fiber network) is mixed with a larger locally generated wave in a square-law detector. The mixer output appears at the intermediate frequency (IF), which is the difference between the carrier frequency of the signal and that of the local oscillator (LO). The IF electrical signal is then amplified and demodulated; this process is in principle the same as that in a microwave system. If the difference frequency is zero, that is, if the signal and the LO are at the same frequency, the technique is called homodyne detection; if the IF frequency is other than zero, it is known as heterodyne detection.

The improvement in the receiver sensitivity of coherent optical systems is attributed to two effects:

(1) improvement of the signal to noise ratio (SNR) for a given signal level due to conversion gain in the mixing process, so that the noise becomes shot noise limited, rather than thermal noise limited,

(2) a further improvement in SNR brought about by the use of a coherent detection scheme (i.e., use of a phase coherent reference obtained from the received signal) as opposed to non-coherent detection (for example envelope detection).

The basic topology of a long-haul coherent optical fiber transmission system is shown in Figure 1.1. The transmitter consists of a laser oscillator and a modulator. Any suitable modulation format, such as Frequency Shift Keying (FSK), Amplitude Shift Keying (ASK) or Phase Shift Keying (PSK) may be used, depending on the system requirements. For some modulation

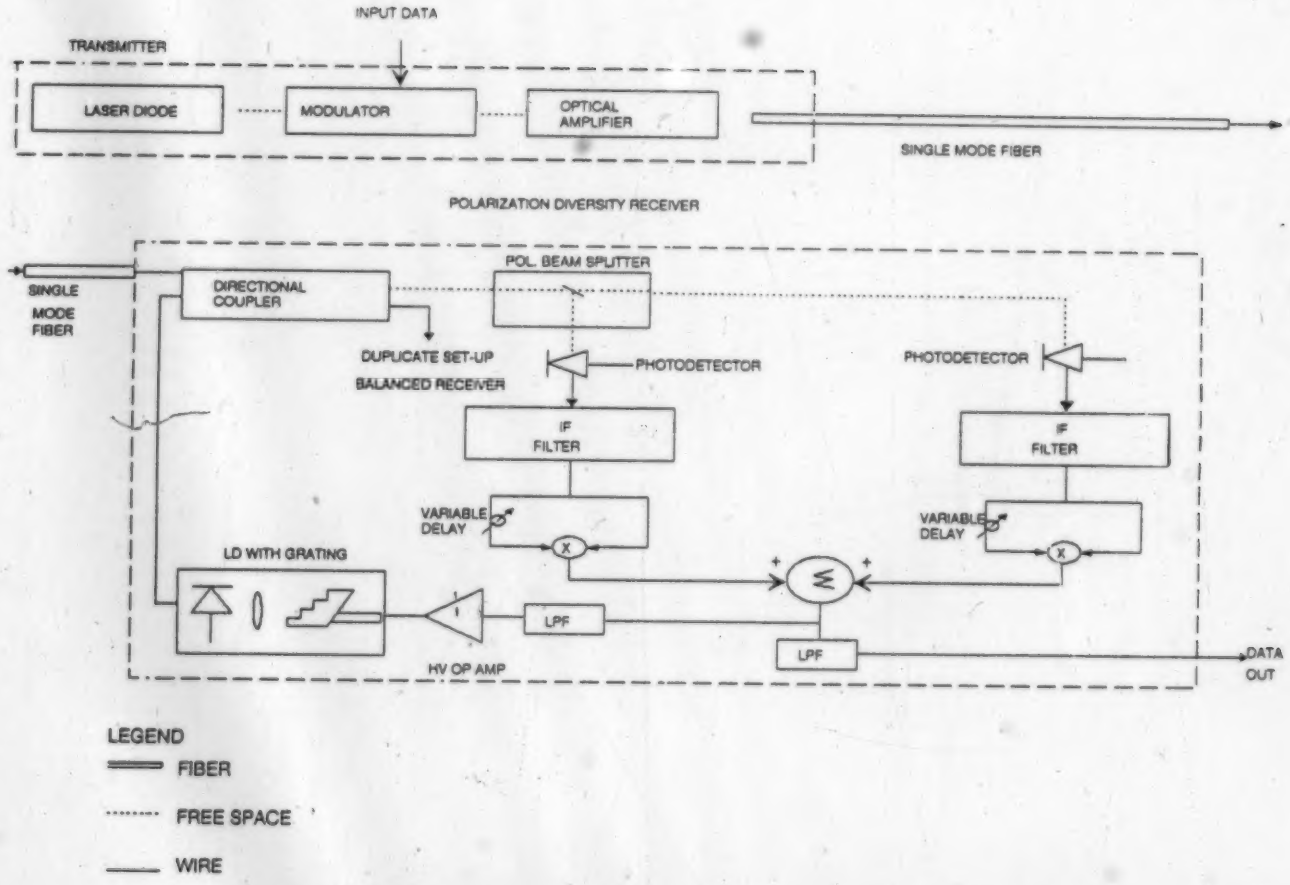

Fig. 1.1 Basic Configuration of a Coherent Long-Haul Optical Fiber Transmission System

formats, such as ASK or FSK, the laser can be modulated directly by varying the injection current while for PSK, external modulators are used. An optical amplifier may be used to boost the optical signal level before or after transmission through the fiber. At the receiver, the IF signal is obtained by mixing the transmitted signal and the LO signal. This IF signal can then be amplified and demodulated.

It should be noted that the polarization state of the LO and that of the received signal must be matched for best performance. There are several techniques used to overcome the problem of polarization mismatch. The most promising is a polarization diversity receiver whereby separate heterodyne detection is used for each polarization state and the outputs are recombined in the receiver electronics.

A more promising application of coherent optical fiber technology is in interoffice and loop-feeder systems, due to its potential for providing many closely spaced multigigabit channels. Figure 1.2 shows a star configuration appropriate for an interoffice network, in which each station is assigned a specific transmitting wavelength. This configuration exhibits the powerful frequency division multiplexing capabilities of coherent communications. Each station receives information from all other offices in the network over its own individual fiber. At any location, the desired channel can be selected by tuning the receiver local oscillator to that channel. There have been several experiments reported on multi-channel coherent systems [1]. However, there is much need for improvement in the devices required for realizing the long-haul or the interoffice topology discussed above. One of the most critical components in any coherent system is a stable optical source which has a

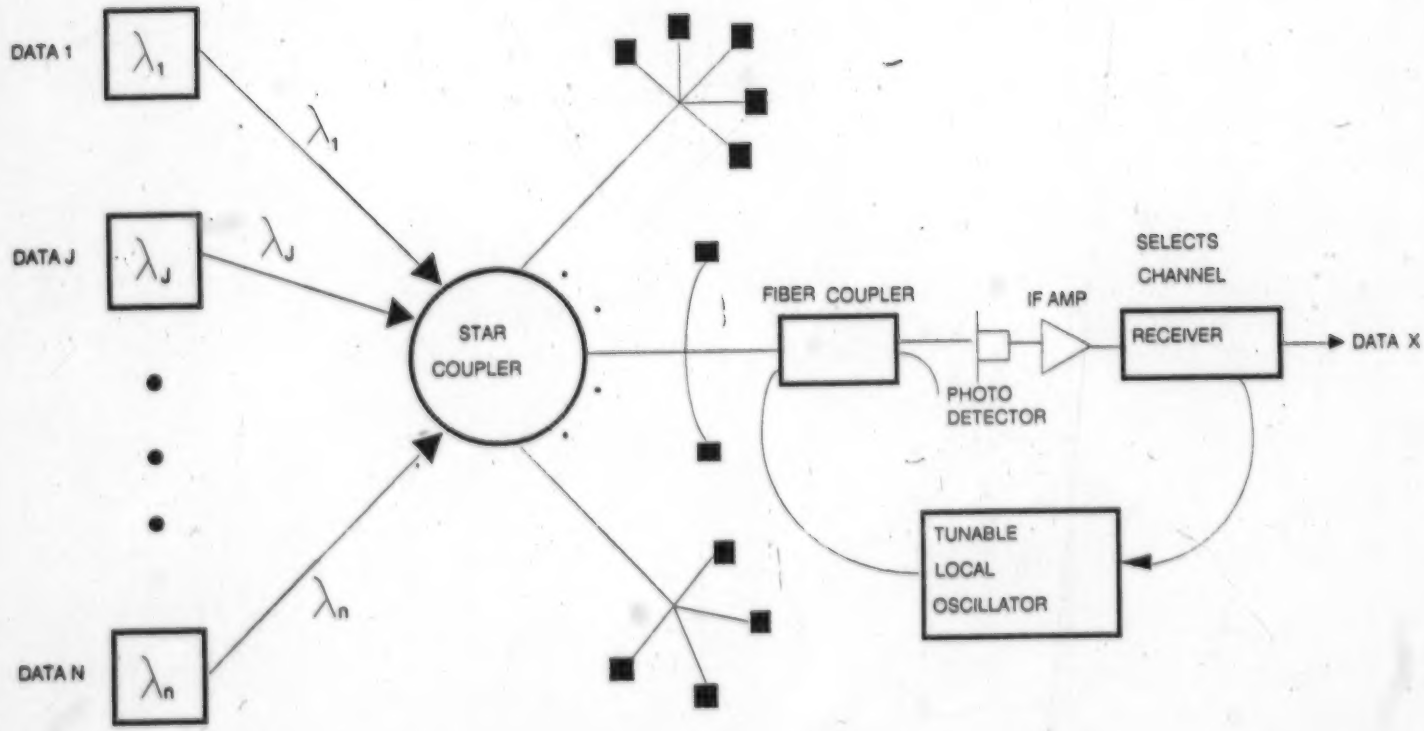

Fig. 1.2 A Star Network Configuration suitable for Interoffice Applications

narrow linewidth. Sources for coherent systems are considered in the next section.

1.2 SOURCES FOR COHERENT SYSTEMS

In order to realize the benefits of coherent detection, the continuous wave (CW) linewidth of the transmitter laser (which provides the optical carrier wave) as well as the CW linewidth of the local oscillator have to be considerably less than the modulation bandwidth. In addition, the lasers must have a long life and a stable and tunable frequency.

Theoretical calculations of the linewidth requirement for a particular modulation scheme (ASK, FSK, PSK DPSK) have been reported in various publications (2-4). Results show that the maximum allowable linewidth increases with transmission bit-rate and depends on the modulation used. The linewidth requirements for various modulation schemes are listed in Table 1. The continuous-wave linewidth of a laser depends on the Q-factor of the cavity and on the output power. Therefore, any endeavors to reduce the linewidth should entail adjusting these parameters. The following are some of the methods currently used to reduce the laser linewidth:

(1) weak optical feedback
(0.01 - 0.1% of output power fed back into the laser cavity)

(2) strong frequency-selective optical feedback
(10 - 25% of output power fed back into the laser cavity)

(3) injection locking

(4) electrical feedback

(5) integrated structures
(monolithic cavities)

TABLE 1

LASER LINEWIDTH REQUIREMENTS FOR DIFFERENT TYPES OF MODULATION[3]

MODULATION TYPE	LINEWIDTH/ BITRATE	POSSIBLE LASER TYPE
ASK, FSK	< 20%	DFB
DPSK	< 0.3%	EXTERNAL CAVITY
PSK	< 0.1%	EXTERNAL CAVITY

Each of these methods has its own merits and the method chosen depends on the application of the source. The linewidths obtained using some of the above techniques are listed in Table 2. Since integrated external cavity lasers show the most promise of being practical sources for coherent communications, future developments are geared towards obtaining narrow-line tunable sources using integrated structures. A monolithic distributed Bragg reflector laser with multiple electrodes has been reported that can be tuned continuously over a 720 GHz frequency range, which has a linewidth of a few megahertz [5].

1.3 MODULATION/DEMODULATION SCHEMES

There are three basic modulation schemes that can be considered for a coherent transmission system. These are:

(1) Phase Shift Keying (PSK)

(2) Amplitude Shift Keying (ASK)

(3) Frequency Shift Keying (FSK)

All three schemes assume a source coherence time much longer than a single pulse period, so that the source may be considered as a synchronous optical carrier.

For PSK heterodyne detection, a combination of a frequency stabilized oscillator and an external guided-wave electro-optic phase modulator is a possible transmitter configuration. External modulators can be divided into two types, intensity and phase modulators. The basic building block of these modulators is a linear waveguide, on the order of 3μm wide, diffused into a lithium niobate base or piezoelectric semiconductor substrate flanked by two

TABLE 2

LINEWIDTH OBTAINED WITH VARIOUS FEEDBACK CONFIGURATIONS

WAVELENGTH(μm)	CAVITY LENGTH	LINEWIDTH	TECHNIQUE EMPLOYED
1.5	1 m	50 kHz	[6]Grating Feedback (weak optical feedback)
1.5	15 cm	10 kHz	[7]Grating Feedback (strong optical feedback)
1.5	-	2 MHz	[5]DBR - Integrated External Cavity Laser
1.3	-	~3 MHz	[8]DFB Laser

electrodes. Since the phase information of the signal is used, the linewidth requirement for PSK systems is more stringent than that required for ASK or FSK [3].

FSK and ASK signals can be generated by directly modulating the injection current of a single-longitudinal mode laser. Each modulation type suffers from the spurious effects of the other type when the injection current is modulated. In cases where the laser is stabilized by the use of strong optical feedback, which degrades the frequency modulation efficiency, an external modulator can be used to generate an FSK signal. The drawback of directly modulating the laser frequency is that the FM response (i.e, the frequency deviation per milliamp) of semiconductor lasers is not uniform as a function of modulating frequency. Several techniques can be used to overcome this non-uniform FM response. One such technique is to use an adaptive quantized feedback equalization scheme at the receiver. In order to implement this technique, only a few passive components need to be added to the decision circuit in the receiver [9].

Optical signals are demodulated by heterodyne or homodyne detection using a local oscillator. To demodulate ASK and FSK signals, two methods are available; coherent or envelope detection. For coherent detection, the phase of the IF carrier is retained and used in the demodulation process; it implies demodulation with an absolute phase reference. The non-coherent detection is essentially an envelope detector (for example, a frequency discriminator for FSK); decisions are made by comparing the magnitude of the envelope of the received signal with a threshold value. For this reason, coherent detection is somewhat more complex and, for about a 1 dB power penalty, non-coherent post detection or envelope detection can be used. For

PSK demodulation, only coherent detection can be used. This requires a phase coherent reference from the received signal. Non-coherent demodulation of PSK signals involves differential detection (DPSK). For DPSK, the phase locked loop (PLL) used in PSK is replaced by a delay line equal to the bit spacing. A significant advantage of PSK or FSK modulation is that a semiconductor laser amplifier can be used as a high power post amplifier to overcome the loss due to the insertion of an external modulator, for example, a limiter or a preamplifier [10].

There are basically two types of linear semiconductor laser amplifiers; the Fabry-Perot-cavity type and the near travelling-wave type. The Fabry-Perot-cavity amplifier (which is a Fabry-Perot laser without AR coating on the facet) is biased just below threshold and achieves amplification by utilizing stimulated emission. The near travelling-wave amplifier is made by anti-reflection coating the laser facets of a Fabry-Perot laser. The near travelling wave amplifiers have a very broad bandwidth and are therefore very useful for amplification of frequency division multiplexed signals.

In homodyne detection, an optical PLL is essential for achieving a high homodyne receiver sensitivity. Homodyne detection has a 3 dB higher sensitivity than heterodyne schemes, but considerable complexity is introduced by the need to phase lock the local oscillator to the received signal. An optical PLL consists of a phase detector (photodetector), a voltage controlled oscillator (LO) and a loop filter. The phase error is detected by the photodetector and fed back to the LO, to effectively track the carrier phase. For binary transmission systems, PSK achieves the highest detection sensitivity [3].

1.4 THESIS OBJECTIVES AND ORGANIZATION

1.4.1 OBJECTIVES

The purpose of this thesis is to obtain an optical source that will be suitable for use in a coherent optical fiber communication system. Since it is intended that this source would eventually be used as an optical carrier, the modulation characteristics of this source will also be investigated. The source will be modulated in frequency by varying the injection current. This is known as direct frequency modulation.

The main objectives of this thesis are as follows:

1. Select a suitable optical feedback configuration (the amount of optical feedback being critical). Consideration must be given to what is experimentally feasible.
2. For strong optical feedback, it is necessary to antireflection coat one of the laser facets. A technique for coating and obtaining the lowest possible reflectivity must be determined.
3. Build the external cavity laser using a diffraction grating for the external frequency-selective reflector.
4. Verify that a source can be obtained that oscillates in a single longitudinal mode; i.e., side mode suppression ratio of greater than 20dB.
5. Measure the range of wavelengths over which single mode oscillation is obtained.

6. Measure the laser linewidth obtained with this configuration. Investigate the behavior at other wavelengths (i.e., obtain a graph of linewidth versus wavelength).
7. Investigate the frequency modulation capability of the external cavity laser diode

1.4.2 ORGANIZATION

In Chapter 1, various aspects of coherent optical fiber systems have been presented. A long-haul and a star topology for coherent systems have been briefly discussed. The characteristics of a source that is required for such a system have also been discussed, along with different modulation and demodulation techniques.

In Chapter 2, the problem of obtaining very low reflectivities for anti-reflection coated laser facets is discussed. A procedure will be described to monitor the reflectivity of the facet while the coating is being deposited onto it. Experimental results will be discussed and the calculation of modal reflectivity will be carried out.

In Chapter 3, the design of an external cavity-controlled semiconductor laser is discussed. Each of the elements that constitutes the external cavity will be discussed in detail. Crucial alignment procedures will also be outlined.

The single longitudinal mode oscillation of the external cavity and the mechanism that causes this will be the topic of Chapter 4. Measurements of side mode suppression ratio and the tuning range capability of the external cavity laser will be presented.

In Chapter 5, the linewidth narrowing factor and the factors that influence line narrowing phenomena will be discussed. Linewidth measurements of the laser with an external cavity tuned at different wavelengths will be presented.

The direct frequency modulation characteristics of the source will be discussed in Chapter 6. A relationship between the linewidth reduction factor and the degradation in frequency modulation capability of the external cavity laser will be presented. Finally, the experimental results obtained for frequency modulation of this laser will be discussed.

In Chapter 7, the major results obtained in this work will be recapitulated and recommendations for further work in this area will be given.

CHAPTER 2

FABRICATION OF ANTI-REFLECTION COATING ON LASER-DIODE FACET

The advantages of using strong optical feedback to obtain narrow linewidth lasers are numerous. For example, the resulting source is fairly insensitive to spurious optical reflections, precise temperature and current control of the laser are not necessary, and the resulting spectrum is essentially independent of chip parameters. However, in order to reach the regime of strong optical feedback, it is necessary to anti-reflection (AR) coat the semiconductor laser diode (LD). In this regime, the feedback level into the LD is typically greater than -10dB [11].

The optimum film characteristics required to obtain a reflectionless layer on LD facets with a thin active region are different from those of a simple quarter-wavelength matching film [12]. In a LD the optical mode confinement factor, Γ, for the active layer is about 0.4. This means that most of the optical field exists in the cladding region. Therefore, the influence of the cladding layer must be incorporated in the design of an AR coating with low reflectivity. For this purpose, a series of theoretical calculations, as described in Reference [12], must be carried out to determine the exact thickness and refractive index of the coating with a certain active area height. However, determining the exact thickness and refractive index of the coating does not guarantee very low reflectivities. This is because the evaporation parameters such as the deposition rate, pressure in the chamber during the deposition process, etc. all affect the final reflectivity obtained with a pre-determined coating thickness and therefore the optical thickness of the coating varies with

these parameters. In view of the foregoing, it was thought essential to monitor the change in reflectivity of each LD while the coating was being deposited, so that the process could be terminated at the optimum point when the reflectivity is the lowest possible under the deposition condition for that LD. In this chapter, a technique that can be used to coat the LD facet is described. The results obtained with various sample diodes are presented. Finally, the procedure to measure the reflectivity of a sample LD is outlined.

2.1 REAL-TIME FACET REFLECTIVITY MONITORING SYSTEM

One way to monitor the change in reflectivity of a LD while a coating is being deposited on it, is to monitor the change in threshold current during the deposition process. The threshold current density of a semiconductor laser diode is given by [13]

$$J_{th} = \{\alpha - [\ln (R_1R_2)]/2\ell\}/\beta \qquad (2.1)$$

where:

β = gain factor

α = internal loss coefficient

ℓ = length of the laser cavity

R_1, R_2 = power reflection coefficients of front and back facets, respectively.

When the back facet is being coated, R_2 either increases or decreases, and assuming that other device parameters remain relatively constant, the

threshold current density will decrease or increase, respectively. As the reflectivity becomes very small, the threshold point vanishes. An increase in threshold current can also occur due to a rise in junction temperature and due to leakage current that may develop during the coating process. However, the threshold current will drop only due to an increase in reflectivity. If the evaporation process is terminated at the point of maximum change in threshold current or until lasing ceases, then a coating thickness is obtained that corresponds to a minimum reflectivity. To attain the minimum possible reflectivity, the refractive index of the coating must also be optimised. For most dielectric materials used as optical films on substrates from the III-V material system, this can be achieved by controlling the rate of deposition and the pressure in the evaporation chamber during the process [12,14].

2.1.1 EXPERIMENTAL SET-UP

Figure 2.1 shows the experimental arrangement for monitoring LD facet reflectivity. The characteristics of the InGaAsP LD used in this experiment are listed in Table 3. The LD was biased at its initial threshold current and pulsed periodically to a higher value. The pulse frequency was 500Hz, with a 20% duty cycle. This pulse generated a corresponding optical power pulse. The amplitude of the current pulse needs to be higher than the expected change in threshold, or the optical power pulse will cease. For the various LDs that were coated, the current pulse amplitude was set at 100mA. As the threshold current increases, the amplitude of the optical power pulse decreases, and this was monitored on a chart recorder and an oscilloscope during the coating process. To ensure that the change in threshold was mainly due to the

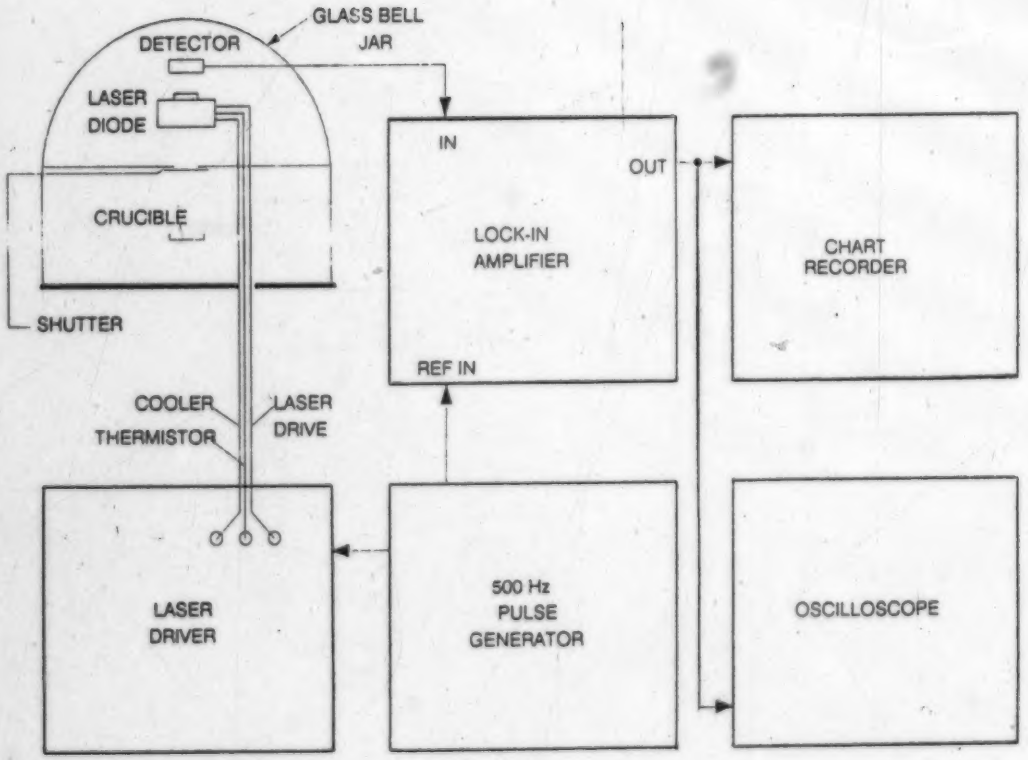

Fig. 2.1 Experimental Set-Up for monitoring LD Facet Reflectivity

TABLE 3

PHYSICAL PROPERTIES OF THE BURIED HETEROSTRUCTURE LASERS USED IN THIS WORK

CHARACTERISTICS	SYMBOL	VALUE	REFERENCE
Threshold Current	I_t	16 mA	b
Wavelength	λ	1.3 μm	a
Length	ℓ	250 μm	a
Stripe Width	s	2 μm	a
Active Region Thickness	d	0.2 μm	a
Refractive Index Active Area	n_a	3.4965	c
Refractive Index of Cladding	n_c	3.2176	c

a. Manufacturers data

b. This work

c. [13]

change in reflectivity rather than in temperature, the laser diode was mounted on a Peltier cooler. The temperature of the laser chip was actively controlled using a thermistor temperature detector to control the current through the Peltier cooler.

The laser to be coated was mounted on a jig with a Peltier cooler and a thermistor and placed in the evaporation chamber (NRC 3115). The facet of the laser to be coated was mounted such that it coincided with the edge of the jig and would therefore be subjected to the vapour directly without being shadowed. The SiO_x film was formed by thermal evaporation with a resistance heated source in a vacuum system. The chamber, which is a glass bell jar, was evacuated to a pressure of about $5X10^{-6}$ Torr using a diffusion pump with a liquid Nitrogen trap. As the current was applied to the source, the SiO_x started vaporizing and the pressure dropped to $7X10^{-7}$ Torr. When the pressure was stable at this point, the shutter exposing the vapour to the facet was opened. Throughout the experiment the pressure was held constant near $7x10^{-7}$ Torr by adjusting the current to the source, so as to achieve a constant rate of evaporation. At various times during the coating process, the shutter was closed and the power versus current curve of the LD was measured. After completion of the experiment, the total thickness was measured to be 6710Å; the total evaporation time was 17.6 minutes. This gives a deposition rate of approximately 6.4Å/sec. The thickness and time indicated here correspond to coating beyond the minimum reflectivity point. The explanation for this is given in the next section.

2.1.2 EXPERIMENTAL RESULTS

The change in peak LD output power versus coating thickness is shown in Figure 2.2. As the evaporation proceeds, the LD output power decreases, indicating an increase in the threshold current and a corresponding decrease in reflectivity of the coated facet. At point D, the power is a minimum; to obtain minimum reflectivity the coating process would normally be stopped at this point. In this experiment, the coating was continued beyond this point in order to verify that the reflectivity would behave as expected. The minimum reflectivity obtained at point D corresponds to a coating thickness of 2573Å. Beyond point D, the output power rises again, indicating an increase in reflectivity. At point E, the reflectivity is almost equal to its starting value. The slight difference is probably due to losses in the coating, and to the fact that the light from the LD is not truly planar. At point F, the reflectivity is again a minimum.

In Figure 2.3 the various optical power versus current curves corresponding to points A to F of Figure 2.2 are shown. The initial threshold current is seen to be 16mA. At points B and C, thresholds of 19mA and 30mA were obtained, respectively. At the point of minimum reflectivity, D, the lasing action has become weak. The curves for points E and F are as expected. At E, the threshold current is 17mA, only slightly greater than the initial value, while at the second minimum, F, the lasing action has again almost ceased.

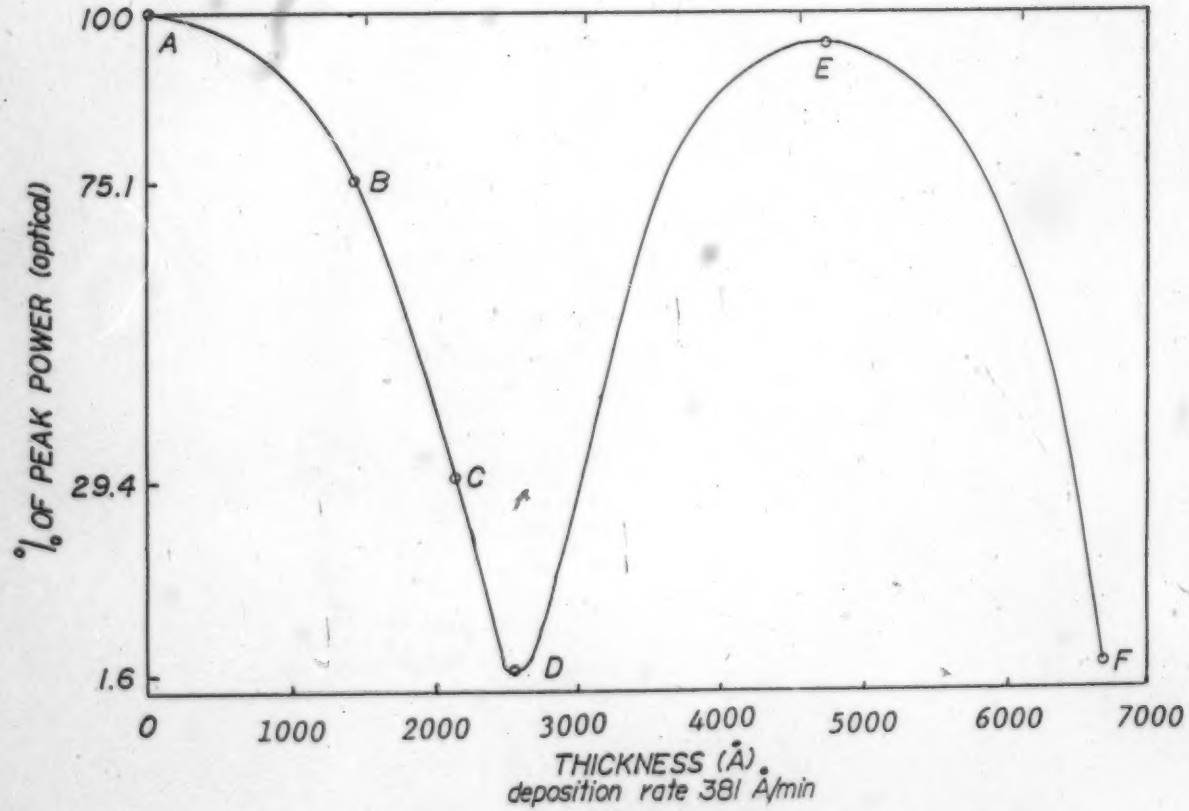

Fig. 2.2 Dependence of LD Optical Power on Coating Thickness

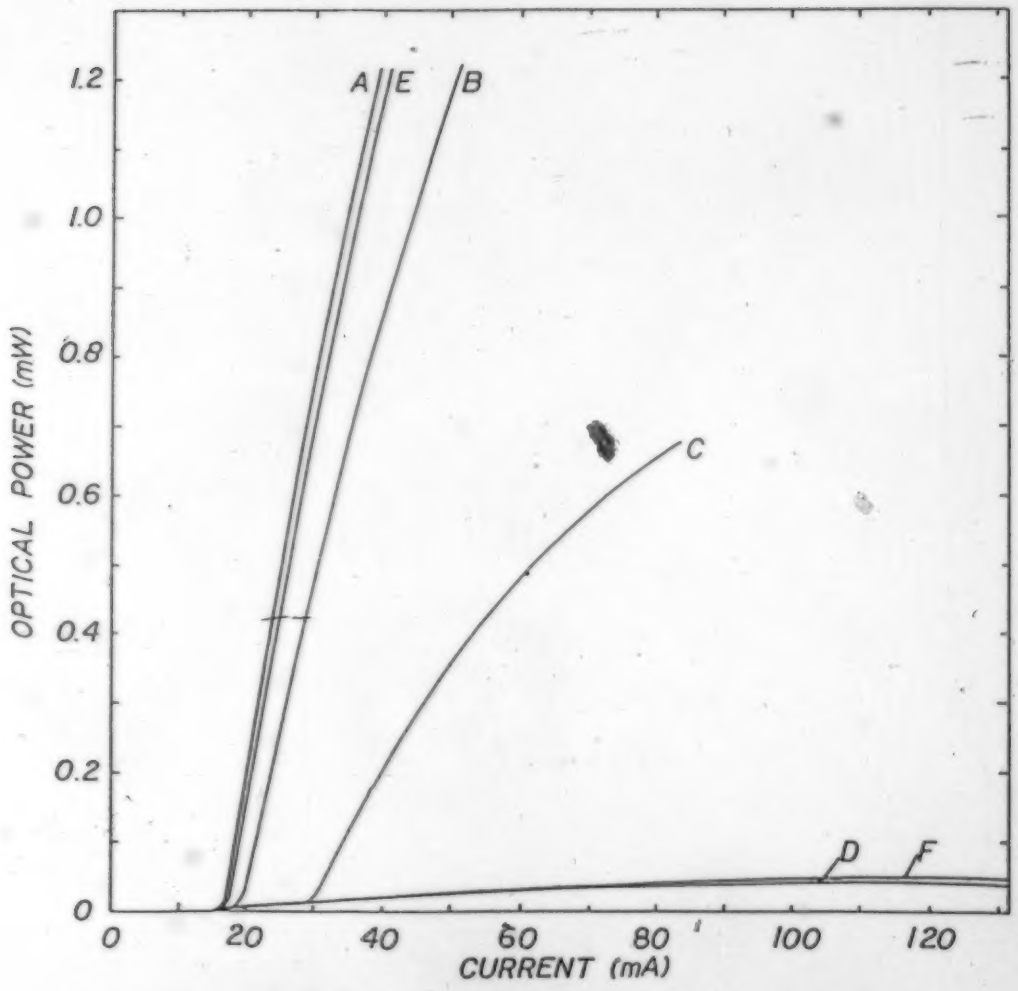

Fig. 2.3 CW Lasing Characteristics at the Points indicated in Fig. 2.2

2.2 MODAL REFLECTIVITY MEASUREMENT

The modal reflectivity can be obtained from a measurement of the power spectral density of the guided amplified spontaneous emission (ASE) below oscillation threshold [15]:

$$P(\lambda) = \frac{K(1+RG)(1-R_{ar})(G-1)}{(1-(\sqrt{R_{ar}R})G) + 4(\sqrt{R_{ar}R})G \sin^2(2\pi n_{eff}\ell/\lambda)} \qquad (2.2)$$

where:

R, R_{ar} = Modal power reflectivity of the uncoated and coated facet, respectively

ℓ, n_{eff} = Laser length and guided wave effective refractive index

G = Guided wave gain

K = Proportionality constant that contains the spontaneous emission rate and photon energy

When $(\sqrt{R_{ar}R})G << 1$, (below threshold), the sinusoidal term in Equation 2.2 shows resonance and antiresonance of the laser diode. R_{ar} can be determined from the above equation by measuring the power ratio of the neighbouring resonant and antiresonant peaks:

$$\frac{P_{max}}{P_{min}} = x = \frac{(1-(\sqrt{R_{ar}R})G)^2 + 4(\sqrt{R_{ar}R})G}{(1-(\sqrt{R_{ar}R})G)^2} \qquad (2.3)$$

Equation 2.3 can be rewritten as:

$$R_{ar}R\,G^2 = \left[\frac{\sqrt{x}-1}{\sqrt{x}+1}\right]^2 \qquad (2.4)$$

In order to determine R_{ar} from Equation 2.3, P_{max} and P_{min} are measured for the transverse electric (TE) and transverse magnetic (TM) modes by obtaining the power spectral density for each of these polarizations. The experimental set-up for this measurement is shown in Figure 2.4. Before the LD is AR coated, the oscillation is usually in the TE polarization [15], and at the threshold current I_t , $G_{TE}R^{TE} = 1$ [15]. Since R^{TE} is known from Ikegami's calculation [16], G_{TE} can also be determined. Therefore, R_{ar} (TE polarization) can be calculated. To determine R_{ar} (TM polarization) the assumptions made in Reference [15] were used. R^{TM} was again determined from Ikegami's calculation and, to determine G_{TM} ,the following relationship was used:

$$G_{TM} = (G_{TE})^{(\Gamma TM/\Gamma TE)} \qquad 2.5$$

where Γ_{TE} and Γ_{TM} are the optical confinement factors for TE and TM polarisation respectively.

Figures 2.5 and 2.6 show the power spectral density for the TE and TM polarization, respectively. From Figure 2.5, $X_{TE} = 1.21$. $R^{TE} = 0.37$, [16] $G_{TE} = 2.70$ and, applying Equation 2.4,

$$R_{arTE} = 0.85 \times 10^{-3}.$$

From Figure 2.6, $X_{TM} = 1.13$ and $R^{TM} = 0.25$. In order to determine G_{TM}, the confinement factors Γ_{TM} and Γ_{TE} must be determined from the laser parameters. The optical confinement factor is defined as follows:

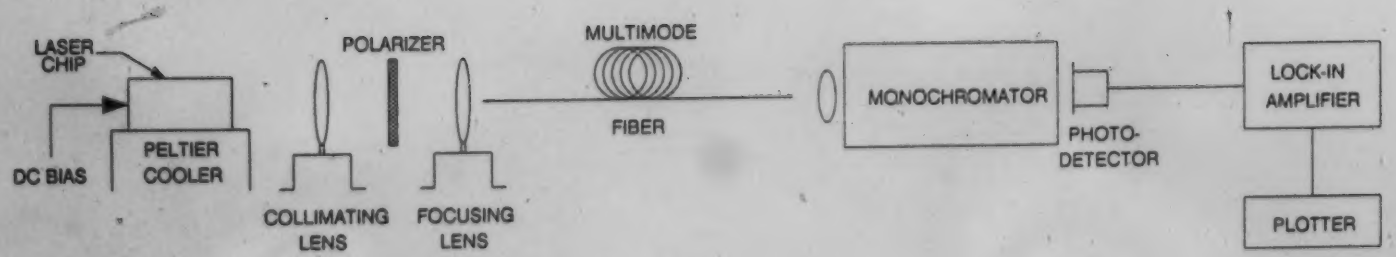

Fig. 2.4 Experimental Set-Up for measuring TE and TM Power Spectral Density

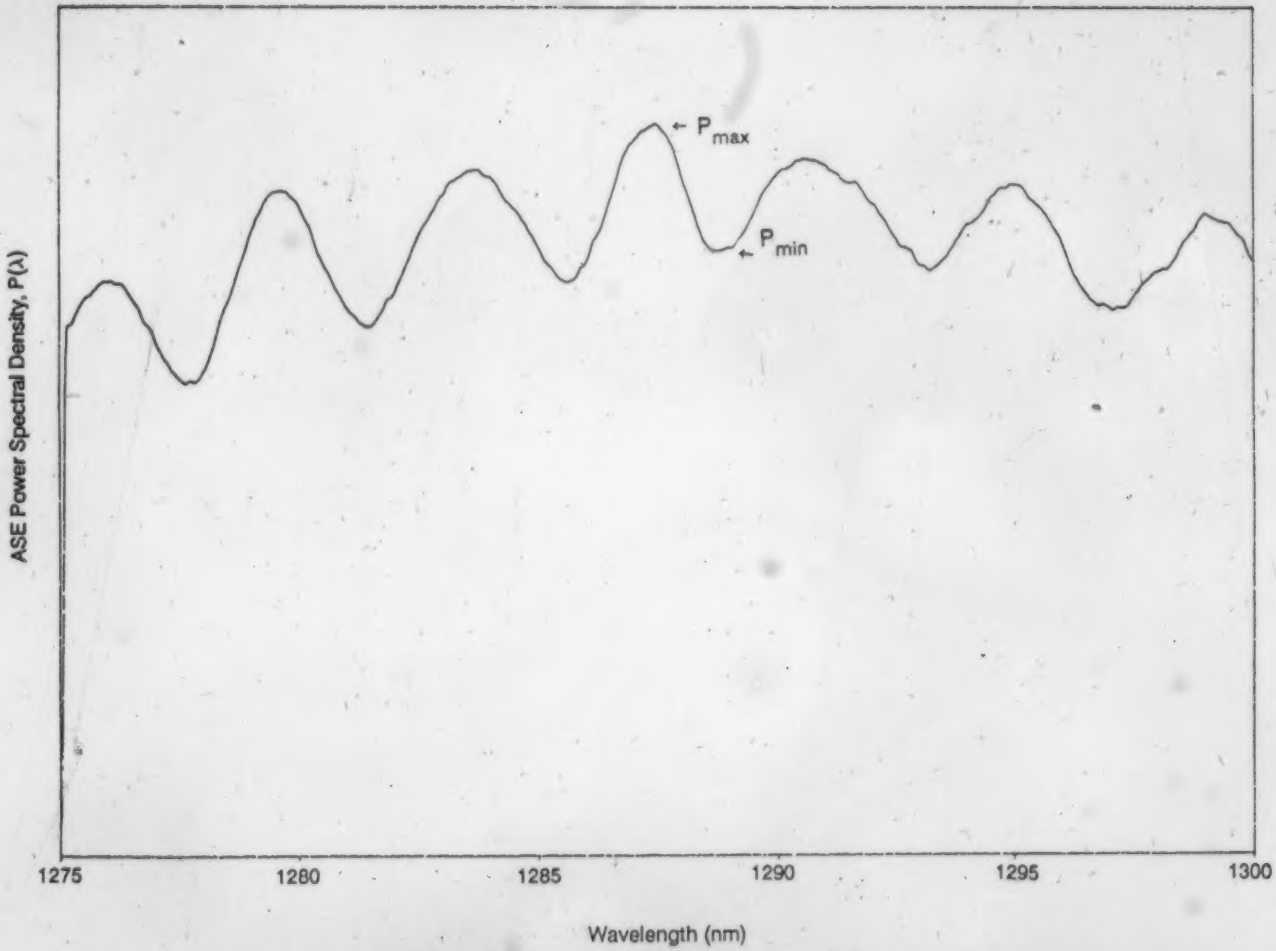

Fig. 2.5 Power Spectral Density of the Guided Amplified Spontaneous Emission for TE Polarisation; I_{bias} = 16 mA

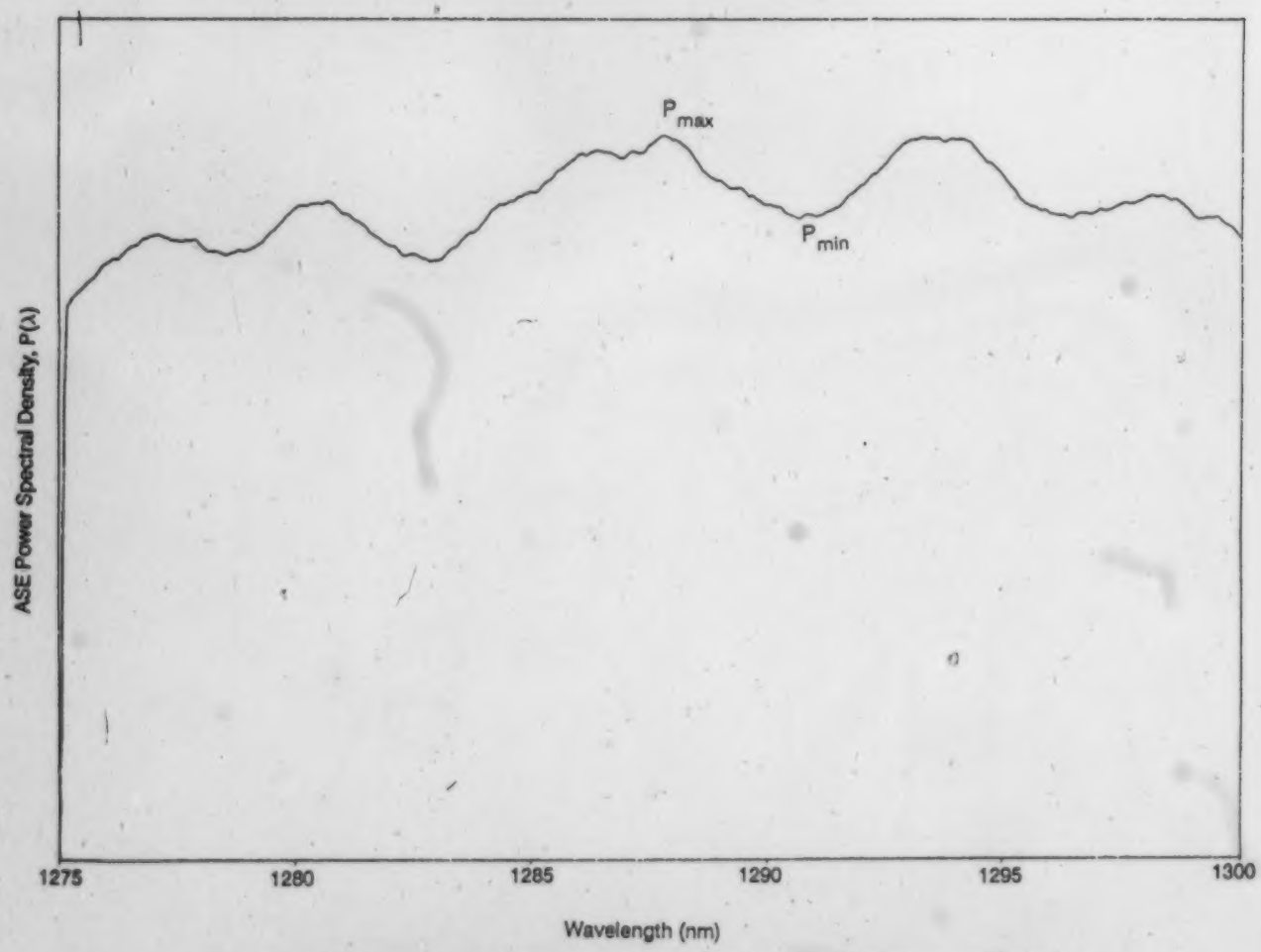

Fig. 2.6 Power Spectral Density of the Guided Amplified Spontaneous Emission for TM Polarisation; I_{bias} = 16 mA

$$\Gamma \overset{\Delta}{=} \frac{\int_d Ey^2(x)\,dx}{\int_{-\infty}^{\infty} Ey^2(x)\,dx} \qquad (2.6)$$

Following the procedure outlined in Appendix A, the following values are obtained for the ratio of the confinement factors, G_{TM} , and finally the reflectivity for TM polarisation, R_{arTM}:

$$(\Gamma_{TM}/\Gamma_{TE}) = 0.896$$

and from Equation 2.5:

$$G_{TM} = 2.44.$$

Using Equation 2.4:

$$R_{arTM} = 0.63\times10^{-3}$$

2.3 SUMMARY

In this chapter the fabrication of an AR coating on LD facet has been discussed. Real time monitoring of the reflectivity while the coating was being deposited is the key to obtaining low reflectivities. The evaporation process, i.e., the pressure in the chamber during coating, and the deposition rate were not optimised for this case since the reflectivities obtained without this optimisation were adequate. However, if it is desired to obtain reflectivities in

the 10^{-6} to 10^{-7} range (for example for semiconductor laser amplifiers), then these parameters must be accurately controlled.

In this chapter the procedure to calculate modal reflectivities was also outlined. The TE and TM power reflectivities obtained for a sample diode with the parameters listed in Table 3 were as follows:

$$R_{ar,TE} = 0.85 \times 10^{-3}$$
$$R_{ar,TM} = 0.63 \times 10^{-3}$$

CHAPTER 3

CONFIGURATION OF THE GRATING LOADED EXTERNAL CAVITY LASER

In this chapter the experimental configuration of the external cavity controlled LD is described in detail. Each of the elements used in the design of the cavity is discussed and critical alignment procedures are outlined. A block diagram of the experimental set-up of the external cavity laser is shown in Figure 3.1. The elements used in the external cavity controlled semiconductor laser are: a movable diffraction grating, a collimating lens, a semiconductor laser diode, an optical isolator and single mode fiber to couple light out so that spectral measurements can be made. Light from the AR coated LD facet is collimated using a microscope objective. The collimated light is reflected off a diffraction grating and the first-order diffracted beam is aligned such that it is reflected back into the LD cavity through the same facet. At the other facet, i.e. the uncoated facet, light can be coupled out for measurement or transmission using a tapered single mode fiber. An optical isolator is required to eliminate spurious reflections from the measuring equipment.

3.1 DESCRIPTION OF EACH OF THE COMPONENTS CONSTITUTING THE EXTERNAL-CAVITY LASER

3.1.1. DIFFRACTION GRATING

The grating used in this experiment is gold coated for higher reflection efficiency and has 1200 lines/mm groove spacing. The power efficiency of the diffraction grating was measured to be 81% at 1300 nm for light polarised in the direction perpendicular to the grooves. The grating is mounted in a gimbal

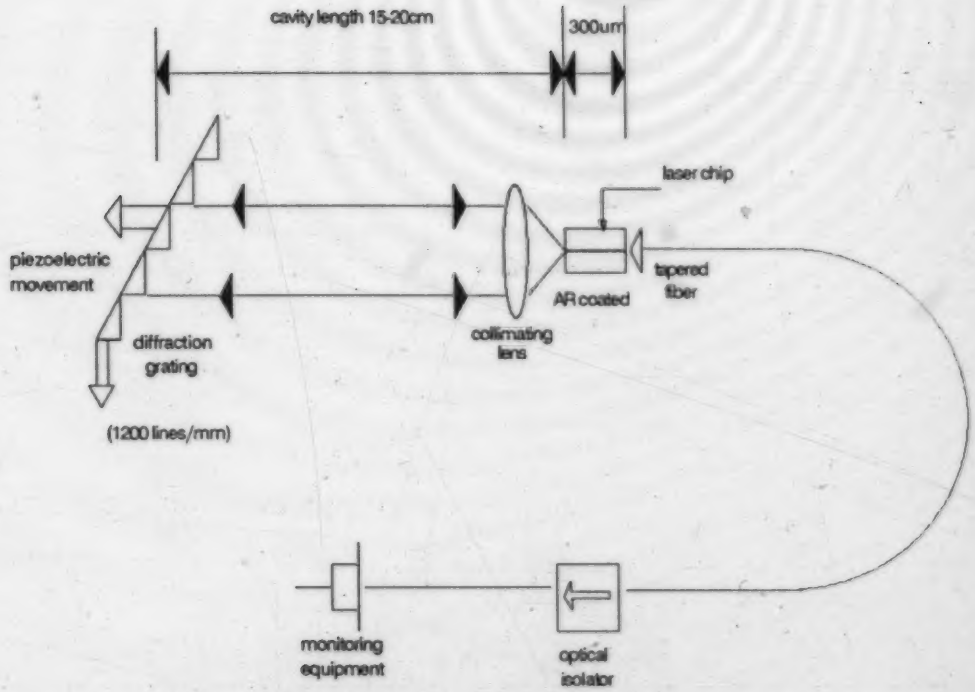

Fig. 3.1 Block Diagram of the Experimental Set-Up of a LD with External Grating Feedback

holder with two angle drives that can be controlled piezoelectrically. One angle (Φ) scans across the grooves thereby selecting a different angle of diffraction for the first-order diffracted beam and, hence, a different oscillating wavelength. The other angle (θ) scans along the grooves and serves mostly for aligning of the diffracted beam back into the LD cavity. Typically the output radiation beam of the LD is characterized by two angles which measure the divergence of the beam in the direction parallel and perpendicular to the junction plane. Usually, the beam divergence in the perpendicular direction is much broader than in the parallel direction and hence more lines on the grating will be illuminated if the grating is mounted with the grooves parallel to the junction plane. However, measurements showed that the highest first-order grating reflection was obtained when the electric field vector was perpendicular to the grooves. This indicated that even after AR coating, the LD continued to emit radiation in the TE polarisation (that is, the electric field vector in the plane of the junction); the TM polarised modes still had higher losses in the LD cavity. Therefore, in order to minimize losses in the overall cavity, the grating was mounted such that the grooves are perpendicular to the junction plane and hence the electric field vector. This is shown in Figure 3.2.

The grating is mounted in the Littrow configuration, that is, the first-order diffracted beam is reflected collinear with the incident beam and re-imaged onto the laser facet. Considerable care must be taken to ensure that the grating is mounted vertically in the holder so that the two angle tilts are decoupled.

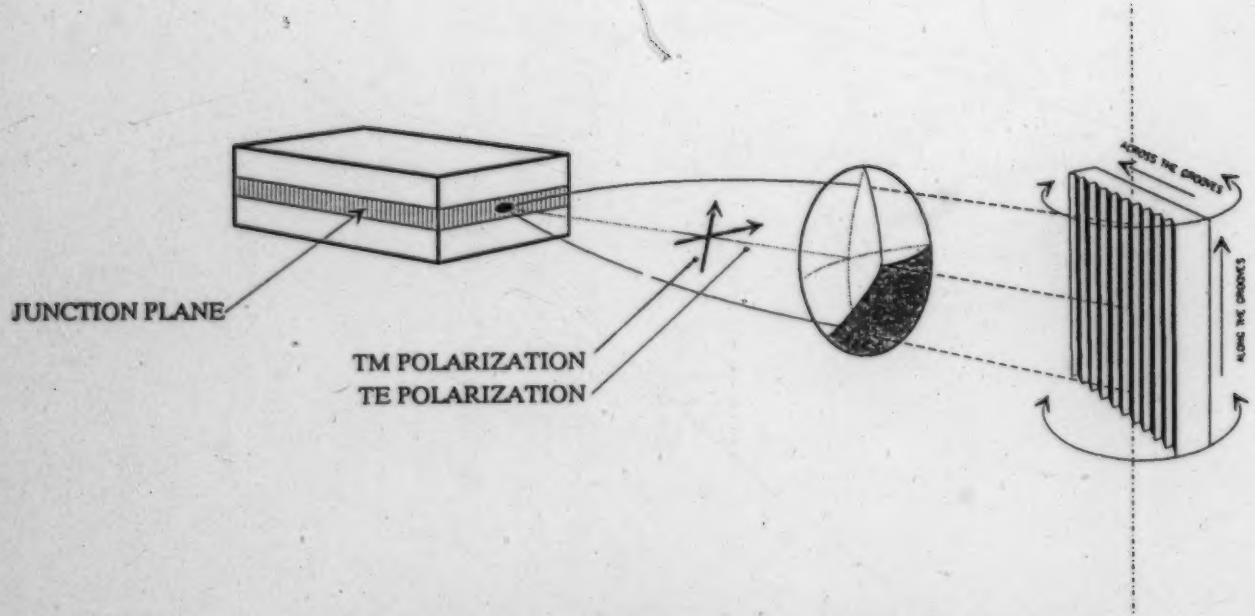

Fig. 3.2 Figure Showing how the Grating is mounted with respect to the LD
The Grooves are Perpendicular to the Electric Field Vector that is
Parallel to the Junction Plane

3.1.2 COLLIMATING LENS

The purpose of the collimating lens is to collect as much radiation from the LD as possible and collimate it onto the diffraction grating. To this end, this lens requires a large aperture ratio. Also, high optical throughput and negligible scatter are necessary to minimize the cavity losses. The collimating lens used in this experiment is a microscope objective with a 0.4 numerical aperture (NA) and 16 mm focal length. The lens is antireflection coated for minimum reflection at 1300 nm. The lens is fully corrected for spherical aberration at this wavelength. For proper imaging the lens has to be mounted such that it is perpendicular to the optical axis and for this reason it is mounted on an XYZ translator. The light collected from the facet of the laser is aligned to have a focus at a point as far away from the laser as possible, i.e., the output beam from the lens is parallel. It cannot be emphasized enough that the accuracy with which the lens is mounted will determine how much of the light reflected from the grating is actually coupled into the LD cavity. In the alignment procedure, it was found that the positioning of the lens along the optical axis (i.e. the distance from the LD), was also critical in entering the regime of strong optical feedback, when at least -10 dB of the light emitted is fed back into the cavity [11].

3.1.3. SEMICONDUCTOR LASER DIODE

The LD used in this experiment is a V-grooved double heterostructure index guided laser. The double heterostructure and narrow stripe geometry supports only the fundamental lateral and transverse mode. Lateral confinement of the mode is obtained by introducing steps in the refractive

index (hence, the name index guided laser). Each lateral mode is associated with a family of longitudinal modes. Therefore, index guided LDs which support only the fundamental lateral mode are desirable because the optical feedback to obtain single longitudinal mode contends only with one family of longitudinal modes. The phenemenon of "homogeneous gain saturation" (see Chapter 4) which causes single longitudinal mode oscillation occurs when there is only one family of longitudinal modes.

The original physical characteristics of the LD used in the external cavity configuration are listed in Table 4. One of the facets (the front facet) of the LD was AR coated according to the procedure outlined in Chapter 2. The following values were obtained for the reflectivity of the TE and TM modes:

$$R_{ar(TE)} = 1.0 \times 10^{-3}$$
$$R_{ar(TM)} = 0.7 \times 10^{-3}$$

The optical power versus current characteristic of the LD was measured from both the uncoated and the coated facet. This is plotted in Figure 3.3. The optical power spectrum of the LD (with one facet coated), measured with a monochromator is shown in Figure 3.4. This spectrum is typical for superluminescent diodes, which oscillate over a broad range of wavelengths. A tapered fiber was used to couple light out of the uncoated facet, so that spectral measurements could be made. The coupling efficiency of the taper was measured to be about 15%. The LD chip on a carrier (as received from the manufacturer) is mounted on a Peltier cooler. The current through the Peltier cooler is controlled by a thermistor temperature control circuit. The circuit diagram of the control circuit and the temperature calibration of the thermistor are shown in Figures B.1 and B.2 in Appendix B, respectively. The laser diode CW bias circuit is shown in Figure B.3. The grating is

TABLE 4

PHYSICAL PROPERTIES OF THE STRIPE GEOMETRY DOUBLE-HETEROSTRUCTURE LASER USED IN THE EXTERNAL CAVITY CONFIGURATION [Figure 3.1]

Manufacturer: Fujitsu FLD130D4SJ-A (InGaAsP)

CHARACTERISTICS	SYMBOL	VALUE	REFERENCE
Threshold Current (before coating)	I_t	13 mA	a
Wavelength of peak intensity	λ_p	1284 μm	b
Length	ℓ	300 μm	a
Stripe Width	s	< 1.5 μm	a
Active Region Thickness	d	0.2-0.3 μm	a
Gain Factor	β	0.12×10^{-1} cm/Amp	a
Internal Loss Coefficient	α	17 cm^{-1}	a
Reflectivity of Uncoated Facet	R	0.35	c

a. Manufacturer's data

b. This work

c. [13]

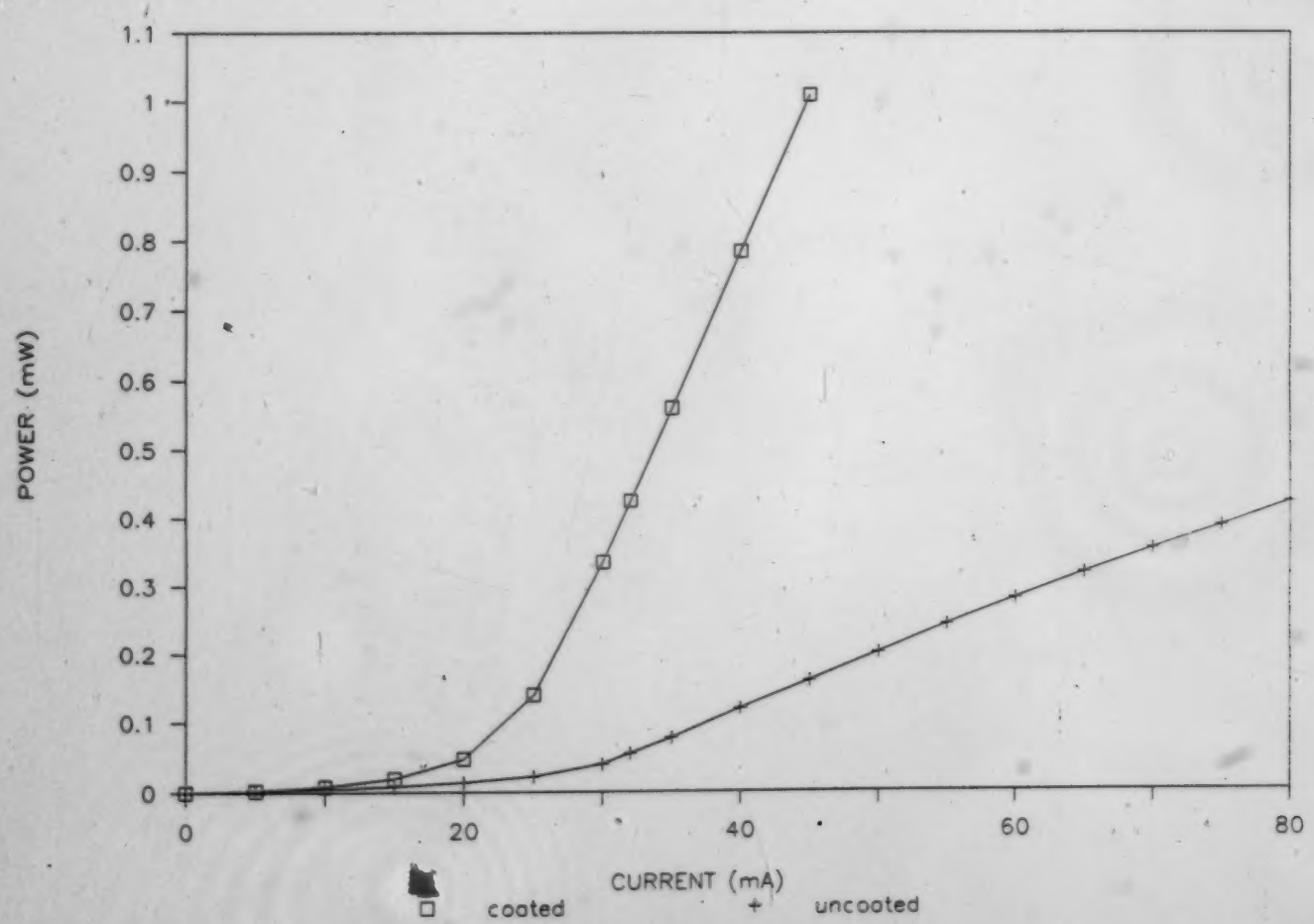

Fig. 3.3 Optical Power versus Current Curve of the Fujitsu LD at T = 17°C

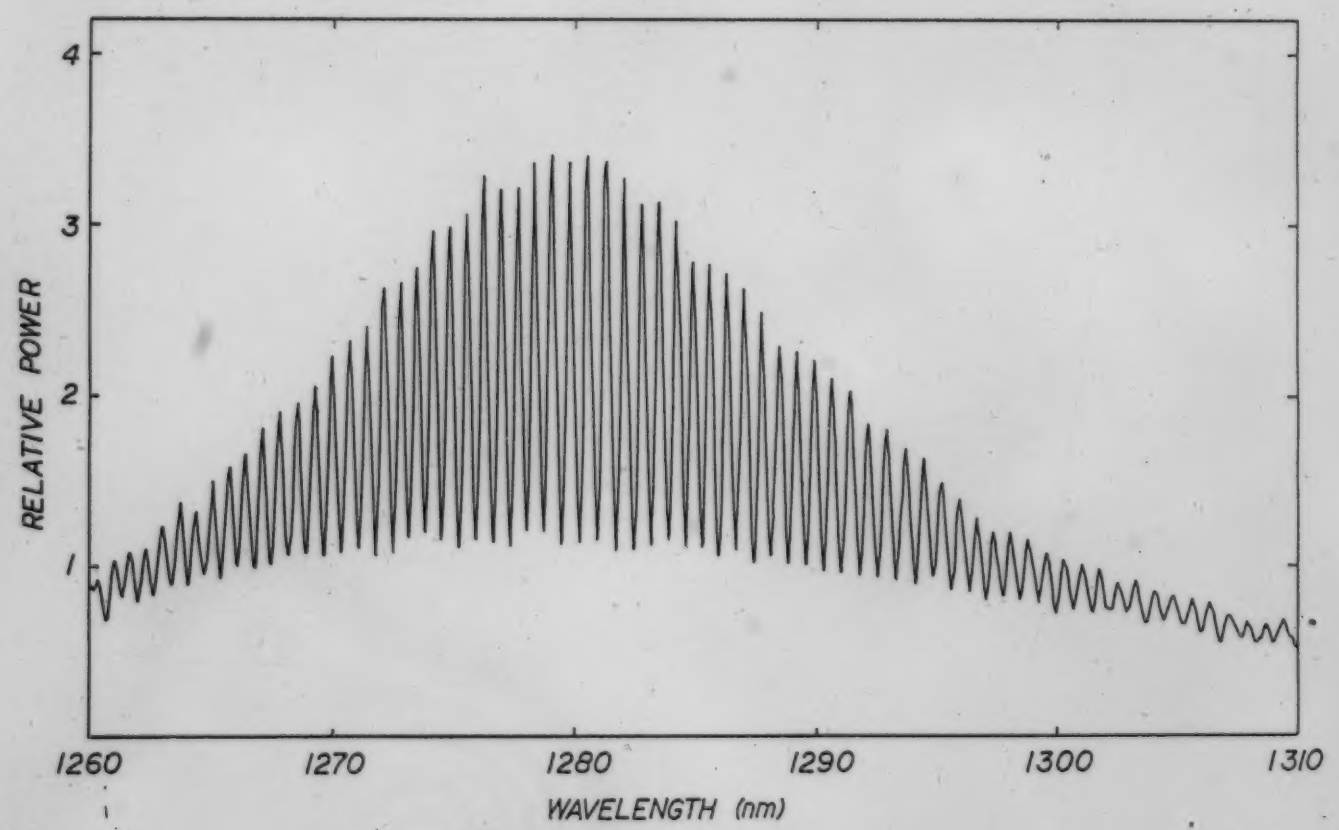

Fig. 3.4 Output Spectrum of a LD with One Facet Coated for Minimum Reflectivity. $I_{bias} = 2.0I_{th}$

placed about 19 cm away from the LD. This distance determines the external cavity length.

3.1.4 OPTICAL ISOLATOR

The reason for using an optical isolator in this set-up is to reduce feedback of laser radiation into the LD from the output fiber. The optical isolator is a non-reciprocal device based on the Faraday or magneto-optic effect. The optical isolator used in this experiment is a NEC device No. OD8313B (λ = 1.3 μm). It provides an isolation of greater than 30 dB and has an insertion loss of 0.5 dB when properly aligned. It is better to install the optical isolator between the LD and the fiber so that all the undesired reflections are blocked. In this set-up however, due to physical constraints, it was necessary to use a short piece of fiber (~1m) between the LD and the isolator. The reflections from this short piece of fiber cause side frequencies, (150 GHz) that are far away from the desired frequency, and which do not fall within the grating response (30GHz, calculated in the next chapter).

If an optical isolator is not installed in the fiber path between the LD and the measuring device,the reflections from the fiber end face cause "noise spikes" at frequency intervals of nv/2L Hz (n is the axial mode number along the fiber, v is the velocity of light in the fiber and L is the length of the fiber used). This is shown in Figure 3.5, where the noise spikes are labelled B,B',C,and C'. In this case, the length of fiber from the laser to the measuring instrument was about 12.5 meters, and hence, these spikes appear about 8 MHz apart. In this experiment, the only feedback of light into the LD that is desired is the reflection from the grating through the coated facet. The feedback of light from the fiber through the uncoated facet must therefore, be

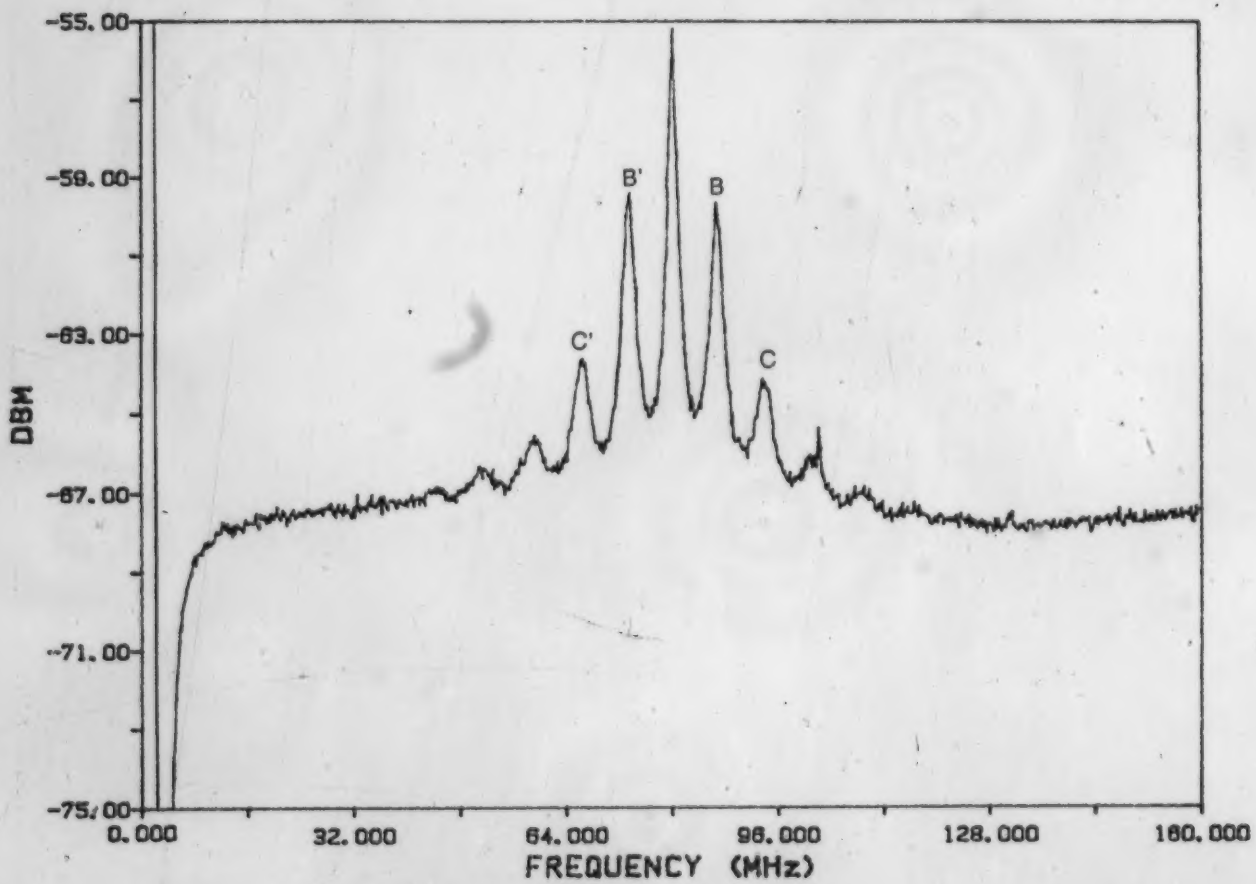

Fig. 3.5 Output Power Spectrum without an Optical Isolator. The "Noise Spikes" resulting from Spurious Reflections are marked by B,B',C and C'.

minimized. It was found that the reflection from the fiber end face to the uncoated facet made it more difficult to operate the LD in the strong feedback regime.

3.2 MEASURING/MONITORING EQUIPMENT

Three different types of measuring equipment were used in this experiment; a monochromator, a Fabry Perot Interferometer and a self-heterodyne set-up. The output power of the laser diode was measured with a calibrated Germanium large-area photo diode. The power readings gave an indication of the level of feedback into the laser cavity since the feedback causes a change in the threshold condition of the LD. These readings can be used to calculate the feedback factor (see Chapter 4).

3.2.1 SCANNING MONOCHROMATOR AND FABRY PEROT INTERFEROMETER

A scanning monochromator (McPherson 270) was used in the configuration shown in Figure 3.6 to measure the spectral properties of the LD light. Direct wavelength measurements can be made using the monochromator. The slit width used for most measurements was about 50 μm, which gives a resolution of 20 GHZ.

For better resolution a Burleigh scanning Fabry Perot interferometer was used in the configuration shown in Figure 3.7. The plate separation was about 1mm with a free spectral range (FSR) of 143 GHZ. The resolution of the Fabry Perot interferometer depends on the finesse of the instrument. The finesse of the instrument depends on the reflectivity and the parallelism of the mirrors and on diffraction losses. Therefore, precision alignment of the

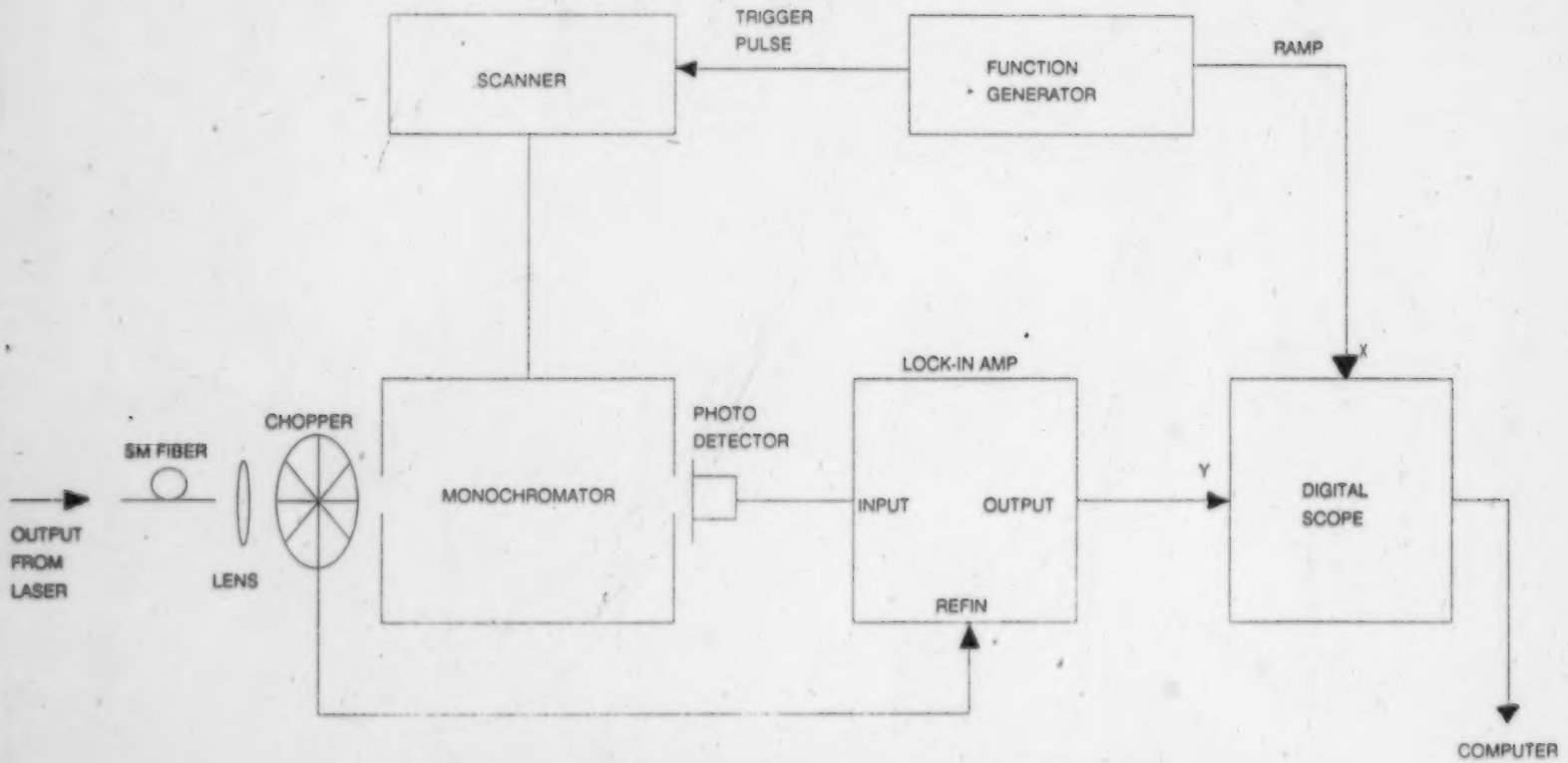

Fig. 3.6 Monochromator Set-Up for Direct Wavelength and Spectral Measurement

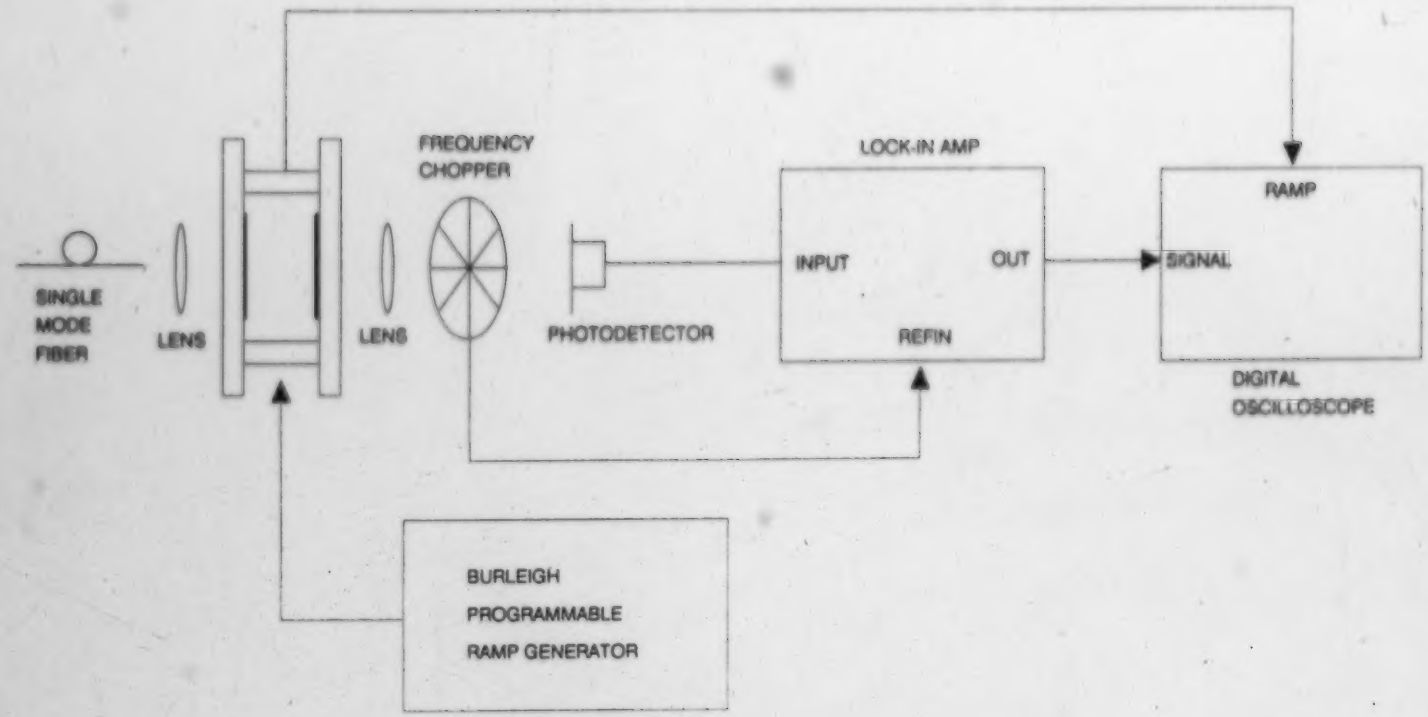

Fig. 3.7 Fabry-Perot Set-Up for High Resolution Spectral Measurement

optical elements is critical to obtain the best resolution. The resolution that can be achieved with a plane Fabry Perot interferometer is about 50 MHz.

The Fabry Perot scans were recorded by a digital oscilloscope and transferred to a computer to evaluate the linewidth. However, the linewidths obtained with the experimental configuration discussed in this chapter were very narrow and a more sensitive method had to be used to obtain an accurate measurement. For this purpose, the self-heterodyne method discussed in the next section was used.

3.2.2 SELF-HETERODYNE SET-UP

The self-heterodyne principle of measuring the linewidth is based on the principle that, when a laser oscillator output beam is divided and recombined after a time delay τ, and is then detected by an optical square law detector, the FM quantum noise in the laser light is converted to intensity fluctuation. The experimental set-up based on this principle [17] is shown in Figure 3.8. The light from the LD is divided into two branches using a 3 dB coupler. The light through branch 1 is passed through an acousto-optic modulator (Matsushita EFL-M 080 Y03) which causes an 80 MHz frequency shift of the first order deflected beam. The light through the second branch is delayed by time τ_d. For this experiment, approximately 700 metres of single mode fibre was used, and hence a delay of approximately 3.8 μsec was achieved. The light from these branches is mixed in a photodetector.

The power spectrum of the output of the photodetector is given by [17]:

$$S(f) = e^{-2\pi\delta f\tau_d}\,\delta(f) + \frac{\delta f}{\pi\{f^2 + (\delta f)^2\}}\left[1 - e^{-2\pi\delta f\tau_d} \times \left(\cos 2\pi\tau_d f + \left(\frac{\delta f}{f} + \frac{f}{\delta f}\right)\sin 2\pi f\tau_d\right)\right] \quad (3.1)$$

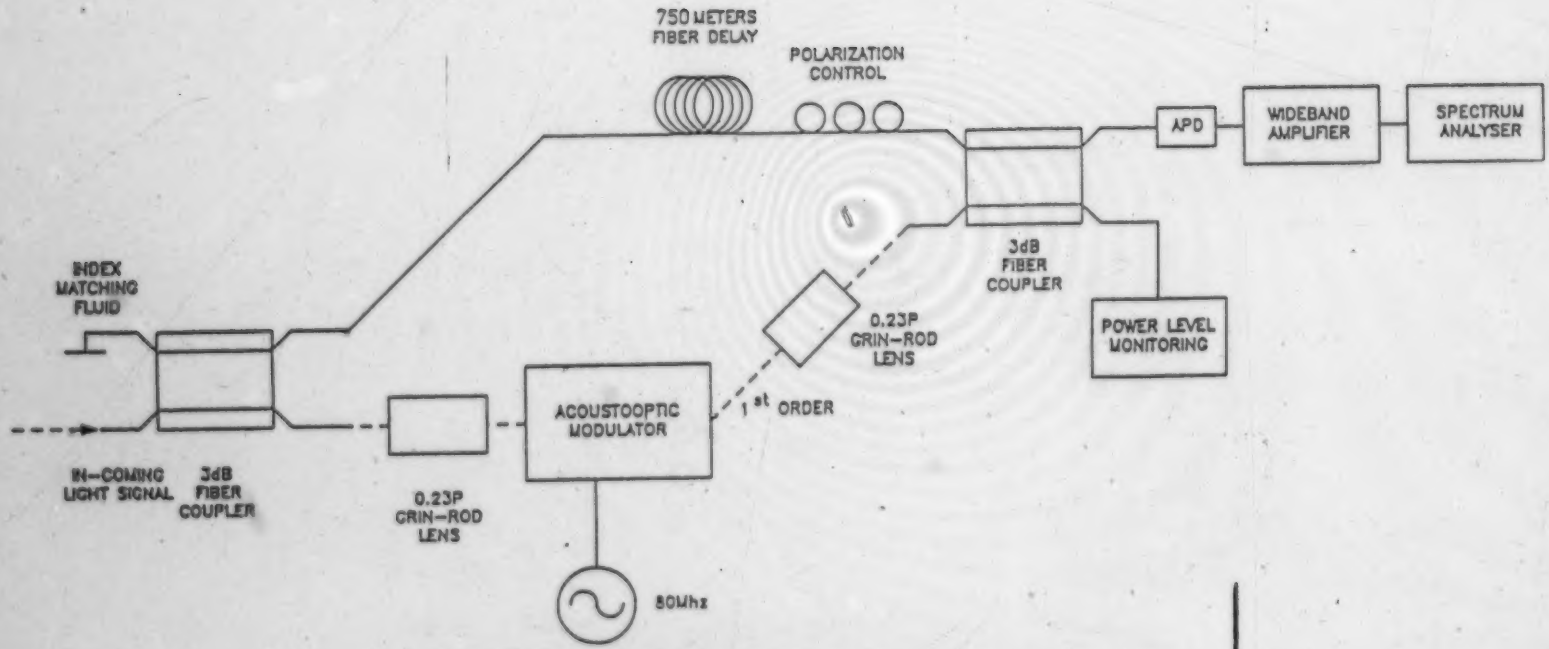

Fig. 3.8 The Self-Heterodyne Set-Up for Measuring Narrow Linewidth. Resolution of this Set-Up is about 250kHz [18]

where

δf = 3 dB spectral width of the IF spectrum.

When the delay time, τ_d is much less than the coherence time, $^1\Xi\delta f$, of the LD, the first term is dominant. For intermediate values of τ_d, the spectrum consists of two parts, the line spectrum due to the delta function part and the continuous portion due to the cosine term in Equation 3.1. When the delay time is much longer than the coherence time (that is $\tau_d >> 1/\delta f$) that is, the phases of the optical fields in the two branches have become totally decorrelated, the power spectrum is true Lorentzian and is given by [17]

$$S(f) = \frac{\delta f}{\pi (f^2 + (\delta f)^2)} \qquad (3.2)$$

The FWHM of the power spectrum is twice as large as that of the original spectrum, since both the paths contain equal FM quantum noise and therefore, the spectral resolution (Δ) of this method is given by [17]:

$$\Delta = 0.5/\tau_d \qquad (3.3)$$

The photodetector used in this set-up is a Germanium APD with an active area of approximately 0.001 mm^2 and responsitivity of 0.8 A/W (gain, M=1) at 1.3 μm.

The output from the spectrum analyzer was transferred to a computer for further analysis to determine the linewidth. When $\tau_d < 1/\delta f$, then in most cases, a best fit curve to the experimental results using Equation 3.1 can be

obtained to determine the linewidth. This will be explained in further detail when the linewidth measurements are discussed in Chapter 6.

3.3 SUMMARY

In this chapter the overall configuration of the external cavity laser has been discussed. It cannot be stressed enough that all the elements in the external cavity must be aligned with extreme precision. For example, during the alignment of the set-up in the laboratory, it was noticed that the positioning of the collimating lens with respect to the laser, was very critical to the amount of reflected light that can be coupled into the laser cavity, thereby determining the domain of feedback (strong or medium level).

Variations in the optical cavity length due to thermal effects can perturb the nearby external cavity modes. It is therefore recommended that the entire external cavity be enclosed in a plexiglass housing which is designed to be reasonably air-tight. This will provide a great deal of acoustic and thermal isolation. It should be noted that for the present experiment stability measures such as these were not undertaken since access was required to all the components in the cavity. Now that the relative position of the various components has been determined and the cavity is characterised to a certain degree, these measures could be implemented.

CHAPTER 4

SINGLE-MODE EXTERNAL CAVITY LASER

The solitary LD without external feedback has a multi-longitudinal mode spectrum with modes spaced approximately 0.8 nm apart, as shown in Figure 3.4. The purpose of optical feedback from the external cavity is two fold:

(1) to obtain a stable single longitudinal mode oscillation

(2) to obtain a narrow spectral linewidth (i.e, highly coherent source)

To achieve these objectives the LD was coupled strongly to an external cavity loaded with a diffraction grating. In this configuration the external cavity is the dominant cavity since the mode selection of the Fabry-Perot cavity (solitary LD) is partly destroyed by AR coating one of its facets. The experimental set-up is shown in Figure 3.1 and discussed in detail in that chapter. In this chapter, the single longitudinal-mode oscillation of the external cavity is discussed. The grating response is calculated to determine the selectivity provided by the grating. The effect of optical feedback on the threshold condition of the laser is also discussed. In the last part of the chapter, the experimental results for the single mode oscillation of the external cavity laser and the tuning range measurements, are presented.

4.1 THE DIFFRACTION GRATING (FILTER) RESPONSE

The diffraction grating in a grating tuned external cavity LD can be viewed as a "reflection filter" with a certain reflection band Δf. The centre

frequency of this band is a variable controlled by the angle of the grating. In this band, there could be a number of possible solutions to the external-cavity resonance condition. This number (N) is dependent on the length of the external cavity L and is given by:

$$N = (2L/c)\cdot\Delta f$$

The reflection band (Δf) of the grating can be accurately determined by solving the boundary value problem for diffraction of the electromagnetic waves by a periodic boundary, taking into consideration the direction, polarization and amplitudes for the various waves. This is covered extensively in Reference [19]. For the purpose of this thesis, it sufficient to determine (Δf) from a scalar aspect of diffraction having to do with the image-forming characteristics of the diffracted waves, when they are limited in size by gratings of finite width. Therefore, the formula used for the calculation of (Δf) of the grating filter is:

$$\Delta\lambda = \lambda/(m\, N_{eff}) \qquad (4.1)$$

where

m = order of scattering

and $$N_{eff} = 2b/(a\cos\phi) \qquad (4.2)$$

where

a = grating constant

ϕ = incident angle

$2b$ = spot size of the incident beam

In this experiment, the first order diffracted beam was fed back into the laser cavity and therefore, m = 1. From the manufacturer's data, the grating constant, 'a' = (1200 lines/mm)$^{-1}$. The incident angle, ϕ, can be determined from the grating equation because the incident angle and the first-order beam are collinear. This is shown in Figure 4.1. The grating equation is given as follows [20]:

$$2a\sin(\theta_m) = m\lambda \qquad (4.3)$$

and for λ = 1300nm, the incident angle $\theta = 50°$.

The spot size of the beam incident on the grating is determined using the following formula and assuming a gaussian beam. [21]

$$[w(z)]^2 = w_o^2 [1 + (\lambda z/\pi w_o^2 n)^2] \qquad (4.4)$$

where:

w_o	=	minimum spot size at z = 0 (spot size of the source)
z	=	distance between source and lens
n	=	refractive index of the medium of propagation

and w(z) is the distance at which the field amplitude is down by a factor 1/e compared to its value on the axis. Figure 4.2 shows these parameters graphically. The spot size w_o at the laser is given approximately by [20]:

$$w_o = \lambda/\pi(\tan\theta_{11}) \qquad (4.5)$$

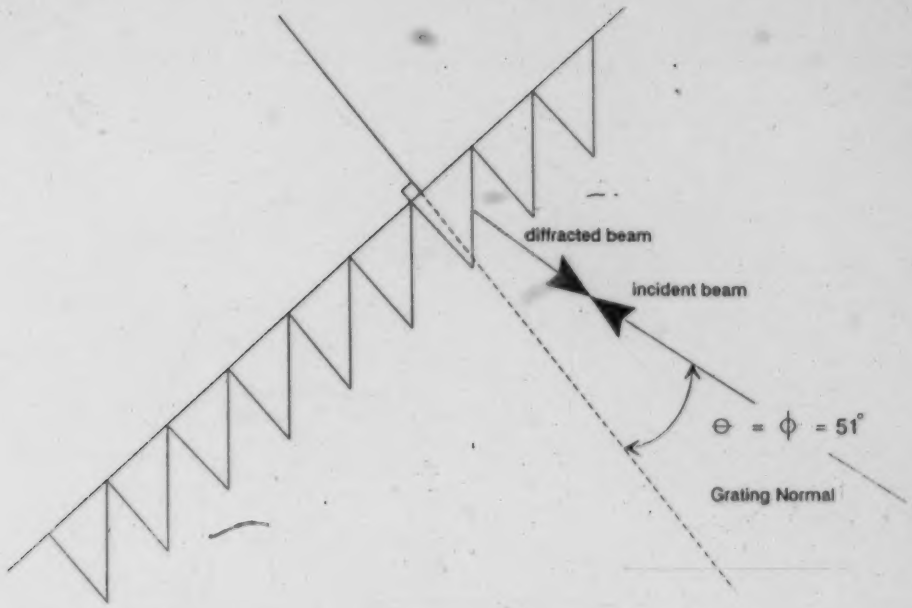

Fig. 4.1 Angular Placement of the Grating

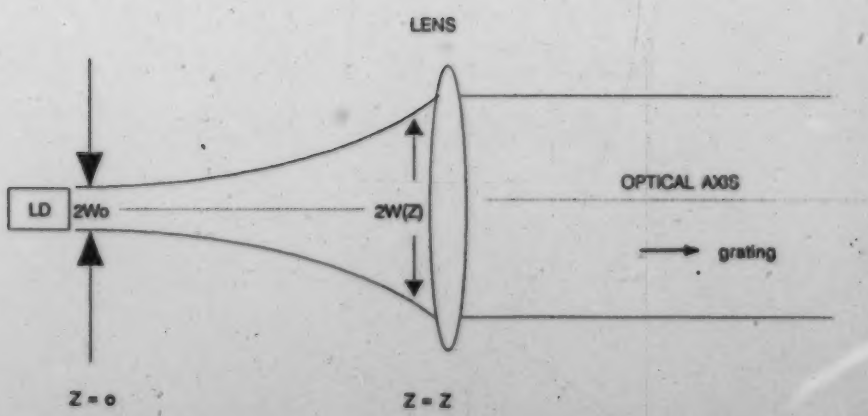

Fig. 4.2 Geometry for Determining the Spot Size of the Beam Incident on the Grating

where θ_{11} is the laser far field pattern divergence angle at 1/e of the field amplitude in the direction parallel to the junction (the data sheet obtained from the manufacturer showing the far field pattern is included in Appendix B, Figure B.4). The following values were used to determine w(z):

$\theta_{11} = 17.5°$

$\lambda = 1.3\ \mu m$

$w_o = 1.3124\ \mu m$

$z = 1.142$ cm (measured)

hence,

$w(z) \simeq 4$ mm $= 2b$ (of equation 4.2)

Now therefore, the FWHM of the grating response is determined by substituting the value for w(z) into Equation 4.2 and then Equation 4.2 into 4.1:

$\Delta\lambda = 1.3 \times 10^{-6} / [4 \times 1200/(\cos 51°)]$

$= 0.17$ nm

$\Delta f \simeq 30$ GHz

The grating response indicates that a band of frequencies (and not a single frequency) is reflected by the grating back onto the LD facet. The LD internal modes are about 140GHz apart. From this it can be concluded that, although the light is reflected in a band of frequencies, this band will not include the next internal mode, that is, only one LD internal mode will be selected at a given orientation of the grating. However, the band of frequencies reflected from the grating may involve several external cavity modes (depending on the length L of the external cavity). Therefore, some external cavity modes may acquire

enough gain (from spontaneous emission noise for example) for oscillation. However, the tendency of the laser would be to oscillate on a mode located at the peak of the grating response, since that mode would have the highest gain.

4.2 THRESHOLD CONDITION

A simple external cavity model with grating feedback is shown in Figure 4.3. The AR coated facet faces the diffraction grating which is placed a distance L away from the laser. The amplitude reflectivities are given by r_1, r_2 and $r_g(\omega)$ for the uncoated facet, the coated facet and the grating, respectively. In this model the coated facet and the grating reflectivity can be combined at the facet, so that the laser cavity can be modelled as having one facet with amplitude reflectivity r_1 (the uncoated facet) as before and the effective reflectivity, r_{eff} as the second facet. The effective reflectivity is given as follows [22]:

$$r_{eff} = \frac{r_2 + r_g(\omega)\exp(i\omega\tau_{ext})}{1 + r_2 r_g(\omega)\exp(i\omega\tau_{ext})} \qquad (4.6)$$

where:

r_2 = amplitude reflectivity of the coated facet

τ_{ext} = $2L/c$ (L = external cavity length, c = speed of light)

and $r_g(\omega)$ is given by:

$$r_g = r_o \exp\left(-(N_{eff}/4)^2 (\omega\zeta - 2\pi m)^2\right) \qquad (4.7)$$

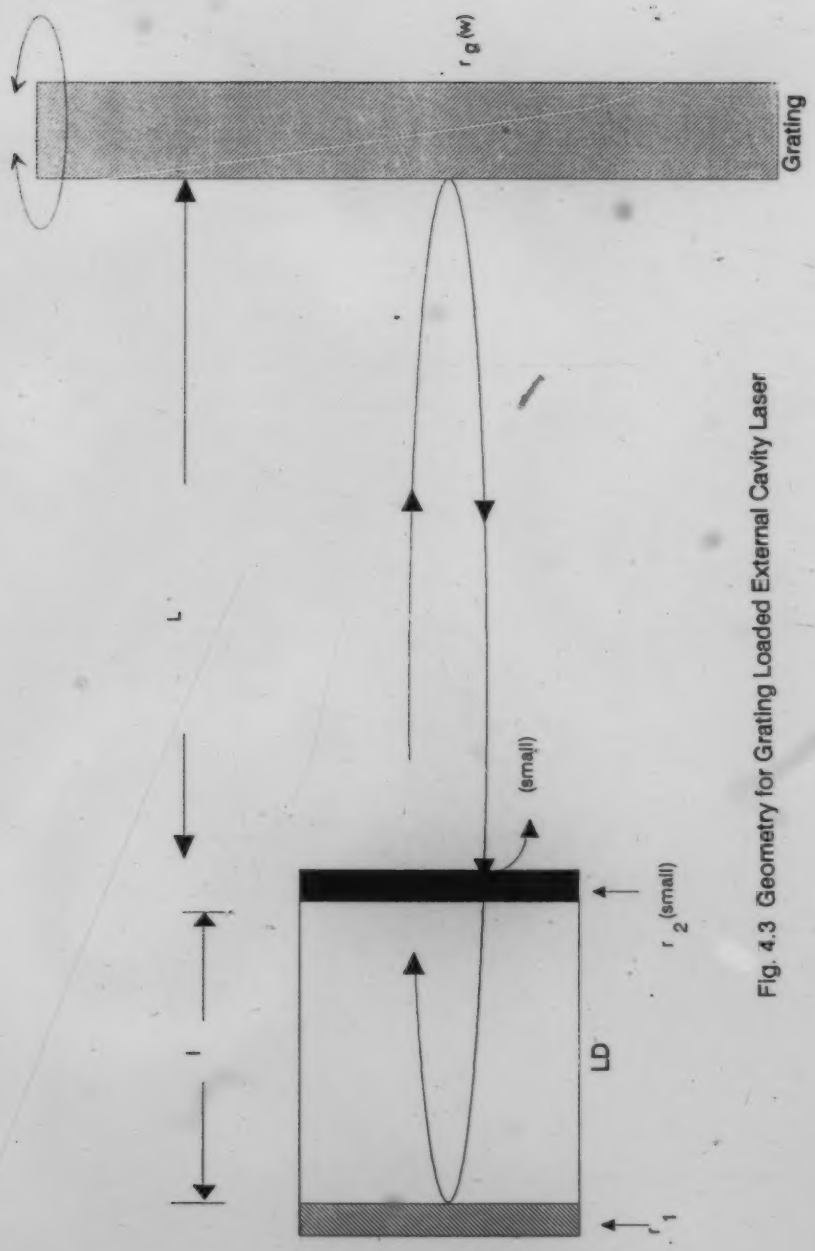

Fig. 4.3 Geometry for Grating Loaded External Cavity Laser

where:

m = order of scattering

r_o = amplitude reflectivity, including loss

$\varsigma = (2a \sin \phi)/c$

and N_{eff}, a, ϕ, 2b are as defined and calculated in the previous section.

The shape factor r_o is a slowly varying function of frequency and for the calculations here it will be assumed to be constant over the frequency range of concern. The power reflection coefficient R_o ($R_o = r_o^2$) (and $r_o \approx |reff|$ at the peak of the grating response) is the ratio of power actually coupled into the laser cavity to the power emitted from that facet and is commonly known as the feedback factor. All the coupling loss, lens transmission loss and grating reflectivity can be included in this factor. There are several methods commonly used for estimating the feedback factor. One of these methods will be presented here and r_{eff} thus calculated will be used for the rest of this thesis.

This method relies on the change in threshold current with reflectivity. By measuring the threshold current of the uncoated LD and the threshold current with feedback, the effective reflectivity or the feedback factor can be calculated. The ratio of the threshold current before coating the LD (I_{th1}), and the threshold current with feedback (I_{th2}) is given as follows:

$$\frac{I_{th1}}{I_{th2}} = \frac{\alpha \ell - \ln(r_1 r_2)}{\alpha \ell - \ln(r_1 r_{eff})} \qquad (4.8)$$

where α, ℓ, r_1, r_2 have their usual definition and r_{eff} is the amplitude reflection coefficient (feedback factor) at the peak of the grating response. From

Figure 4.4 which shows the experimental optical power versus current (L-I) plots with and without feedback, it is found that I_{th2} = 13.5mA. From manufacturer's data and at 17°C, I_{th1} = 11.4mA. Using the values given in Table 4 for r_1, r_2, α and ℓ and Equation 4.8, r_{eff} is found to be equal to 0.44, and therefore about 20% of the power emitted from the facet is coupled back into the laser cavity.

With the effective reflectivity given by Equation 4.6, the threshold gain condition of the external cavity laser can be written as (gain = losses, at threshold):

$$g_{th} = \alpha - (1/\ell) \ln (r_1 | r_{eff} |) \quad . \tag{4.9}$$

and the threshold current (I_{th}) is given by [13]:

$$g_{th} \cong \beta J_{th} = (\beta/\ell s) I_{th}$$

$$I_{th}(\omega) = (\ell s/\beta) (\alpha - (1/\ell) \ln (r_1 r_{eff}(\omega))) \tag{4.10}$$

where:
- α = internal loss coefficient
- β = device gain factor
- ℓ = length of laser cavity
- s = stripe width

With the assumption that at λ = 1284nm (the wavelength at which the plots of Figure 4.4 were measured) the external cavity laser operates at the peak of the grating response, $r_g = r_o$ in Equation 4.7. Using Equation 4.11 and the parameters listed in Table 4, and with r_{eff} ~ 0.44 (calculated above), the threshold current is found to be 13mA. From the (L-I) plots shown in

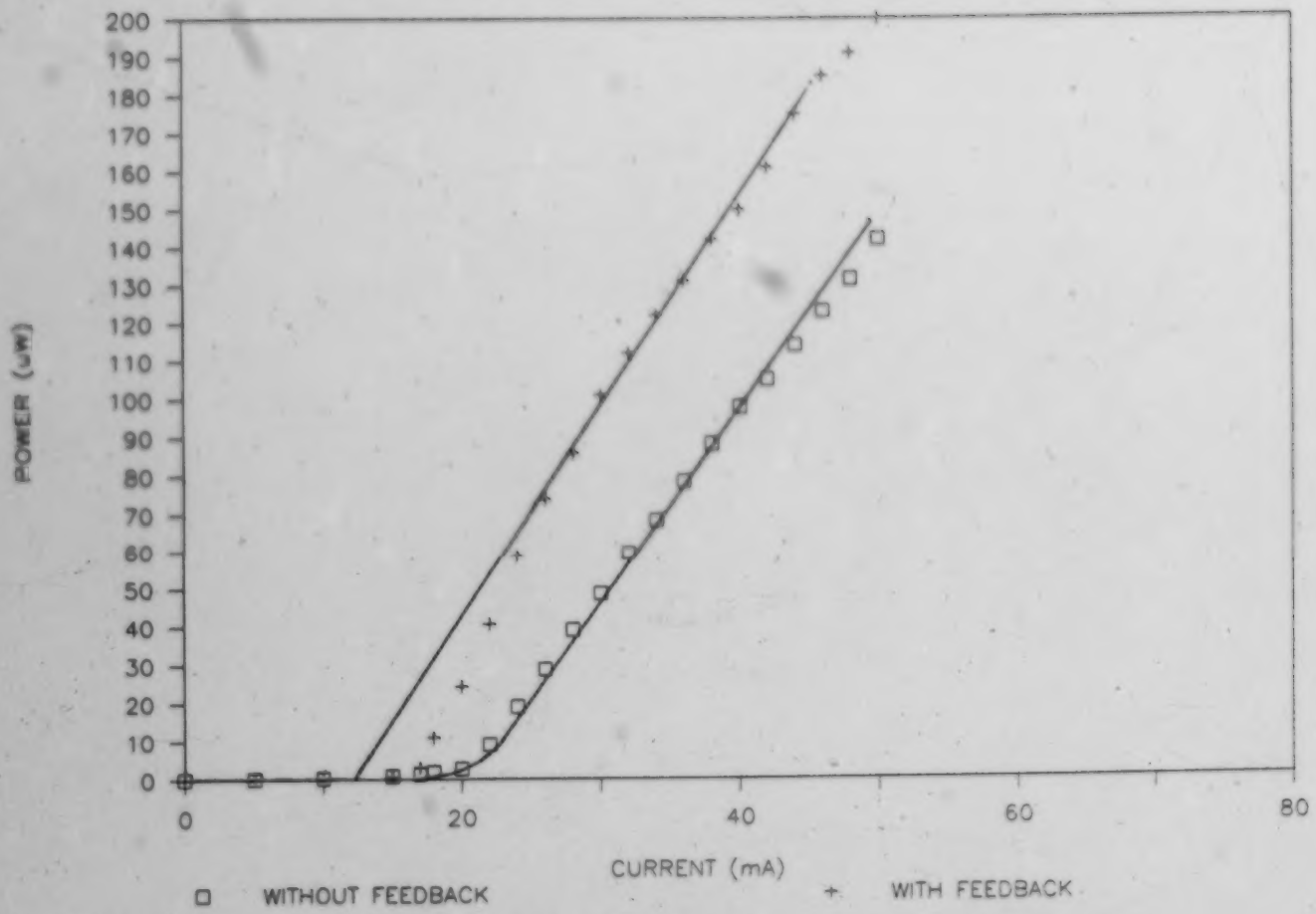

Fig. 4.4 Optical Power versus Current Plot with and without Feedback measured from a Fiber Coupled to the Uncoated Facet.
T = 17°C and λ = 1284nm

Figure 4.4, the threshold current of 13.5mA is obtained with grating feedback. The threshold current of the LD with external feedback is significantly reduced from the threshold current of the coated LD which is about 20mA in Figure 4.4. This is consistent with Equation 4.10 since r_{eff} is much larger than the reflecivity of the coated facet. The threshold current of the coated device without feedback cannot be accurately measured because with the low reflectivity of the coated facet, the threshold point is not very distinct.

4.3 DISCUSSION OF SINGLE MODE OSCILLATION

When a strong coherent beam is injected into the laser cavity, the mode favoured by the external cavity (the dominant cavity in the strong feedback configuration) will oscillate. This occurs due to a phenomenon called the "homogeneous spectral saturation of laser gain", which can be explained in the following manner:

The pump (injection or bias current in the case of a LD) establishes a population inversion (in the absence of feedback) of a certain value. In the presence of the optical field, more stimulated emission events are encouraged (that is, transitions from a higher energy level to a lower level), so that, a new population inversion density equilibrium, which is less than the previous one, is established. This reduction in the population inversion density equilibrium, which results in a reduction of the gain coefficient due to the presence of an electromagnetic field, is called "gain saturation". This process is depicted in Figure 4.5 where it is shown that the gain coefficient is reduced throughout the entire line profile when an atom gives up its internal energy to the stimulating field. Therefore, single mode oscillation is not critically dependent upon the frequency selectivity of the Fabry Perot laser, nor is it due to the wavelength

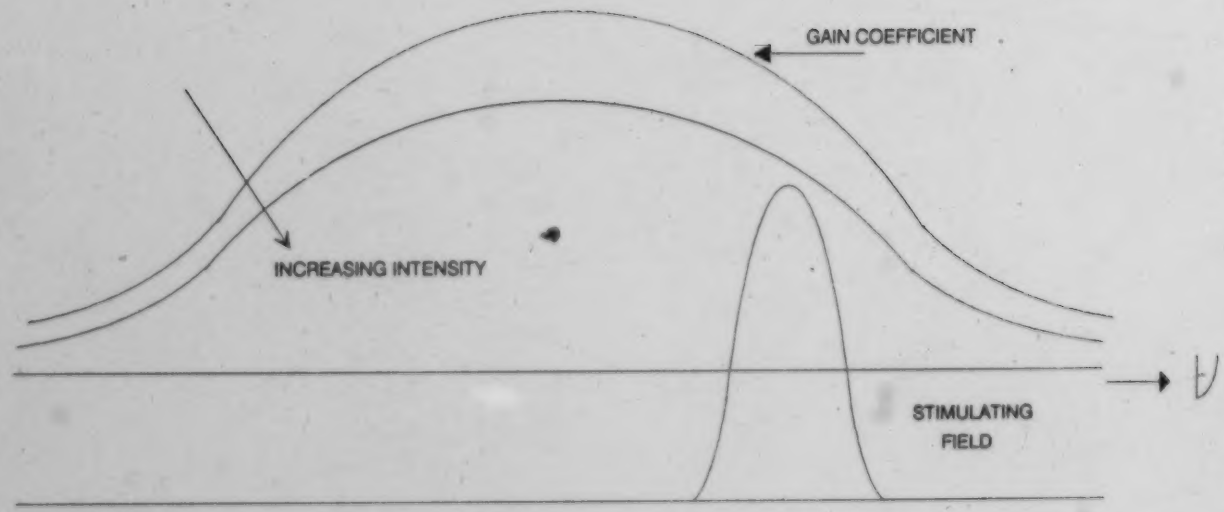

Fig. 4.5 Depiction of Homogeneous Saturation of Gain

selectivity provided by the grating. It occurs because one cavity mode acquires most gain from the energy stored in the population inversion and depletes all the carriers from the other cavity modes.

However, the grating is an important element of the cavity design. First, it provides wavelength selection and thereby limits the number of "possible solutions" of the external cavity modes (depending upon the FWHM of the grating response). Secondly, the use of a grating (frequency selective device) in the external cavity enables laser operation to occur at frequencies away from the frequency that satisfies the minimum threshold condition. The minimum threshold condition forces the laser to operate at a frequency where the external cavity phase ($\omega \times \tau_{external}$, where τ is the round trip time in the external cavity and ω is the operating frequency) is equal to an integral multiple of 2π. With grating feedback, the phase of the returned light is not critical because the internal mechanism of the laser cavity adjusts the overall gain (which is frequency dependent) to compensate for the phase mismatch. It was observed in the laboratory that there is a tendency for the external cavity laser to oscillate in a mode that maximizes the feedback. That is, the gain of the mode, enhanced by the injected carriers, will be further pulled towards a higher gain to compensate for the phase mismatch. It may be argued at this point that this frequency of oscillation would be the frequency where a minimum linewidth is obtained. The basis of this claim lies in the observations made in the laboratory. The grating angle was fine adjusted at a particular wavelength to obtain the maximum output power. This procedure always resulted in a narrower linewidth than the linewidth obtained without this optimization. This increase in power resulted from an increase in gain of that mode.

4.4 EXPERIMENTAL RESULTS FOR SINGE MODE OSCILLATION AND TUNING RANGE

Two of the most significant experimental results of the external cavity controlled LD are the obtaining of a single longitudinal mode oscillation and the wide range of wavelengths over which single mode oscillation may be obtained, called the tuning range. In the following two sections, results of the single mode oscillation and the tuning range measurements are given.

4.4.1 SIDE MODE SUPPRESSION RATIO

Figures 4.6 (a) and (b) show the spectrum of the external cavity LD at bias currents of 1.5 I_{th} and 2.3 I_{th}, respectively (where I_{th} is the threshold current of the laser with feedback). The spectral measurements were made with a scanning Fabry Perot interferometer with a free spectral range of 143 GHz.

The figure of merit for a single mode LD is determined by the power in the oscillating mode as compared to the power in the side modes. This figure of merit is called the side mode suppression ratio. Figure 4.7 shows the spectrum of the LD at 2.3 I_{th} on a vertically expanded scale (x100). On this expanded scale side modes are not evident; therefore, the side mode suppression ratio is greater than 20dB. This figure is within specification for single mode lasers available commercially. In order to verify that the side modes are not concealed, the cavity was misaligned slightly so that a side mode would appear. This is shown in Figure 4.8(a) on a thousand times vertically expanded scale. Figure 4.8(b) shows (again, x1000 vertical scale) that the side mode disappears when the cavity is brought into alignment. This indicates a side mode suppression ratio of better than 30 dB. It should be

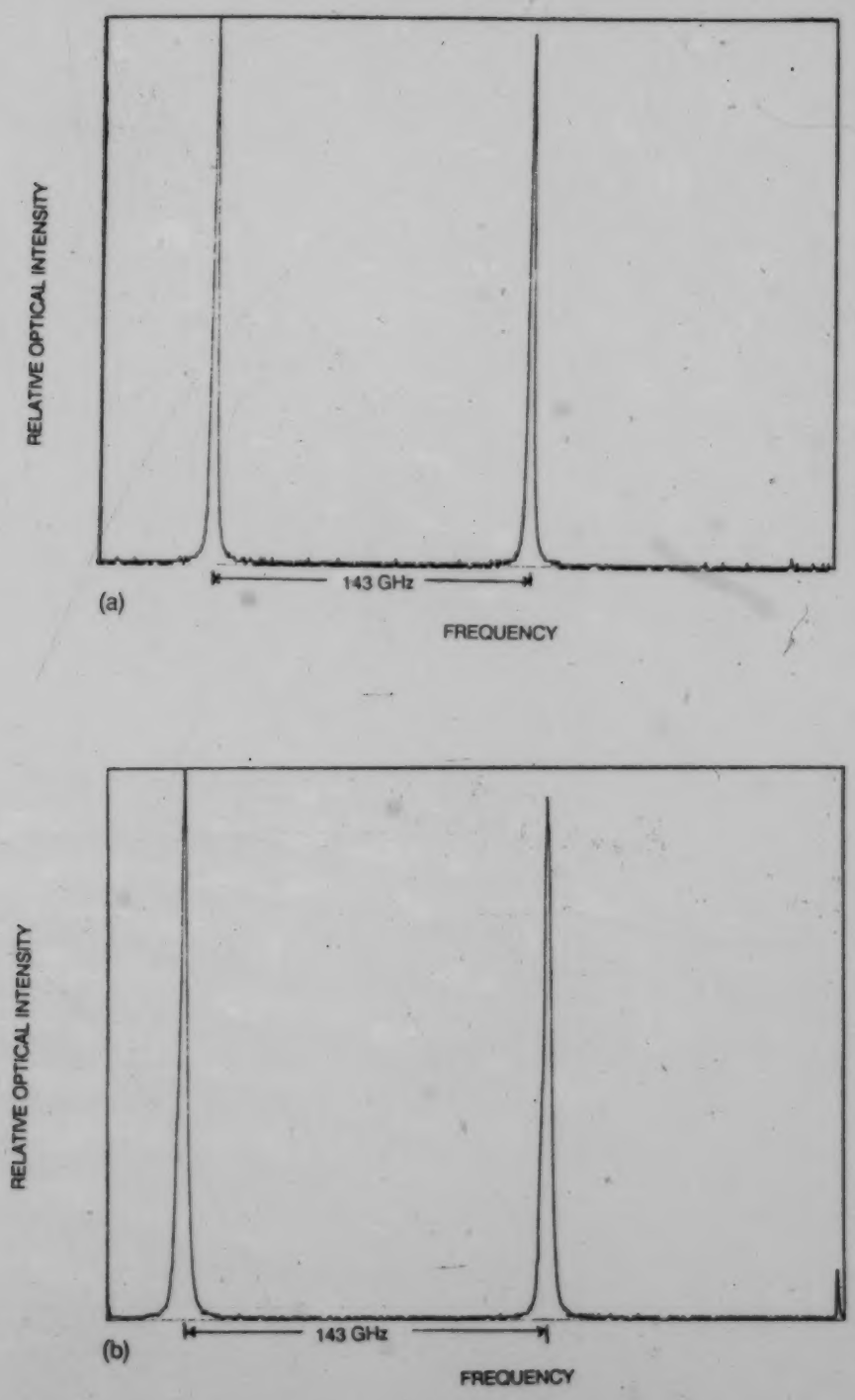

Fig. 4.6 Spectral Output of External Cavity Laser ,(Two Spectral Orders are displayed over One Ramp Period) (a) $I_{bias} = 1.5I_{th}$ (b) $I_{bias} = 2.3I_{th}$

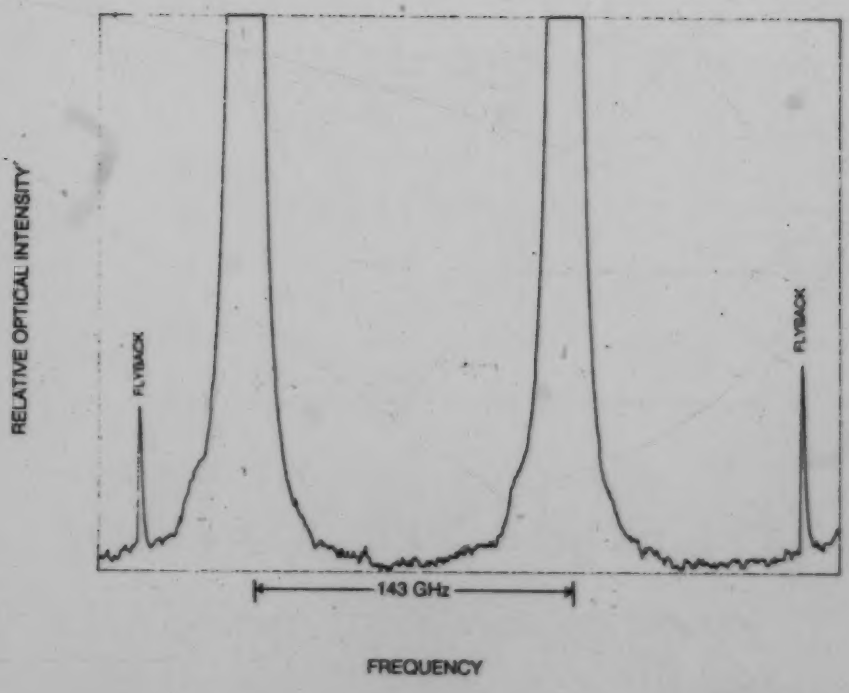

Fig. 4.7 Spectral Output of External Cavity Laser with $I_{bias} = 2.3 I_{th}$. Two Spectral Orders are shown over One Ramp Period. Enlarged 100times, as compared to Fig.4.6.

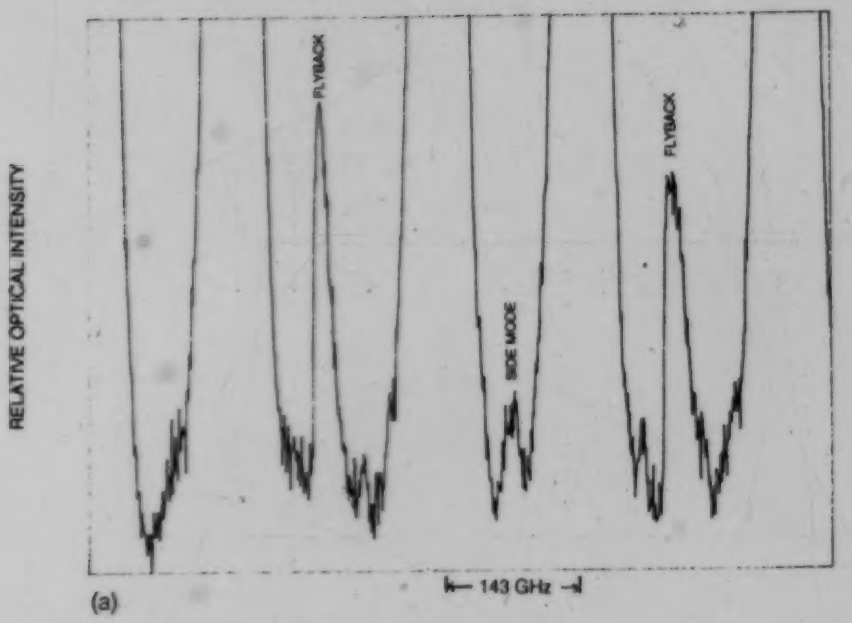

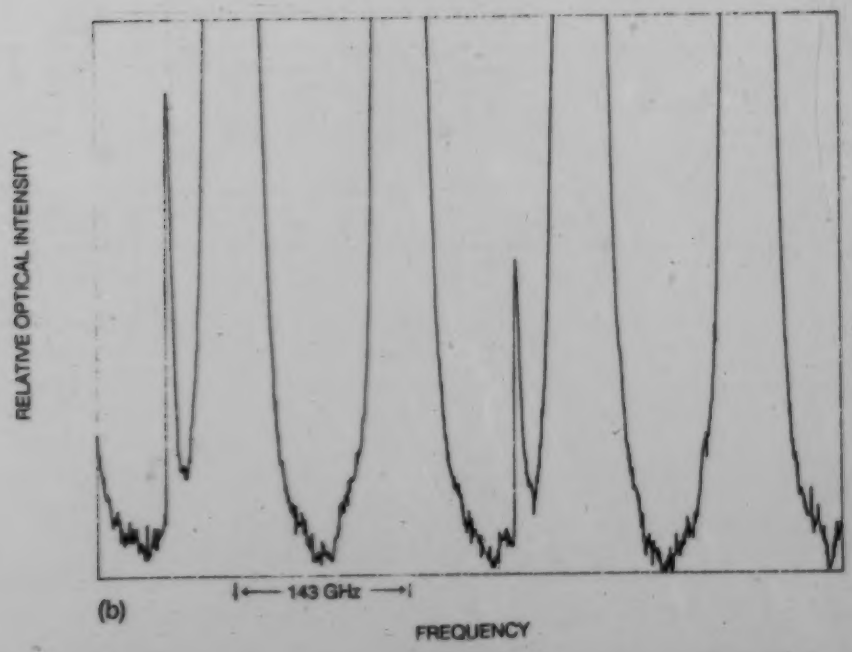

Fig. 4.8 Spectral Output of External Cavity Laser with $l_{cav} = 2.3l_{ch}$. Two Spectral Orders are shown over Two Ramp Periods. Enlarged 1000 times, as compared to Fig.4.6.
(a) slightly misaligned cavity to show where a side mode may develop.
(b) aligned cavity; side mode non-existent

noted that an accurate measurement of side mode level was limited by the noise level.

It was found experimentally that single mode oscillation did not critically depend on the length of the external cavity. It could be obtained for various cavity lengths, such as, 15, 18 and 21 cm.

4.4.2 TUNING RANGE MEASUREMENTS

The coarse tuning of the external cavity laser is accomplished by rotating the grating and selecting each of the longitudinal modes of the laser cavity. These modes still appear due to the non-ideal anti-reflection coating applied to the laser facet. The micrometer controlling the rotation of the grating produces a tilt angle of 6.6 arc-seconds per μm. If a piezoelectric drive is used, then a tilt angle of 0.07 arc-seconds per volt is obtained.

Figure 4.9 shows the wavelength tuning of the laser modes due to rotation of the grating. A tuning range of approximately 40 nm (7,000 GHz) was obtained in this manner. The spectrum is shown only for selected grating angles so as not to clutter the graph. It should be noted, however, that by rotating the grating, tuning of the laser in between the internal modes is also obtained; for example, at 1286, 1288.2 and 1288.5 nm, as shown on the graph. It can be surmised that since, a very low reflectivity of the coated facet was obtained, continuous tuning of the external cavity laser is possible. However, this should be investigated more closely before a definite claim can be made.

Tuning of the external cavity laser between the laser longitudinal modes can also be achieved by inserting an etalon in the cavity. This intra-cavity

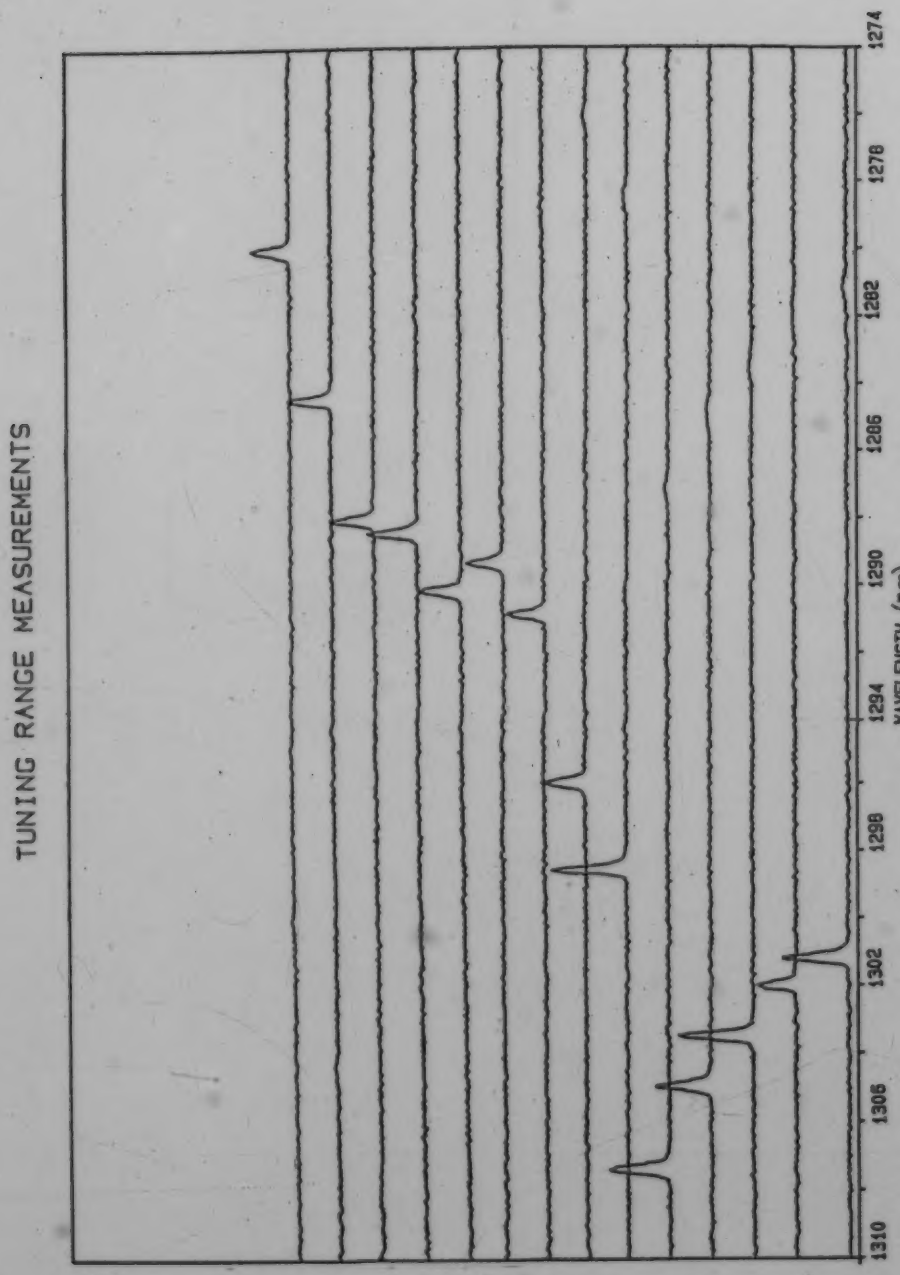

Fig. 4.9 Wavelength Tuning of Laser Modes obtained by rotation of the Grating

etalon serves two purposes. It will provide extra wavelength selectivity and hence, more stability of the oscillating mode. Secondly, by adjusting the etalon along with a fine adjustment of the grating, tuning in between the laser internal modes will be achieved. If a shift in laser oscillating frequency of a few megahertz (depending on the external cavity length) is desired, then the external cavity length can be adjusted. If the length is adjusted by half a wavelength, the frequency of the oscillating mode can be shifted by c/2L where c is the speed of light and L is the length of the external cavity.

4.5 SUMMARY

In this chapter the single mode oscillation of the external cavity LD was discussed. The solitary LD is a multi-longitudinal mode device, whereas the external cavity LD oscillates in a single longitudinal mode with a side mode suppression ratio of greater than 30dB.

The FWHM of the grating response was calculated to be approximately 30 GHz,which is narrow enough to ensure that only one internal cavity mode is selected. With the grating feedback, the threshold current of the LD was calculated to be 13 mA, and found experimentally to be 13.5 mA.

In the last section, the tuning range measurements were presented. It was found that the laser could be tuned over 40 nm (7,000 GHz) wavelength range by rotating the grating. Ideally, with this external cavity configuration, the laser emission can be continuously tuned over a very wide range of wavelength. The best result obtained so far by Wyatt et. al. [7] is a 55nm tuning range (i.e. 10,000 GHz) at 1.5 μm. The precision with which the cavity

is aligned and the quality of anti-reflection coating applied to the laser facet will eventually determine the continuous tunability of the laser emission.

CHAPTER 5

SPECTRAL LINEWIDTH OF EXTERNAL CAVITY CONTROLLED LASER

According to Tkach et. al. [11], there are five distinct regimes of feedback, depending on the fraction of light that is fed back into the laser cavity. In the first regime, with very low levels of feedback, line narrowing or broadening is observed depending on the phase of the returned light. In the second regime, mode hopping is observed for light returned out of phase with the laser field. In regime 3, which is a very narrow region with feedback levels of -45 dB to -39 dB, the laser operates in a single narrow line. However, with higher feedback levels, that is in regime 4, line broadening is observed; this phenomenon is known as "coherence collapse". In regime 5, where the feedback levels are higher than -10 dB, stable single narrow line oscillation is observed. This level of feedback is obtained only when the facet through which light is fed back into the laser cavity is AR coated. In this regime, the laser ideally operates in a long cavity with a short active region and the feedback dominates the field in the LD. The linewidth in this configuration is narrowed for all phases of returned light, and is generally insensitive to all other reflections.

5.1 SPECTRAL LINEWIDTH DISCUSSION

The basic reason for a finite spectral linewidth in a solitary LD is the phase fluctuation of the laser field induced by two independent processes,

namely:

(1) The phase change caused by continuing spontaneous emission events above threshold.

(2) The change of cavity resonant frequency due to the refractive index change caused by the carrier density fluctuation.

When the laser is operated in an extended cavity, the phase fluctuation due to spontaneous recombination is greatly reduced. This is seen from the following discussion: It is assumed first of all that the number of spontaneous photons emitted above threshold is fairly constant, whereas the number of stimulated photons continue to rise [23]. The photon lifetime for a solitary LD is given by:

$$\tau_{ph,s} = n\ell/[c(\alpha\ell - \ln\sqrt{(R_1R_2)})] \qquad (5.1)$$

where:

c = velocity of light

n = group refractive index

ℓ = length of laser cavity

α = internal absorption coefficient

R_1, R_2 = facet reflectivities

Equation 5.1 must be modified when the laser is operated with an external cavity due to the increased length. This equation becomes:

$$\tau_{ph,e} = (n\ell + L)/[c(\alpha\ell - \ln\sqrt{(R_1R_2)})] \qquad (5.2)$$

where:

L = length of external cavity

It can be seen from Equation 5.2 that, due to the essentially loss free propagation in the cavity of length L, the photon lifetime is considerably increased and thereby the spontaneous phase perturbation is significantly reduced, since the number of spontaneous photons is constant above threshold whereas the number of stimulated photons continues to rise. The effect of this increase in photon lifetime on the linewidth can be explained by a simplified argument as follows: In an ideal case, when the coupling between the two cavities (laser cavity and the external cavity) is accomplished without any loss or reflection, that is, when the AR coated facet has zero reflectivity, the linewidth ($\Delta\nu$) is proportional to the inverse square of photon lifetime[23].

$$\Delta\nu \quad \alpha \quad \left(\frac{1}{2\pi\tau_{ph}}\right)^2 \tag{5.3}$$

Therefore,

$$\frac{\Delta\nu_{EXCAV}}{\Delta\nu_{SOL}} \quad \alpha \quad \left(\frac{\tau_{Ph,s}}{\tau_{Ph,e}}\right)^2 \tag{5.4}$$

or, from Equations 5.1 and 5.2

$$\frac{\Delta\nu_{EXCAV}}{\Delta\nu_{SOL}} \quad \alpha \quad \frac{1}{(1 + L/n\ell)^2} \tag{5.5}$$

Equation 5.5 shows that the line is narrowed by a factor which is the square of 1 plus the ratio of the optical lengths of the two cavities. This ratio can also be viewed as the ratio of the length of time the photon spends in the external cavity and in the laser cavity.

However, there is one drawback with the above argument, namely the assumption of zero reflectivity of the coated facet. In a practical situation, $R_2=0$, does not occur, so there is a residual reflectivity that has be be considered. For this case, the passive external feedback can be described by a complex frequency dependent field reflection coefficient at the AR coated facet. This reflection coefficient is given by Equation 4.6. Having residual facet reflectivity is not a disadvantage in all cases. In a case where there is strong feedback with no frequency selective device such as a diffraction grating in the external cavity, the laser operates at the minimum threshold point, that is, the external cavity phase (ω x τ where ω is the operating frequency and τ is the external cavity round trip time) is an integral multiple of 2π. Under these conditions, it is shown in Reference [24] that spectral linewidth increases with an increase in the residual reflectivity. However, if a frequency selective device is incorporated in the external cavity, then operation can occur away from the minimum threshold point (that is when the external cavity phase does not equal an integral multiple of 2π).

If the laser is operated at a point or frequency that is optimally detuned* then the non-zero residual reflectivity causes a substantial decrease in linewidth. This is shown to be the case in Reference [25]. Physically, this line narrowing can be explained as follows. If the external cavity becomes resonant, then the photon will make several round trips in the external cavity, thus increasing the effective length of the cavity and causing further narrowing of the linewidth. In other words, the increase in effective end-reflectivity of the active cavity with optical frequency, due to the external cavity being resonant, contributes significantly to linewidth reduction.

---

* detuning can be defined mathematically as ($\delta\omega/\Delta\omega$ x 360) where $\delta\omega$ = detuning from the internal cavity modes and $\Delta\omega$ = internal mode spacing.

Besides reducing the perturbation caused by spontaneously emitted photons, the external cavity laser decouples the oscillating laser frequency from the strong dependence on the refractive index fluctuations within the active cavity. The mode frequencies for the compound cavity are given as follows[23]:

$$f_q = qc/[2(n\ell + L)] \tag{5.6}$$

where:

q = mode number

ℓ = laser cavity length

L = external cavity length

n = refractive index

The derivative of f_q with respect to n is given by

$$\frac{\partial f_q}{\partial n} = \frac{-qc(2\ell)}{[2(n\ell + L)]^2} \tag{5.7}$$

and the relative changes in f_q due to refractive index fluctuation can be found by dividing

$$\frac{1}{f_q}\ \frac{\partial f_q}{\partial n} = -(1/n)(1+L/n\ell)^{-1} \tag{5.8}$$

As seen from Equation 5.8, the fluctuations in mode frequencies due to refractive index fluctuation are reduced by a factor of $(1 + L/n\ell)$.

In the above argument it was seen that, by increasing the length of the cavity, narrower linewidths can be obtained. The increase in cavity length enables more energy to be stored in the cavity, thereby obtaining higher Q (quality factor) values. By coupling the laser efficiently to a high Q cavity,

narrower linewidths are obtained. However, with very long cavity lengths, mechanical perturbations such as acoustic and thermal variation within the external cavity can cause frequency drifts.

5.2 THEORETICAL CALCULATION OF LINEWIDTH

In this section, an attempt will be made to estimate the linewidth theoretically. It should be understood that certain factors such as α, (the linewidth enhancement factor) and the percentage of power coupled into the active cavity can only be estimated. When the actual numbers are assigned to these parameters, a justification for such assignment will be given.

Several different formulas for the calculation of the linewidth of an external cavity laser in a strong frequency-selective feedback configuration have been proposed, examples of which are given in References 22-23, 26-27. However, for this thesis, the formula given in Reference [24], and proven to fit experimental results in Reference [25], will be used. Thus, the linewidth of an external cavity laser with strong frequency selective feedback is given by [24]:

$$\Delta\nu = E_{cv} WF' (1 + \alpha^2) / 4\pi P \qquad (5.9)$$

where:

E_{cv} is the spontaneous emission rate into the mode, given by[24]

$$E_{cv} = n_{sp} v_g (\alpha\ell - \ln (\sqrt{R_1}\,|r(\omega)|) \qquad (5.10)$$

W represents the ratio of the output power P to the photon number in the laser cavity, given by:

$$W = \frac{v_g h\nu}{\ell} \ln\{(\sqrt{R_1}\,|r(\omega)|)^{-1}\}\{1 + \frac{\sqrt{R_1}}{|r(\omega)|}\frac{1-|r(\omega)|^2}{1-R_1}\}^{-1} \qquad (5.11)$$

F' in Equation 5.9 represents the effect of the external cavity parameters such as the angle of the grating, the length of the cavity, and the reflectivity of the grating. F' is given by [24]:

$$F' = [1 + \frac{1}{\tau_{in}} \mathrm{Re}\{j\frac{1}{r(\omega)}\frac{dr(\omega)}{d\omega}\} - \frac{\alpha'}{\tau_{in}} \mathrm{Im}\{j\frac{1}{r(\omega)}\frac{dr(\omega)}{d\omega}\}]^{-2} \qquad (5.12)$$

All the various symbols used in Equation 5.9, 5.10 and 5.11 are defined as follows:

α' = linewidth enhancement factor

P = power emitted from the uncoated facet (R_1 in this case)

n_{sp} = spontaneous emission factor

v_g = group velocity

α = internal laser cavity loss coefficient

ℓ = laser cavity length

R_1 = reflectivity of the uncoated facet

h = Plank's constant

ν = lasing frequency ($\omega/2\pi$)

τ_{in} = round trip time of laser resonator ($2\ell/v_g$)

$r(\omega)$ is the same as r_{eff} given by Equation 4.6, which is repeated here for convenience.

$$r(\omega) = \frac{r_2 + r_o \exp(-(N_{eff}/r)^2 (\omega\zeta - 2\pi)^2) \exp(i\omega\tau_{ext})}{1 + r_2 r_o \exp(-(N_{eff}/r)^2 (\omega\zeta - 2\pi)^2) \exp(i\omega\tau_{ext})} \qquad (5.13)$$

where:

r_o = grating reflectivity including the losses

and all other variables are as defined earlier for Equation 4.6.

In order to calculate the linewidth ($\Delta\nu$), a value for each of the parameters listed above has to be either measured or estimated. The linewidth enhancement factor α' (which is defined as the ratio of the change in real and imaginary part of the refractive index) was chosen to be -5. There are several published values [28] for this factor and they vary in range from negative 3 to negative 8. This is a very difficult parameter to measure and agreement has not been obtained when different methods of measurement are used. The precise measurement of α', which in itself is a topic of study is outside the scope of this thesis; $\alpha' = -5$ has been used since this agrees well with the values published in Reference [28]. It should be noted that the behavior of a LD with an external cavity will depend on the value of α'. A qualitative explanation will clarify this point. The light reflected back into the cavity lowers the threshold gain. This causes a reduction in carrier density and an increase in refractive index (due to the negative value of $d\mu/dn$ where μ is the group refractive index and n is the carrier density). This leads to a change in the phase relation between the laser light and the reflected light, hence determining the behavior of the LD in the extended cavity.

The spontaneous emission factor, n_{sp}, is taken to be 4.6 [29]. The power emitted from the uncoated facet, is about 3mW (from manufacturer's data sheet) at 2.3 I_{th} (all the measurements were made at this bias current;

36mA). v_g is c/4 where c is speed of light and 4 is the group index for InGaAsP lasers. α, the internal cavity loss coefficient and the ℓ, the length of the laser cavity, and the reflectivity R_1 of the uncoated facet is given in Table 4. For the effective reflectivity $r(\omega)$, the grating parameters such as N_{eff} and the grating constant, "a", have already been given in Chapter 4. Also, with the losses included, the reflection coefficient of the grating, r_o, is found, in Chapter 4, to be 0.45. A computer program (listed in Appendix C) is used to evaluate the linewidth using Equation 5.9. A further analysis was carried out to investigate the behaviour of linewidth with detuning from a certain wavelength corresponding to an internal cavity mode. The detuning is defined as the frequency deviation from a laser internal mode divided by the internal mode spacing.

$$\phi \text{ (detuning angle)} = \frac{\omega - \omega_o}{\Delta\omega} \times 360^\circ \qquad 5.14$$

where:

ω_o = frequency of a laser internal cavity mode

ω = operating frequency

$\Delta\omega$ = spacing of the internal cavity mode ($c/2n_g\ell$)

(n_g = group index, ℓ = length of laser cavity)

The results of the computations are shown in Figure 5.1 and 5.2. In Figure 5.1, the linewidth is plotted for several different wavelengths. It is seen that the average linewidth is about 3 kHz. In Figure 5.2 the linewidth has been plotted against detuning angle for the wavelength λ_o = 1298 nm. The minimum linewidth (at λ_o = 1298 nm) with optimum detuning is found to be 2.1 kHz. The optimum detuning angle is 110° which corresponds to an operating wavelength of 1298.2 nm. These results agree reasonably well with

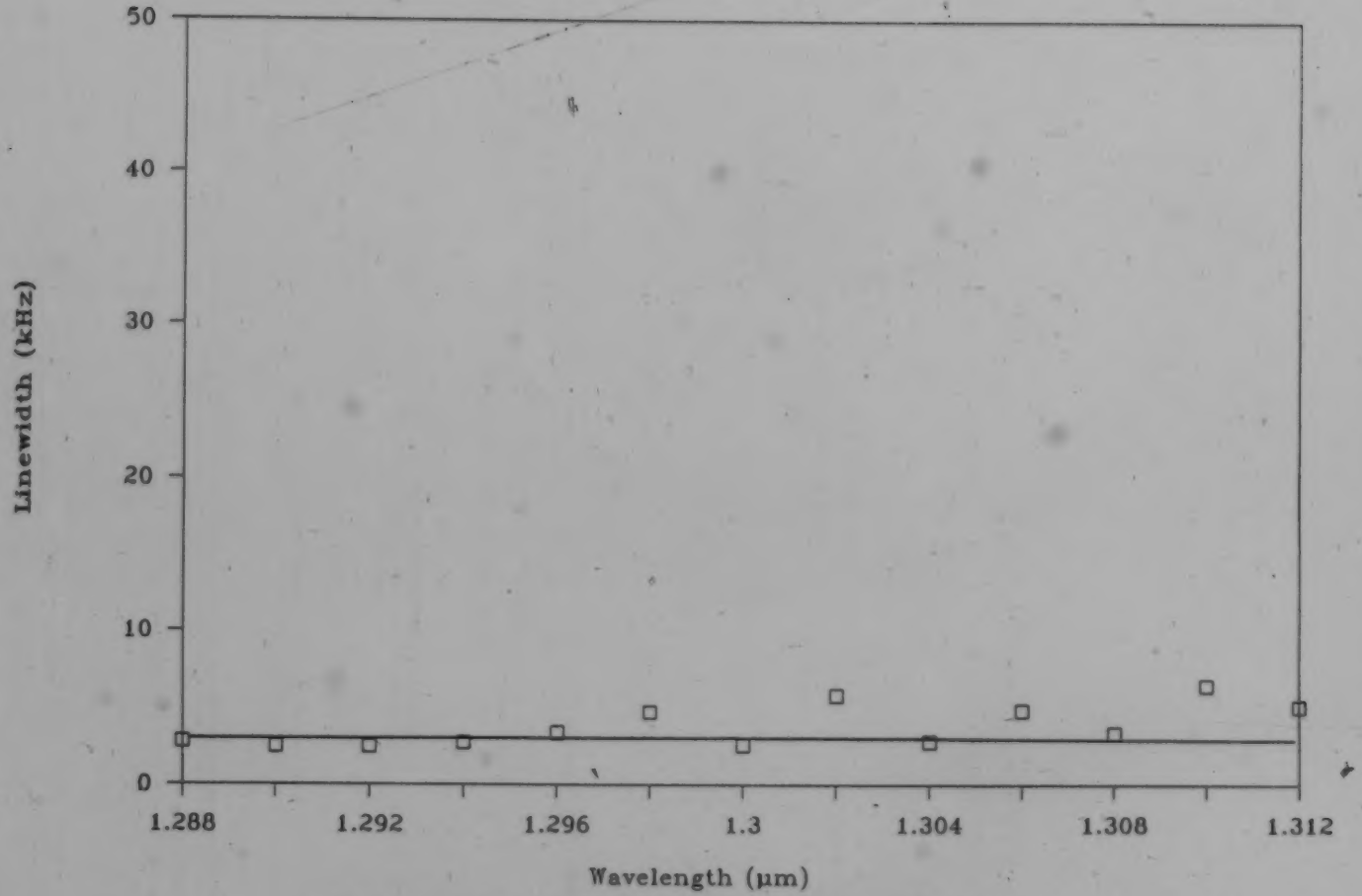

Fig. 5.1 Theoretical Calculation (Equation 5.9) of Linewidth of the External Cavity LD at various Wavelengths. Average Linewidth ~ 3 kHz

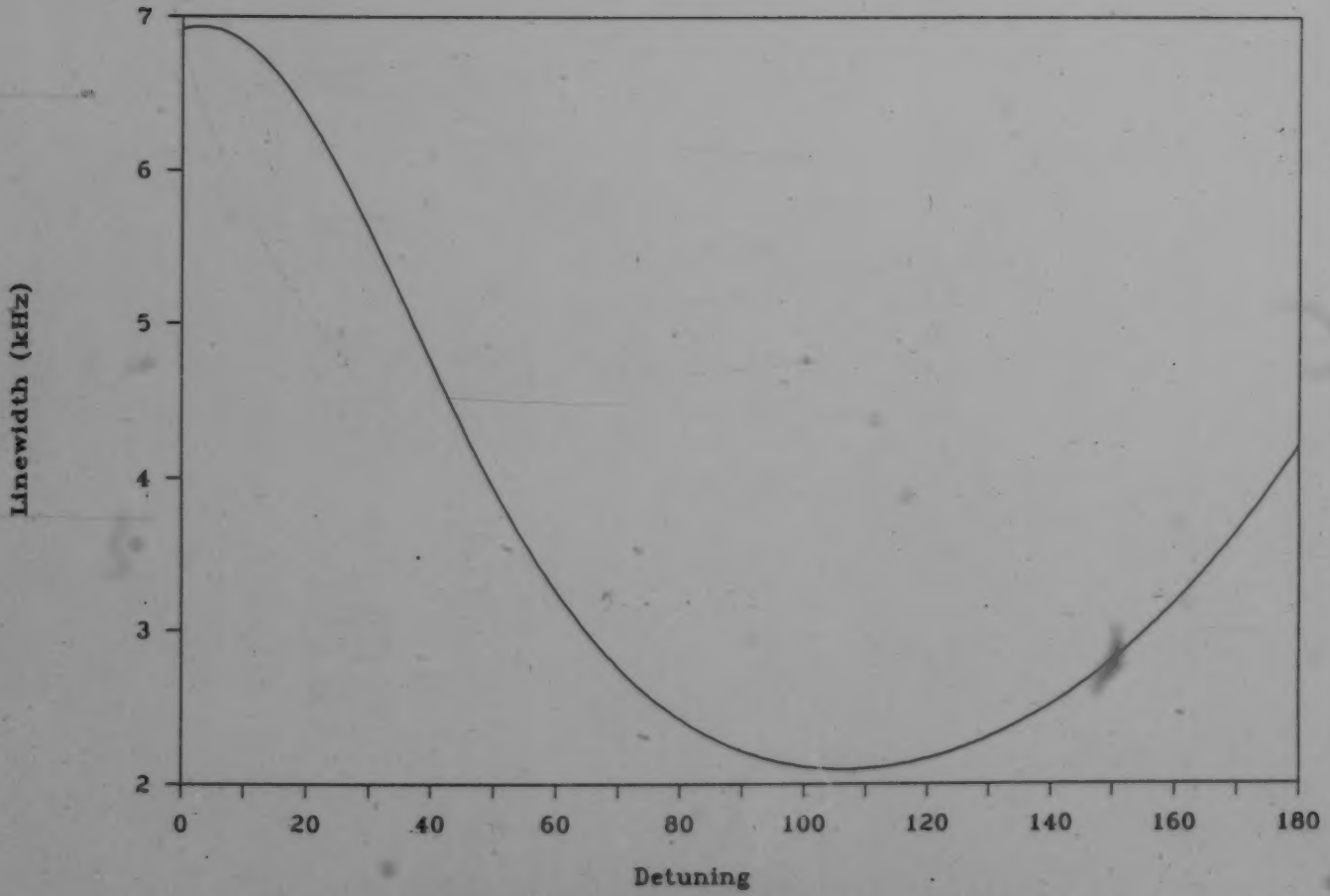

Fig. 5.2 Theoretical Calculation of Linewidth when the Oscillating Frequency is Detuned from the Internal Cavity Mode; λ = 1298 nm

those presented in Reference [25] which show that an appropriate detuning from the laser internal cavity mode resulted in a narrower linewidth.

5.3 EXPERIMENTAL RESULTS

The linewidth of the external cavity laser was measured using the self-heterodyne interferometric technique described in Chapter 3, Section 3.2.2. From Equation 3.1, it can be seen that, as the delay time (τ_d) increases (that is, with longer fiber length), the power shifts from the delta function peak to the Lorentzian pedestal, and finally when the delay time τ_d is much longer than the laser coherence time, the power spectrum is strictly Lorentzian, as indicated by Equation 3.2. This happens when the phases of the optical fields in the two branches of the self-heterodyne set-up are totally decorrelated.

Figure 5.3 shows the power spectrum obtained from the self-heterodyne set-up for the measurement of linewidth. The picture shows side lobes in the wings of the power spectrum. These are due to the exponential portion of the power spectrum formula of Equation 3.1. This occurs when the linewidth is less than the inverse of the delay time τ_d (which determines the resolution). Therefore, in this case, the approximate formula of Equation 3.2 is not valid and the exact formula of Equation 3.1 must be used since the delay line could not be extended. It is not practicable to increase the delay line for the measurements reported here because in order to measure a linewidth of 10 kHz, a fiber length of more than 36 km would be required [30]!

Therefore, Equation 3.1 must be used to perform the analysis on the experimentally acquired data for power spectrum at the output of the detector of the self-heterodyne set-up. By curve-fitting the pedestal portion of the power spectrum, an estimation of the linewidth can be obtained. Figure 5.4

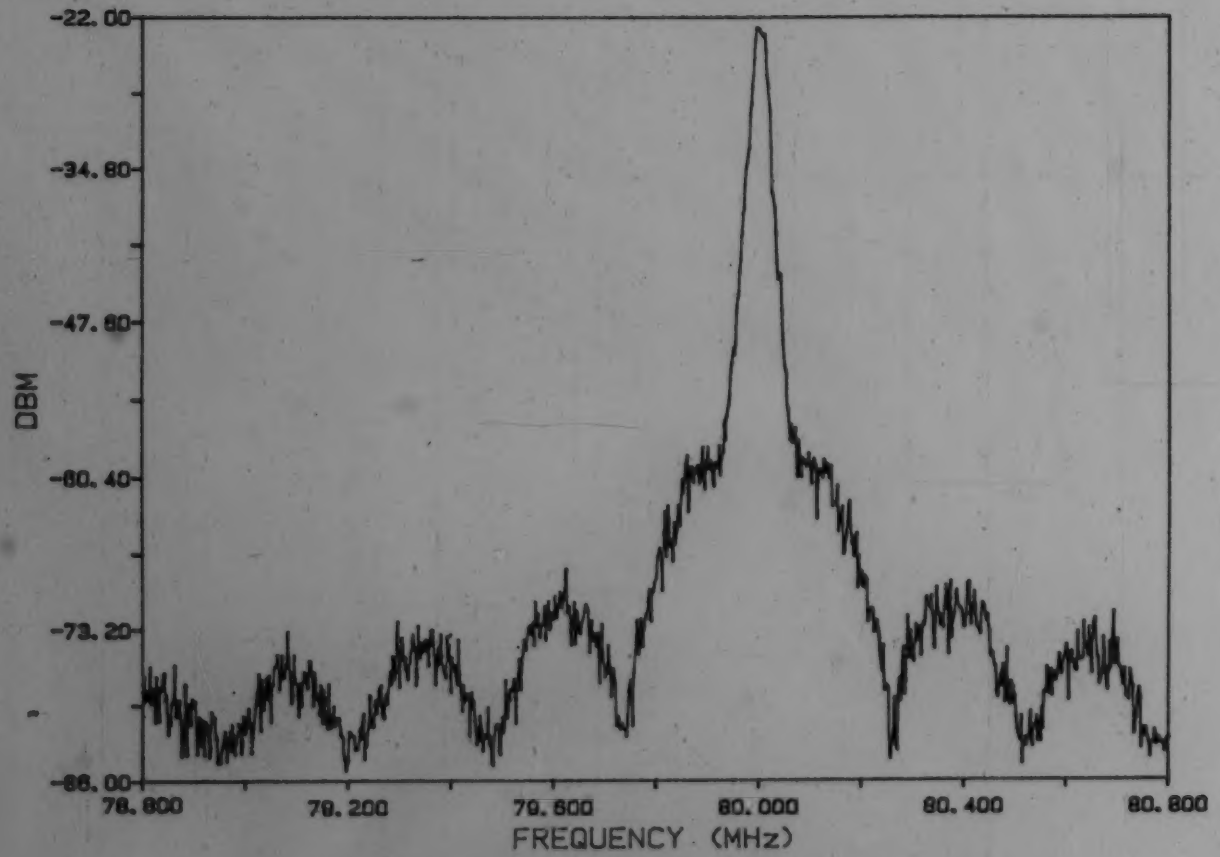

Fig. 5.3 Optical Power Spectrum for Linewidth Measurment using Delayed Self-Heteroydyne Technique. λ = 1289nm, $I_{bias} = 2.3I_{th}$

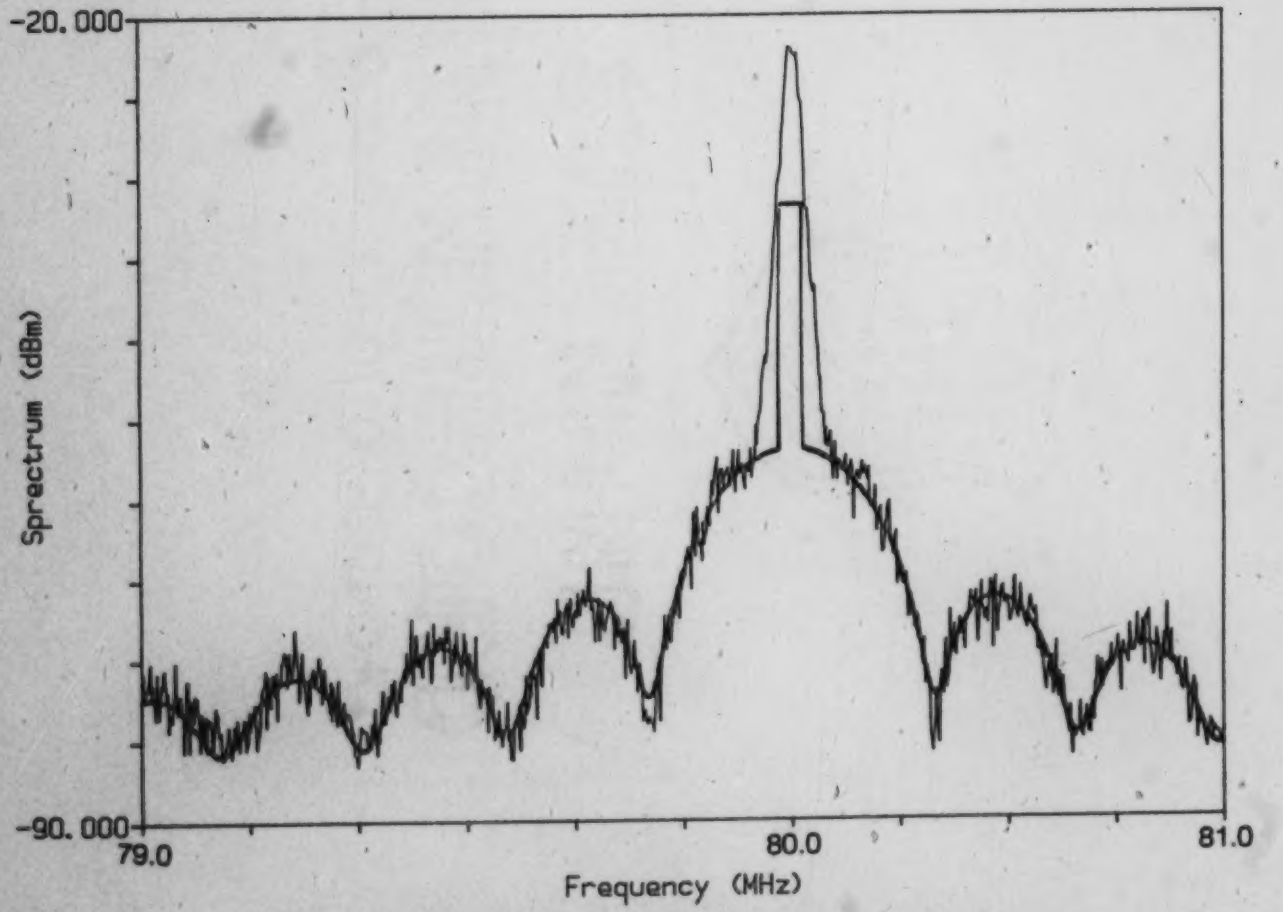

Fig. 5.4 Best Fit Curve for Experimental Results of Fig. 5.3. Fitting Parameters: τ_{fit} = 3.8μsec, fitting range: 78.8 - 79.8 MHz. Linewidth ($\Delta\nu$ = 4 kHz)

shows the results obtained from the self-heterodyne measurement with a fiber delay line of approximately 3.8 μsec and a curve fitted to the data. Using curve fitting over the frequency range 78.8 MHz to 79.8 MHz, a linewidth of 4 kHz was obtained. This estimate compares, within experimental and measurement error, to the theoretically obtained value of 3kHz at $\lambda \approx 1289$ nm (see Figure 5.1)

Similar measurements and curve fitting analyses were carried out at other wavelengths such as 1291 nm, 1296 nm, 1301 nm, 1303 nm, 1308 nm and 1312 nm. The data obtained from the self-heterodyne measurements and the curve fitting graphs are shown in Figures 5.5, 5.6, 5.7, 5.8, 5.9 and 5.10, respectively. A graph of linewidth versus wavelength is plotted in Figure 5.11. All the above measurements were carried out at a constant output power of 3 mW from the uncoated facet. The average linewidth obtained experimentally is about 9 kHz. It is desirable that the linewidth of the external cavity LD remain narrow and does not vary significantly over its wide tuning range. Linewidth measurements for a wider range of wavelengths was not done since these measurements would not have revealed any new information.

Another theoretical comparison to the experimental result can be obtained from the model proposed by Kazarinov et. al. [27]. They define the linewidth narrowing factor F as follows:

$$F = 1 + A + B \tag{5.15}$$

where they attribute A to be due to the increase in roundtrip time in the external cavity and B to the resonance caused in the external cavity due to residual facet reflectivity. The linewidth according to them, is then reduced by F^2. According to the model presented in [27] and calculations carried out in

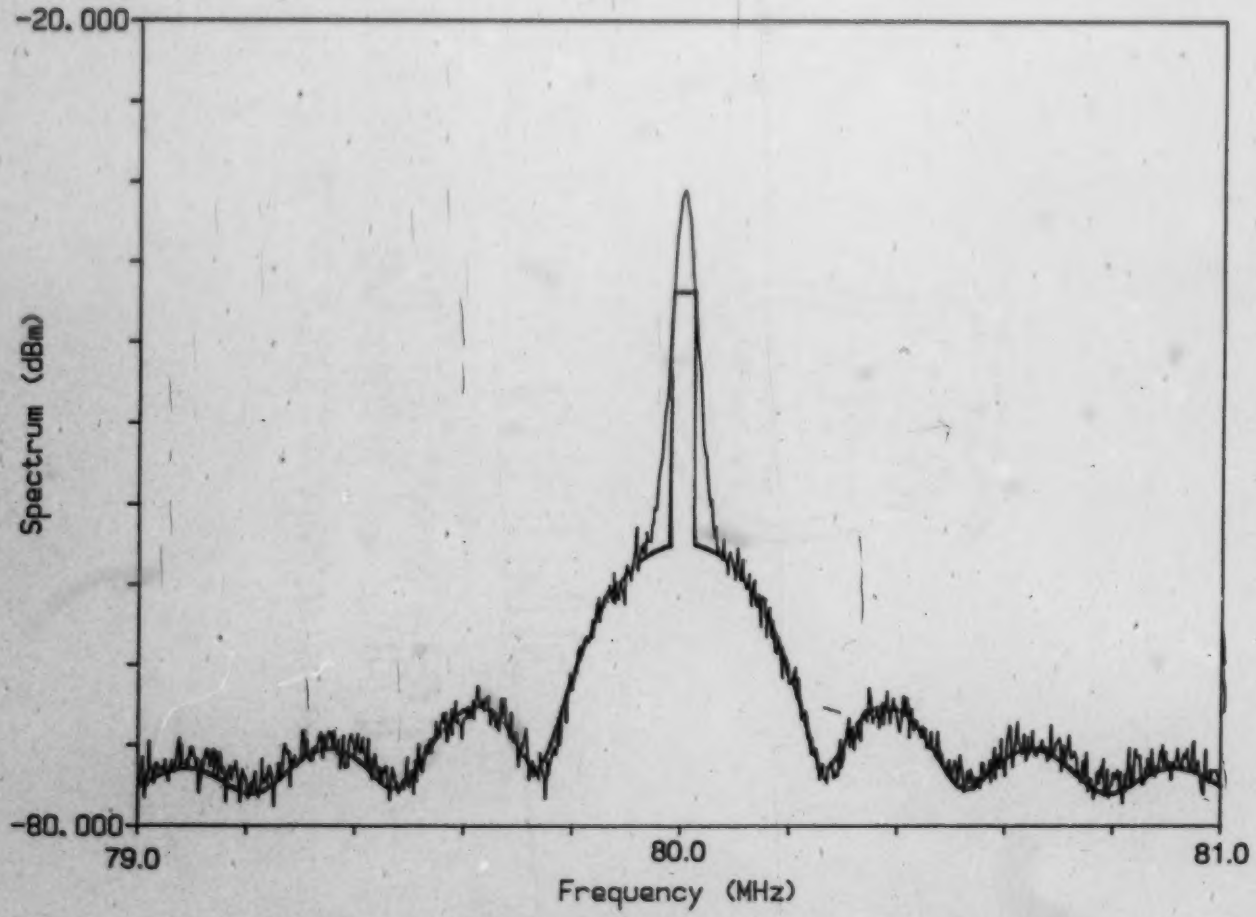

Fig. 5.5 Results of Linewidth Measurement and Best Fit Curve at λ = 1292nm, $I_{bias} = 2.3I_{th}$
Fitting Parameters: τ_{fit} = 3.8μsec, fitting range: 79.0 - 79.9 MHz. Linewidth ($\Delta\nu$ = 7 kHz)

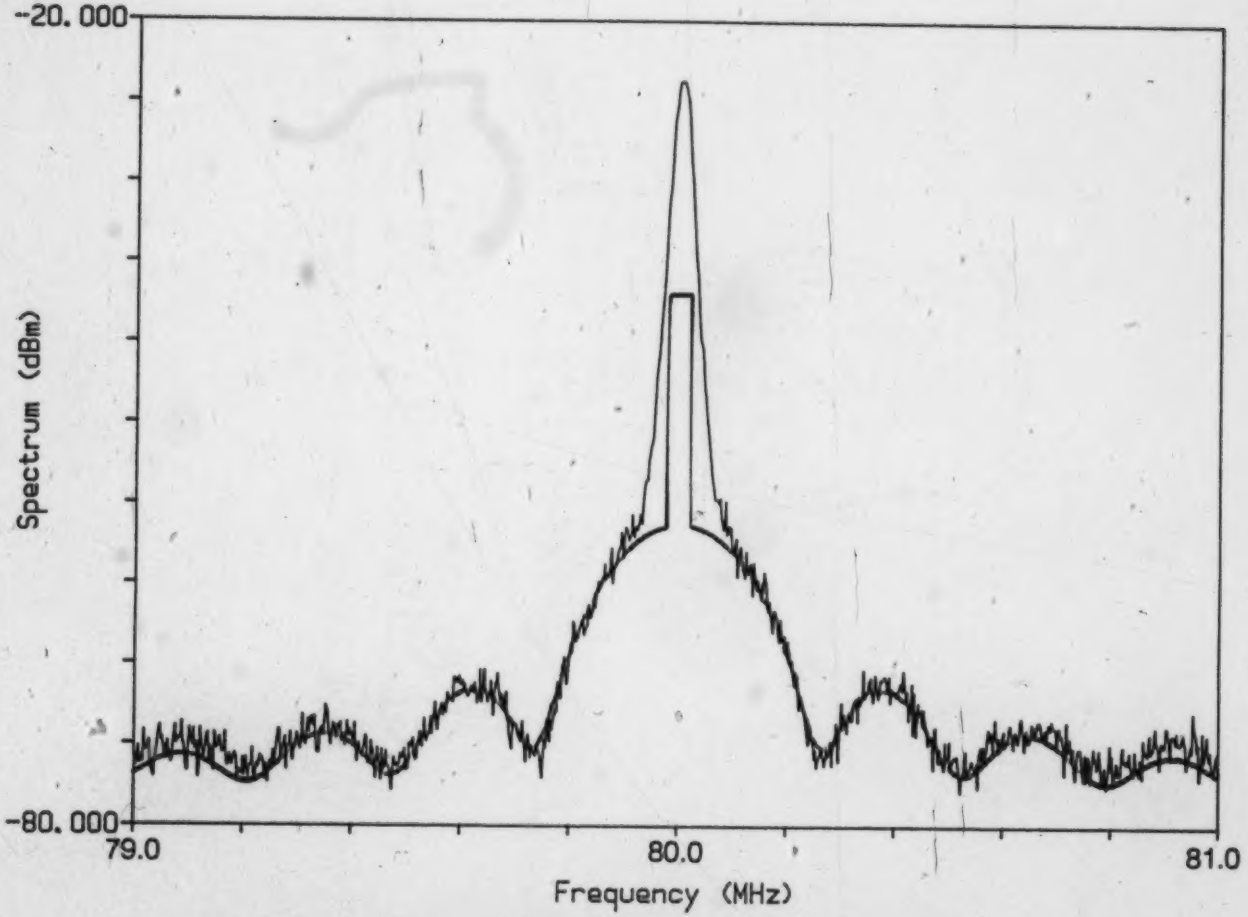

Fig. 5.6 Results of Linewidth Measurement and Best Fit Curve at λ = 1296nm, $I_{bias} = 2.3I_{th}$
Fitting Parameters: τ_{fit} = 3.8μsec, fitting range: 79.0 - 79.9 MHz. Linewidth ($\Delta\nu$ = 9 kHz)

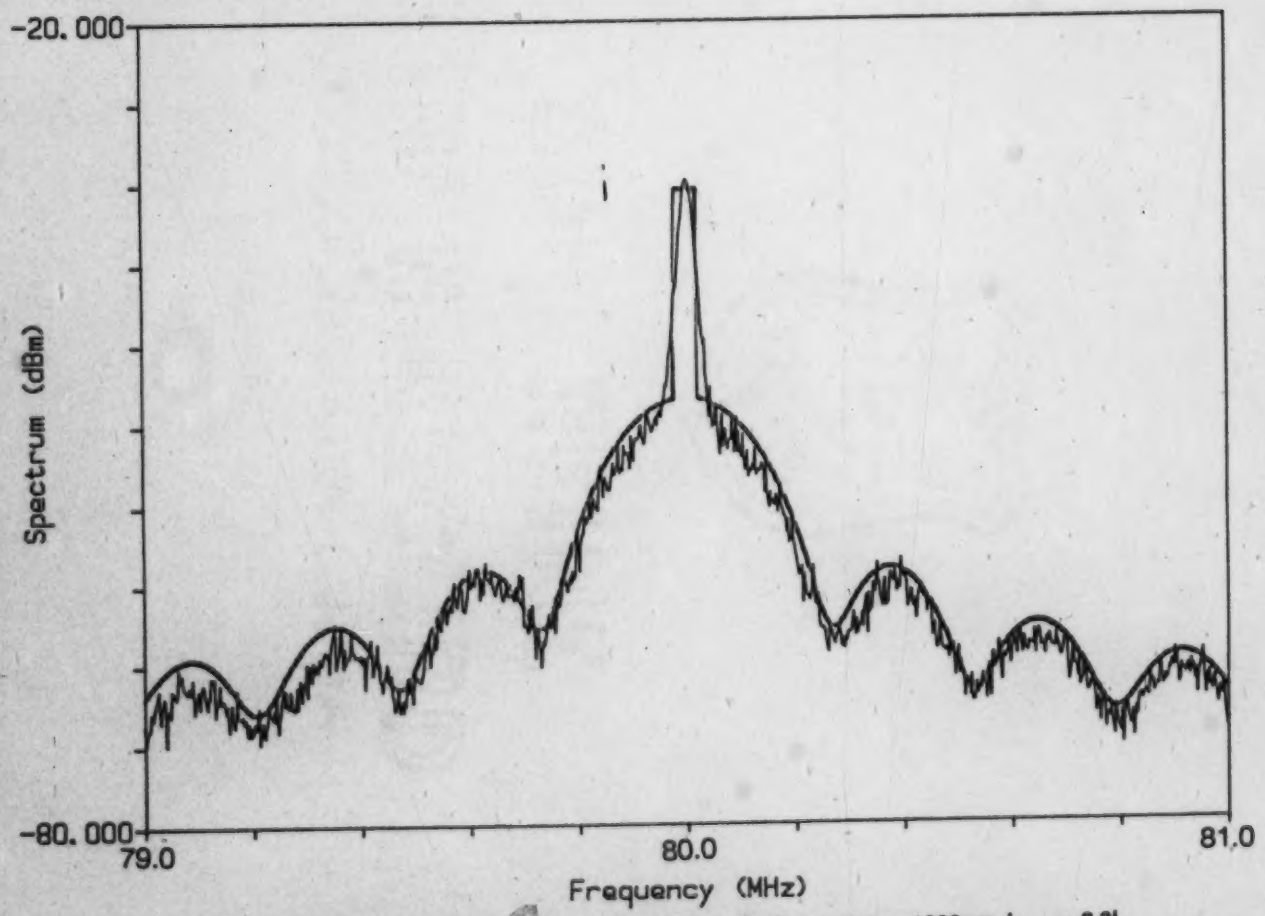

Fig. 5.7 Results of Linewidth Measurement and Best Fit Curve at λ = 1302nm, $I_{bias} = 2.3I_{th}$
Fitting Parameters: τ_{fit} = 3.8μsec, fitting range: 79.0 - 79.9 MHz. Linewidth ($\Delta\nu$ = 13 kHz)

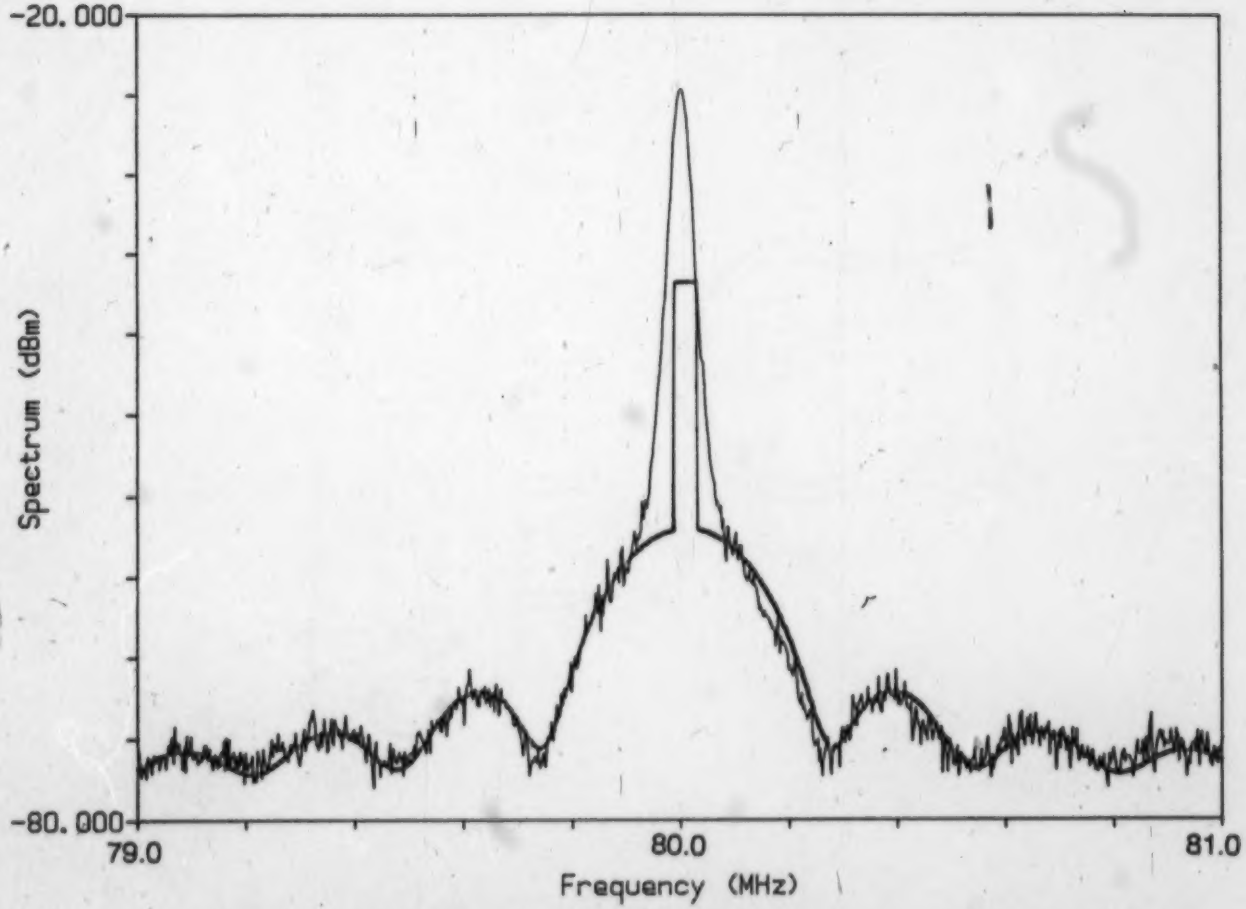

Fig. 5.8 Results of Linewidth Measurement and Best Fit Curve at λ = 1303nm, $I_{bias} = 2.3I_{th}$
Fitting Parameters: τ_{fit} = 3.8μsec, fitting range: 79.0 - 79.9 MHz. Linewidth ($\Delta\nu$ = 7.7 kHz)

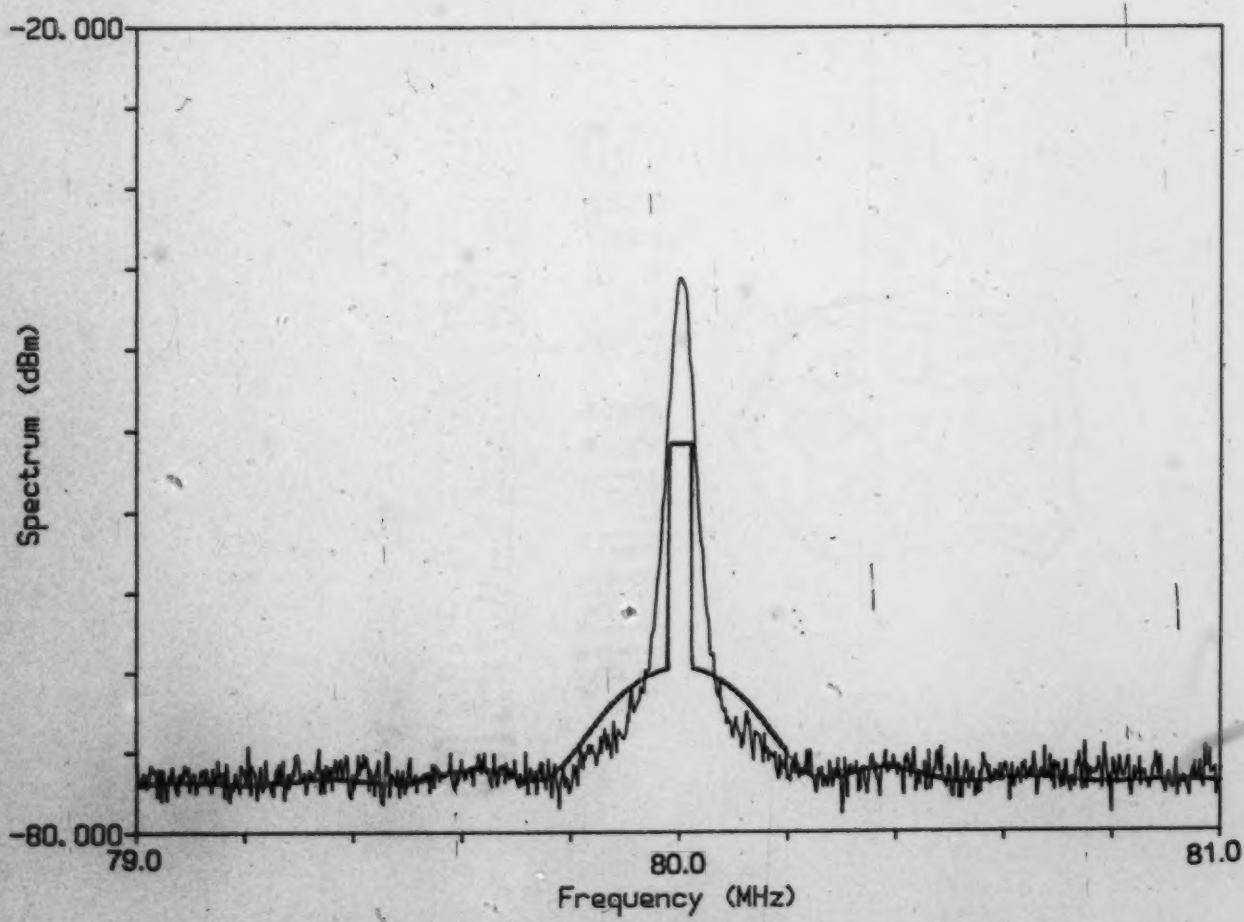

Fig. 5.9 Results of Linewidth Measurement and Best Fit Curve at λ = 1308nm, $I_{bias} = 2.3I_{th}$
Fitting Parameters: τ_{fit} = 3.8μsec, fitting range: 79.0 - 79.9 MHz. Linewidth ($\Delta\nu$ = 10 kHz)

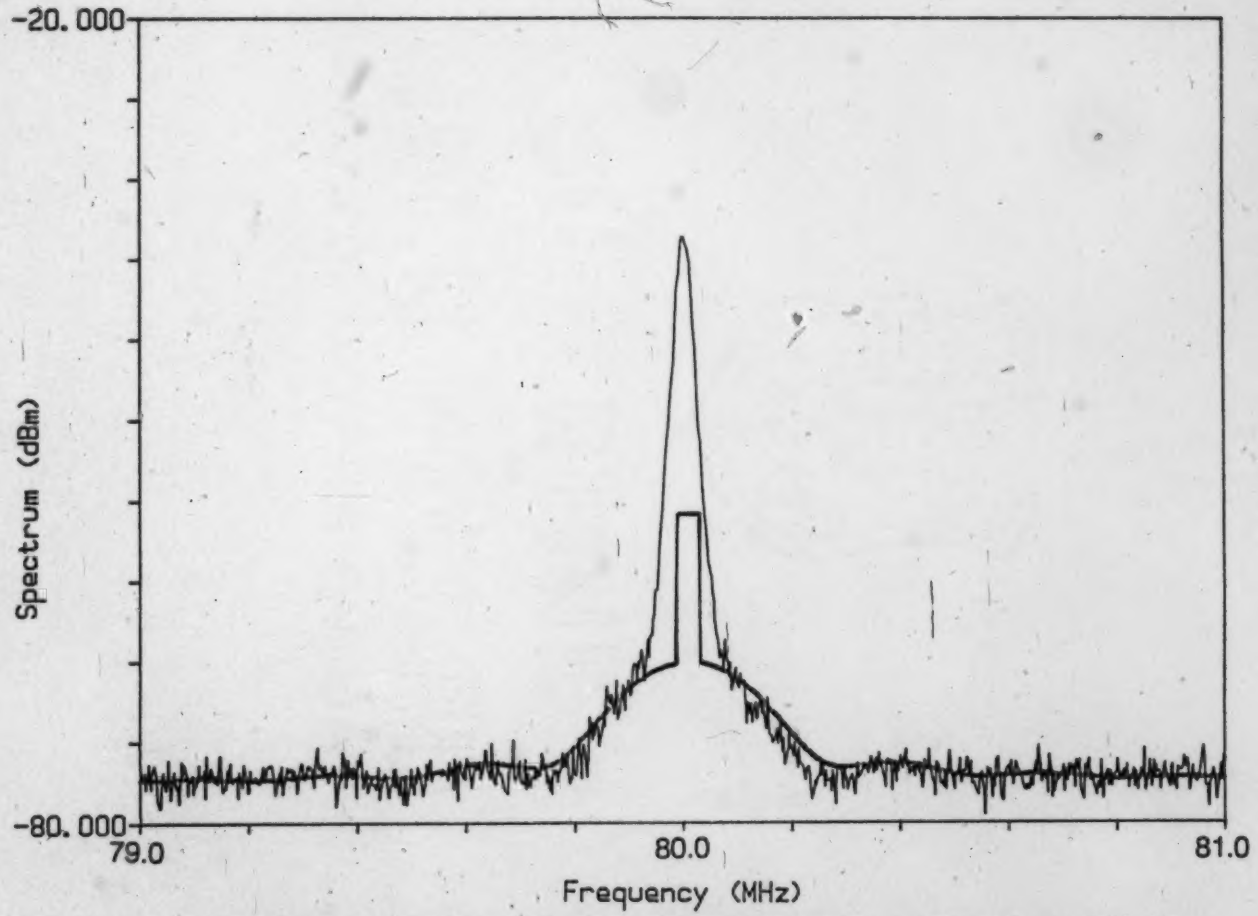

Fig. 5.10 Results of Linewidth Measurement and Best Fit Curve at λ = 1312nm, $I_{bias} = 2.3I_{th}$
Fitting Parameters: τ_{fit} = 3.8μsec, fitting range: 79.0 - 79.9 MHz. Linewidth ($\Delta\nu$ = 30 kHz)

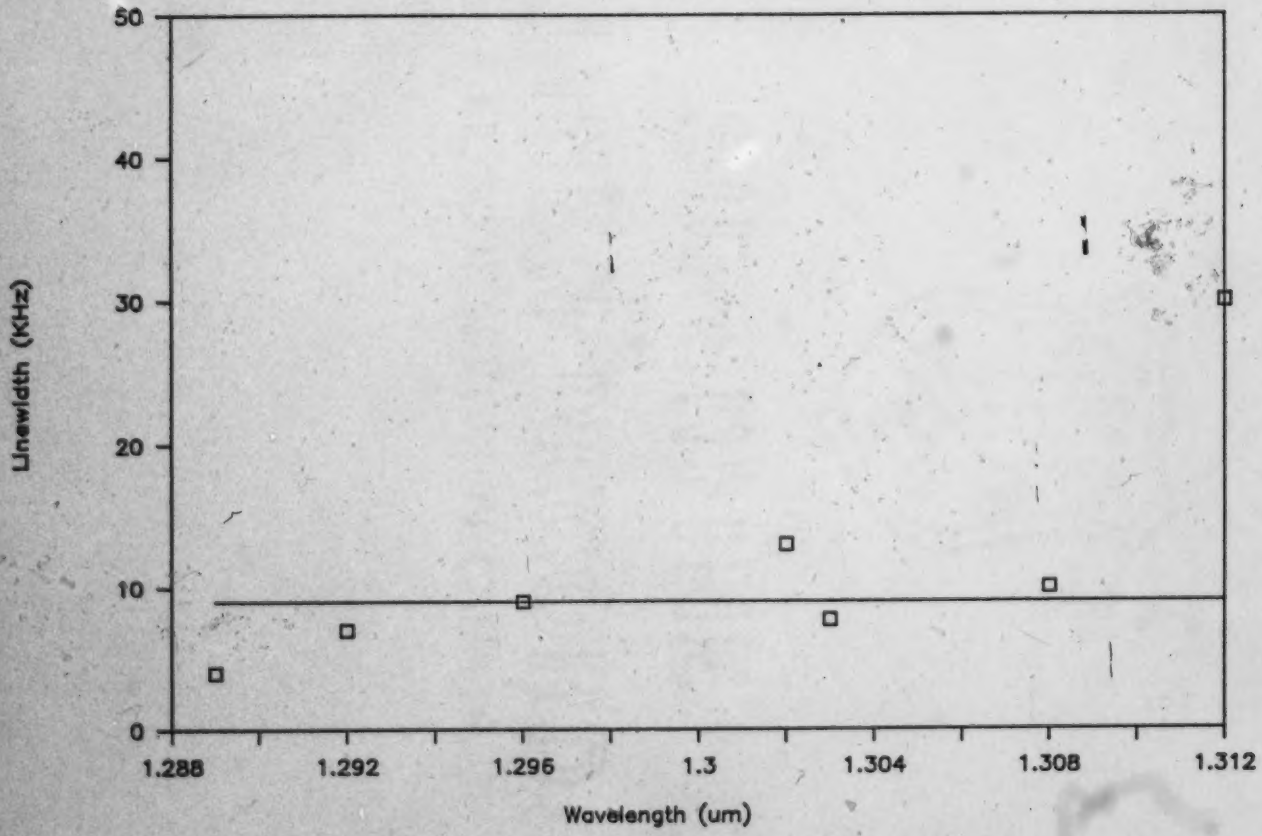

Fig. 5.11 The Linewidth Measurement at various Wavelengths obtained using Best-Fit Curve Analysis

[31] for this case, a linewidth reduction factor F is found to be equal to 180. With a linewidth of the solitary LD of approximately 100 MHz and F = 180, the linewidth of the external cavity LD is found to be:

$$\Delta\nu_{CAV} = \frac{\Delta\nu_{SOL}}{F^2} = \frac{1 \times 10^8}{(180)^2} \approx 3 \text{ kHz}$$

where:

$\Delta\nu_{CAV}$ = external cavity linewidth

$\Delta\nu_{SOL}$ = solitary laser linewidth

This value is in reasonable agreement with the linewidth calculated in the previous section using Equation 5.9 and the values obtained experimentally.

5.4 SUMMARY

In this chapter, the line narrowing due to frequency selective feedback was discussed. There are mainly two factors that contribute to the line narrowing. Firstly, the spontaneous phase perturbation is significantly reduced due to a considerable increase in photon lifetime by the extended cavity. Secondly, the residual reflectivity at an optimally detuned frequency, causes the external cavity to become resonant at that frequency. This means that the photon makes several round trips within the external cavity for each roundtrip through the active cavity. This effectively increases the external cavity length thereby greatly enhancing the linewidth narrowing.

Theoretically, linewidth of approximately 3 kHz has been calculated. Experimentally, for a 19 cm external cavity, a linewidth of about 9 kHz is obtained. Best linewidth measurement of 4 kHz was obtained at λ = 1289 nm

is . For most wavelengths of interest, 1289-1308 nm, the linewidth is narrow; within 5 kHz of the average value of 9 kHz.

CHAPTER 6

MODULATION OF EXTERNAL CAVITY LASER

Frequency Shift Keying (FSK) is an attractive modulation technique for two main reasons:

(1) It can be produced by direct modulation of LD injection current, and

(2) the signal power level can be boosted at the transmitter or along the transmission path using an optical amplifier without incurring a penalty due to intensity noise in the optical amplifiers.

Before FSK can be used as a modulation format, the FM capability of the external cavity LD as compared to that of a solitary LD must be investigated.

The refractive index change caused by temperature modulation for low frequency injection current modulation and by carrier density modulation for high frequency current modulation results in a change in laser oscillation frequency. However, the FM response (that is, the frequency deviation versus modulation frequency) of solitary LD is not uniform and compensating circuits are required to correct this non-uniform behaviour [3]. In the frequency range below 10 MHz the FM characteristics are governed by thermal effects caused by the modulation current. In this range the FM response decreases monotonically from several gigahertz per milliamp to less than a 100 MHz/mA at a modulation frequency of about 10 MHz. The frequency deviation in the frequency range from 50 MHz to 1 GHz is constant. The deviation depends on dc bias current in this frequency range. The FM response shows a resonant characteristic at about 1 GHz due to relaxation oscillation [32]. The discussion above pertains to a solitary laser diode; the FM response of a LD is altered considerably when strong optical feedback is applied to it.

6.1 DEGRADATION OF FREQUENCY MODULATION CAPABILITY OF LD IN AN EXTERNAL CAVITY

The improvements in frequency stability and spectral linewidth reduction are obtained at the cost of a reduced frequency modulation capability. It is a well known fact that direct frequency modulation capability of solitary LD degrades when external grating feedback is used [27,33]. Before a formal derivation of the reduction in frequency modulation capablity is carried out, the physical reasoning for this will be presented. Assume that an extended cavity laser has one of the facets AR coated so that, the reflectivity of that facet is zero (for simplicity). In this case, the photon lifetime is considerably longer than in a solitary laser. In a solitary laser the photon lifetime is a few nanoseconds, which means that the laser can be modulated at frequencies up to a few gigahertz. Comparing the photon lifetime in a solitary LD and that in an extended cavity laser, the following relationship is obtained:

$$\tau_{c,sol} = n\ell/[c(\alpha\ell - \ln \sqrt{R_1 R_2})] \tag{6.1}$$

$$\tau_{c,ext} = (n\ell+L)/[c(\alpha\ell - \ln \sqrt{R_1 R_g})] \tag{6.2}$$

The symbols c, n, ℓ, α, L, R_1, R_2, R_g retain their usual definition. Taking the ratio of Equation 6.1 and 6.2 and neglecting the loss term difference, the following increase in photon lifetime is obtained:

$$\tau_{c,ext} = \tau_{c,sol}\,(1 + L/n\ell) \tag{6.3}$$

Therefore, from these preliminary arguments it can be seen that the modulation capability must decrease by a factor of at least $(1+L/n\ell)$.

A further insight can be obtained by considering the location of the external cavity modes, which are determined by the cavity length. The oscillation frequency deviation range $2\Delta f_{max}$ without mode jumping (that is, the deviation does not exceed the frequency separation of the external cavity modes) is given by [33]:

$$\Delta\omega_{max} \cdot \tau_2 + F\sin(\Delta\omega_{max} \cdot \tau_2) = \pi \qquad (6.4)$$

where:

τ_2 = $2L/c$, c = speed of light

L = external cavity length

F = measure of feedback influence

$\Delta\omega_{max}$ = maximum deviation of oscillation frequency

For large F, the maximum deviation can be approximated by [33]:

$$\Delta f_{max} = (2\tau_2(1+F))^{-1} \qquad (6.5)$$

To obtain a numerical value for the maximum frequency deviation, a cavity length of 19 cm (experimental value) and a value of F = 180, as calculated in the previous chapter is used:

$$\Delta f_{max} = 3x10^8/(2 \times 2)\ 19x10^{-2}(1+180)$$

$$\Delta f_{max} = 2.2\ MHz$$

Therefore, the maximum frequency deviation that can be obtained without mode jumping for a cavity length of 19cm and strong optical feedback is 2.2 MHz. In the next section a comparison will be made with the frequency deviation that can be obtained experimentally.

6.2 EXPERIMENTAL RESULTS OF THE MODULATION CAPABILITY OF A LD IN AN EXTERNAL CAVITY

The diagram of the circuit used to obtain frequency modulation is shown in Figure 6.1. The laser is dc biased at $2.3I_{th}$ and the modulating signal is ac coupled to it. The amplitude of the ac signal is controlled by varying the current through the current source Q3. The current through the LD is controlled by the GaAsFET, Q1. The pulse response of a sample laser diode and the eye diagram at a data rate of 320Mbit/s is shown in Figure 6.2(a) and (b), respectively. It should be noted that these diagrams show only the behaviour of the circuit; the LD used to characterize the circuit did not have a coated facet.

Frequency modulation (FM) was detected by using a delayed self-heterodyne method. The delayed self-heterodyne method has been previously used to measure the spectral linewidth of the LD (with high resolution). Other interferometric methods using a Fabry-Perot interferometer or a Michelson's interferometer can also be used for FM detection. However, the self-

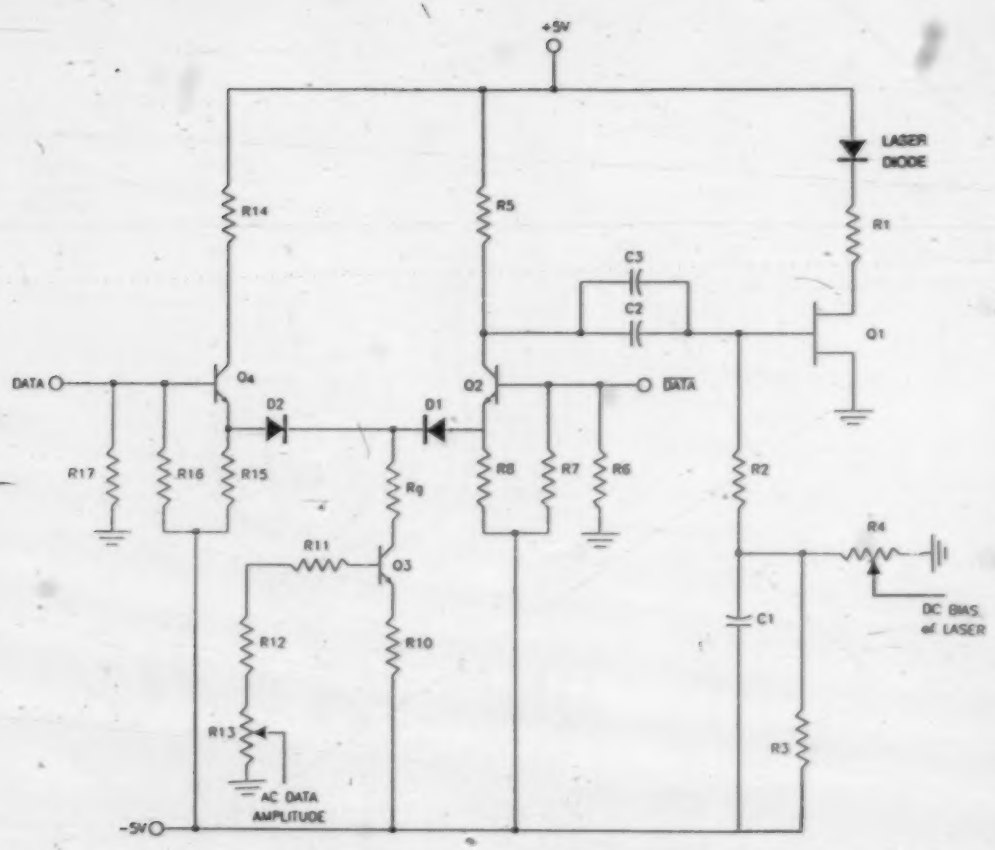

Q1	=	GaAs FET (NEC900076)	R1	=	10 Ω
Q2,Q4	=	BFQ67	R2,R3	=	1K Ω
Q3	=	2N222A	R4,R13	=	5K Ω
C1	=	50nF	R5,R14	=	50 Ω
C2	=	0.1uF	R6,R17	=	82 Ω
C3	=	100pF	R7,R16	=	130 Ω
D1,D2 - for switching current from one arm to the other			R8,R15	=	1.2K Ω
			Rg	=	25 Ω
			R10	=	15 Ω
			R11	=	390 Ω
			R12	=	2K Ω

Fig. 6.1 Circuit Diagram of Laser Driver for High Bit Rate Modulation

(a)

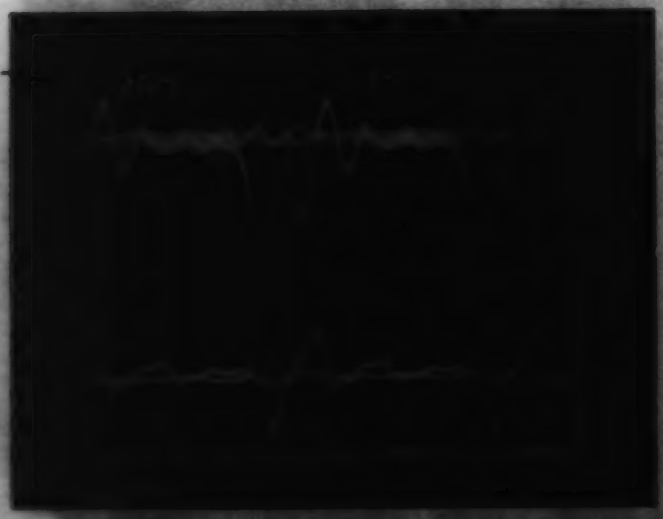

(b)

Fig. 6.2 Modulation Response of solitary LD modulated at 320 Mbit/sec.
The Diagram shows characteristics of the Driver Circuit of Fig. 6.1
(a) Pulse Response of a sample solitary LD
(b) Eye Diagram

heterodyne set-up was the most convenient method of detection in this case. The power spectrum, S(f), of the beat signal of a laser diode modulated directly by a sinusoidal current is given by [34]*:

$$S(f) = (\pi)^{-1} \sum |J_n(2m\sin(\omega_m \tau_d/2)|^2 \{2\Delta\nu/[(f-nf_m)^2+(2\Delta\nu)^2]\} \qquad (6.6)$$

where:

$\Delta\nu$ = linewidth of the unmodulated LD

τ_d = delay time due to single mode fiber

m = frequency modulation index

f_m = modulation frequency

The above power spectrum can be compared to a "normal" FM power spectrum in that, in Equation 6.6, the Bessel functions, J_n are normally a function of β which is the modulation index. Therefore, in the above case, the modulation index can be interpreted as $2m\sin(\omega_m \tau_d/2)$. As indicated in Reference [34], the modulation index $2m\sin(\omega_m \tau_d/2)$ can be measured from the ratio of the carrier and the first-order sideband levels in the high-frequency modulation region (i.e $\Delta\nu < f_m$) with a small modulation index. In the low-frequency modulation region when the side-bands cannot be resolved, the frequency deviation can be measured from the width of the sideband spectrum.

The power spectrum of a frequency modulated LD is shown in Figure 6.3 (a) and (b) for a modulation frequency of 230 kHz. In Figure 6.3 (a) the linewidth is optimally narrowed; that is, the linewidth reduction is maximum. In Figure 6.3 (b) the linewidth reduction factor is relaxed and therefore the linewidth is not as narrow as in Figure 6.3 (a). For identical parameters, i.e., the bias current

* The non-essential constant terms are not included.

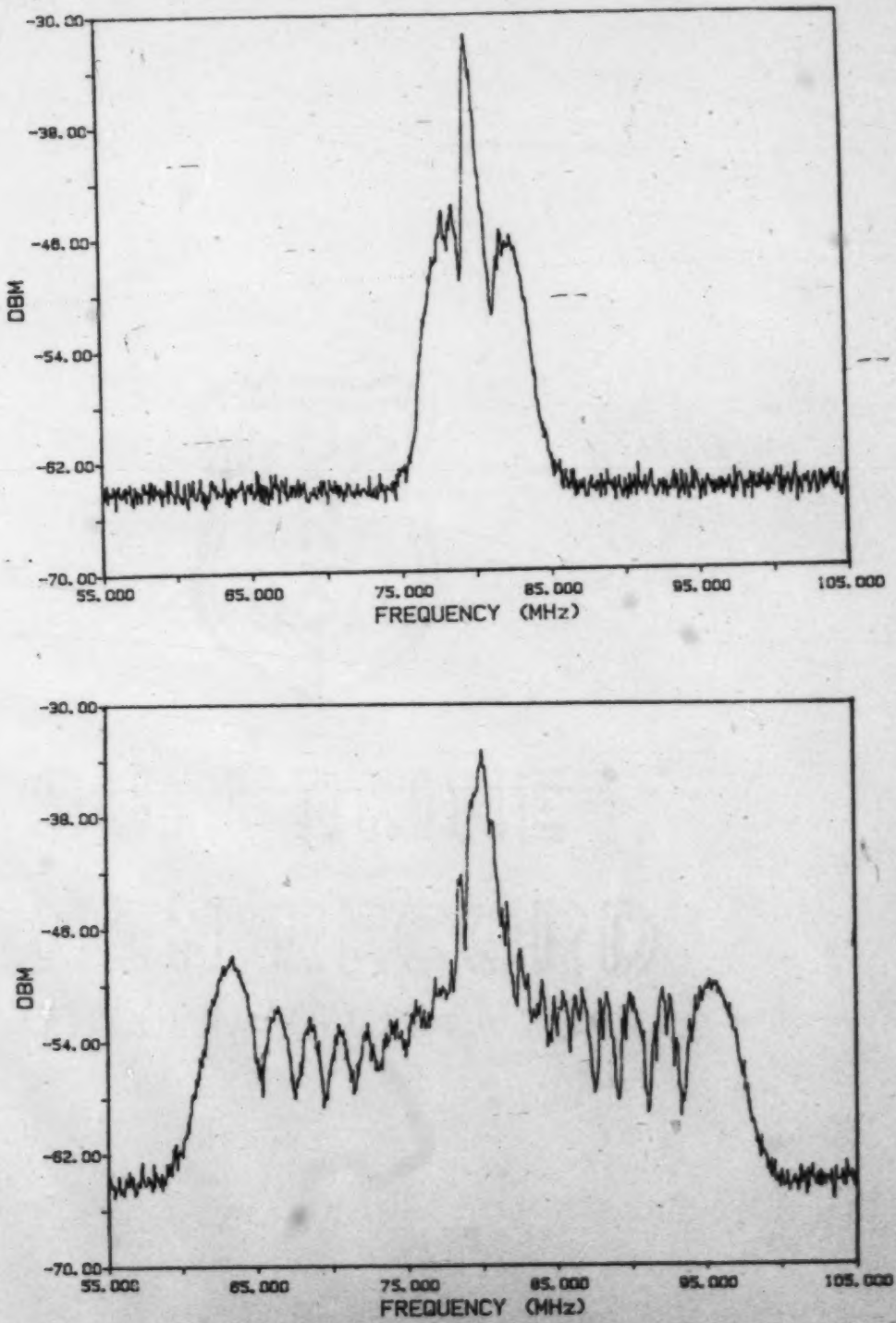

Fig. 6.3 Power Spectrum of Frequency Modulated LD at 230 kHz Sinewave $I_{bias} = 2.3I_{th}$ and ΔI = 1mA pp
(a) Optimally narrowed linewidth Δf = 2.75 MHz
(b) ~ 14 times wider linewidth Δf = 10.5 MHz

$I_{bias} = 2.3I_{th}$ and the modulation current, ΔI = 1mA pp, it is seen that the frequency deviation in (a) is about 2.75 MHz whereas, when the linewidth is not optimally narrowed as in (b) the frequency deviation is about 10.5 MHz. Unfortunately when these measurements were being performed, a precise measurement of the linewidth could not be obtained. A rough estimate would indicate that the linewidth in Figure 6.3(a) is about 14 times narrower than the linewidth in Figure 6.3 (b). However, these graphs clearly show the degradation in frequency modulation capability with increase in linewidth reduction factor.

A second set of measurements was performed to investigate the effect of increasing the modulation depth (i.e the amplitude of the modulation current). Figure 6.4 (a) and (b) show the power spectrum; Figure 6.4 (a) is the power spectrum graph when the current modulation depth is 2 mA pp and Figure 6.4 (b) shows the power spectrum when the modulation depth, ΔI is 3.2 mA pp. It can be seen from a comparison of the two spectra, that the power spectrum degrades considerably when a large modulating current is used to obtain a wider frequency deviation than the maximum obtainable deviation without mode hopping.

Modulation at other frequencies such as 100 kHz and 50 MHz was also tried. At 100 kHz, the frequency deviation could not be discerned however, some linewidth broadening was noticed. At 50 MHz, the sidebands could be resolved, but the spectrum was complicated by the appearance of external cavity modes and by the 80 MHz frequency shift due to the self-heterodyne set-up. An output power spectrum of LD under 50 MHz sinewave modulation is shown in Figure 6.5. Notice that the lower sidebands J_{-2}, J_{-3} etc. are folded over at 0 Hz, and also appear shifted by 80 MHz. The other point of interest is that, for the sidebands J_1, J_{-1} etc, the amplitude cannot be measured exactly since each of these sidebands is the sum of several sidebands multiplied together due to the

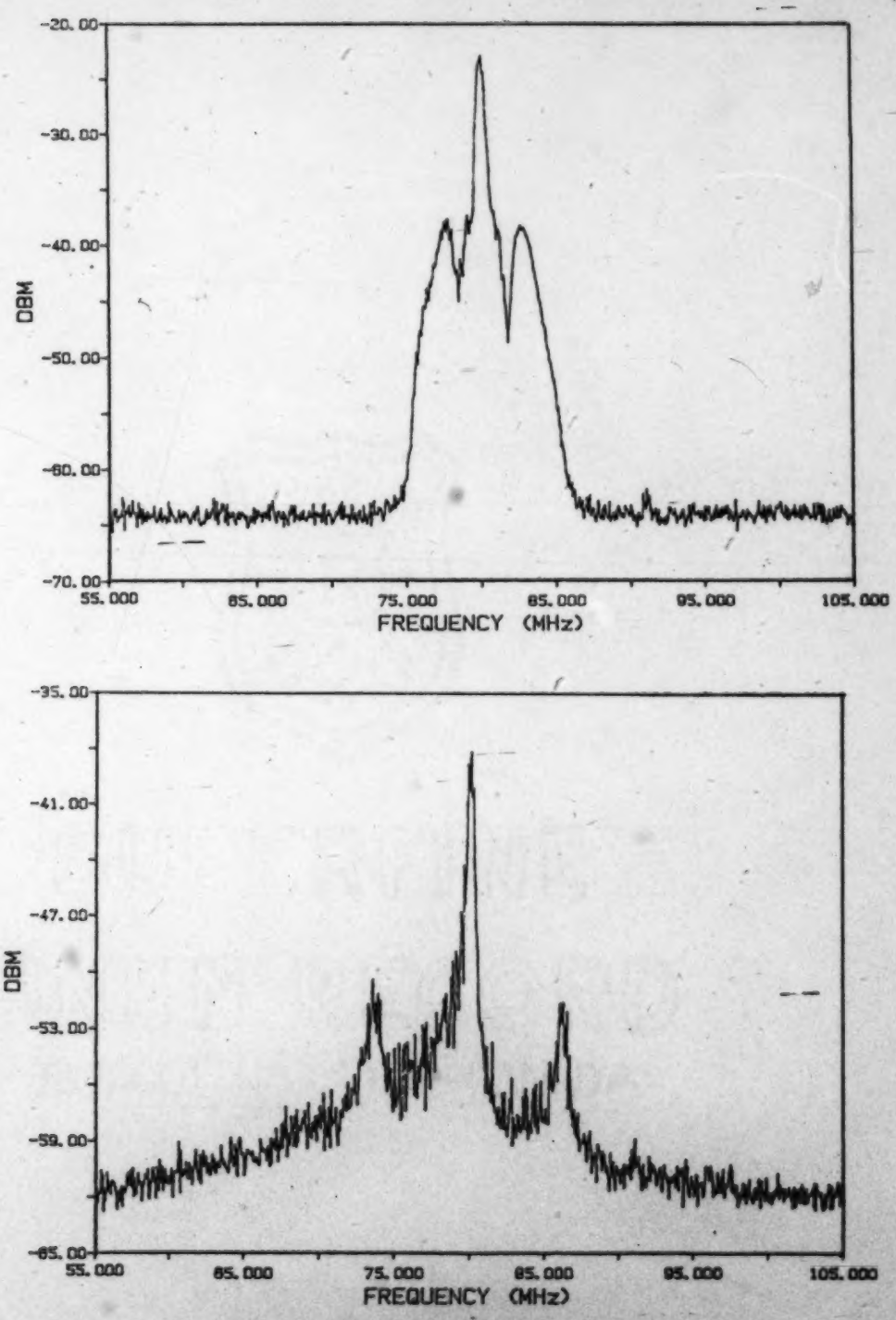

Fig. 6.4 Power Spectrum of Frequency Modulated LD at 230 kHz Sinewave
$I_{bias} = 2.3I_{th}$ and optimally narrowed linewidth
(a) ΔI = 2mA pp; Δf = 3.25 MHz
(b) ΔI = 3.2mA pp; Δf = 5.75 MHz

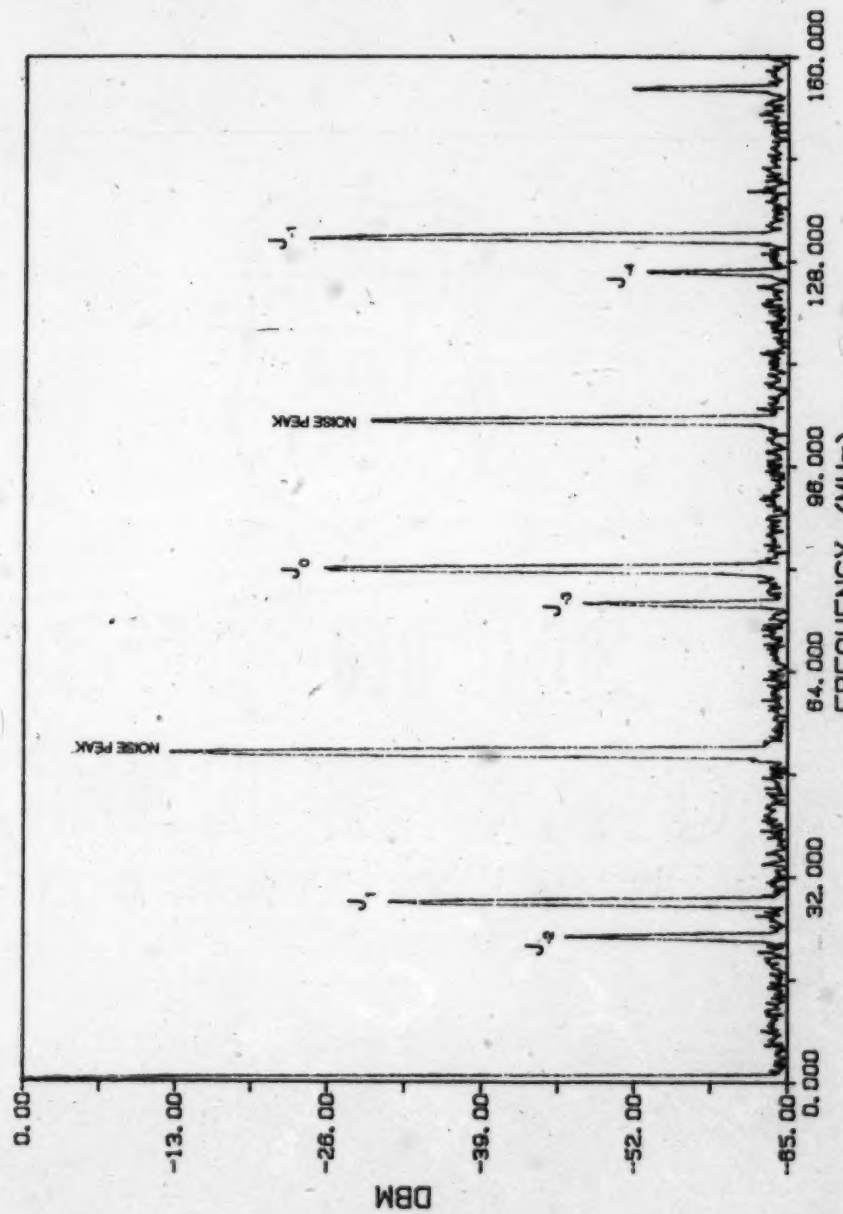

Fig. 6.5 Power Spectrum of LD under 50 MHz Sinewave Modulation
$I_{bias} = 2.3I_{th}$ and $\Delta I = 4.0mA$ pp

convolution process occurring in the self-heterodyne set-up. For example, if the original unshifted spectrum consists of three side-bands as follows:

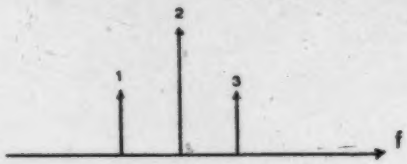

and now these are shifted by 80MHz

then due to convolution the following is obtained:

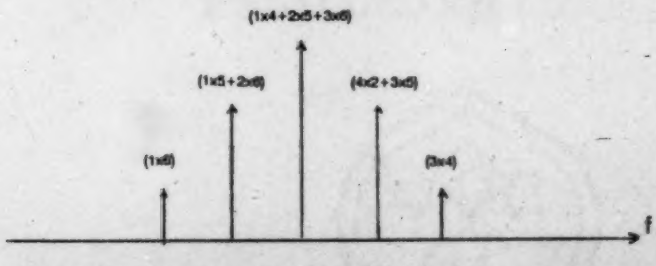

Therefore, no definite conclusion about the modulation index can be made from the ratio of carrier to sideband amplitudes. The amplitude of the sidebands also is affected by the spurious AM component contained in the directly frequency modulated output. However, if the 80 MHz shift due to the acousto-optic modulator is eliminated, then only the AM component is impressed on the sidebands and this can easily be subtracted since this effect causes an assymetrical sideband spectra [32]. The acousto-optic modulator could not be turned off, since continuous monitoring of the linewidth under modulation was required. The order of sidebands indicated in Figure 6.5 is obtained by considering the foldover of frequencies at 0 Hz and the 80 MHz shift. However,

with complications introduced by the 80 MHz shift during the convolution process in the self-heterodyne set-up the sidebands may not be as indicated in the Figure 6.5, although no other explanation is known at this time. The modulation at 50 MHz and the detection using the self-heterodyne set-up was an extra step carried out to test the limit of the detection method and also the modulation capability of the source.

6.3 SUMMARY

In this chapter the modulation capability of a LD, strongly coupled to a grating loaded external cavity was discussed. It was found that the FM modulation capability of such a laser degrades by (1+F), where F is the linewidth narrowing factor discussed in the previous chapter. The maximum frequency deviation with the present set-up (19 cm external cavity length) without mode jumping was found to be 2.2MHz. The measure of frequency deviation was experimentally determined by modulating the laser diode at 230KHz (sinewave modulation) with a modulation depth ΔI = 1mA pp and was found to be about 2.75MHz, confirming the calculated result. It was also shown, that if the linewidth narrowing factor is not optimum (the line was not very stable at this point), a wider frequency deviation could be obtained. The self-heterodyne technique used to detect the FM modulation seemed to give reasonable results when the frequency deviation could be directly measured from the spectrum.For higher modulation rates where the FM side-bands could be resolved, the amplitude of these sidebands was altered by the convolution process and the 80 MHz frequency shift of the acousto-optic modulator and therefore, conclusive measurements of the modulation index could not be made.

CHAPTER 7

SUMMARY AND CONCLUSION

The key requirement for a coherent fiber optical communication system is a source (a semiconductor laser diode for practical systems) that has "adequate" spectral purity, stability and a certain degree of tunability. This thesis is concerned with obtaining such a source.

The scheme for obtaining the narrow linewidth source investigated in this thesis falls under the broad category of optical feedback. About 20% of the light leaving one of the facets of the laser is coupled back into the laser cavity through the same facet, after being reflected from a diffraction grating. Such a scheme is known as a strong frequency selective feedback configuration. In order to be able to feed 20% of the light back into the laser cavity, the facet through which the light is fed back has to be anti-reflection (AR) coated. It is difficult to obtain very low reflectivities for AR coatings on LDs; due to their very thin active areas, the thickness of the coating has to be precisely calculated, taking into consideration the portion of the electric field in the cladding and the core. This procedure does not guarantee that low reflectivities will be obtained since the refractive index of coatings used on III-V material systems varies with the deposition process parameters such as the pressure and the rate of deposition. These parameters therefore, have to controlled precisely. In view of this, it was considered essential to monitor the laser facet reflectivity while the coating was being deposited onto the facet. Such a scheme was designed and reflectivities as low as 8×10^{-4} were obtained reproducibly without adjusting the deposition process parameters.

The AR coated laser was then placed in an external cavity loaded with a diffraction grating. In this configuration, the laser oscillated in a stable single longitudinal mode with a side mode suppression ratio of more than 30 dB . The laser could be tuned over a 43 nm (7,000 GHz) range by rotating the grating.

Linewidth measurements were made using a delayed self-heterodyne technique. These measurements showed that the laser with an external cavity had a very long coherence time. The narrowest linewidth obtained was 4 kHz at 1286 nm. Measurements at other wavelengths gave a linewidth of about 9 kHz ± 3 kHz. Therefore, it can be concluded that the linewidth of the external cavity LD is stable and narrow over a wide range of wavelengths and can therefore be operated at any of these wavelengths.

As laser diode phase noise decreases with optical feedback, the frequency modulation capability is also decreases. It was found that the maximum frequency deviation without any mode jumping is only about 2.2 MHz for a 19 cm external cavity length. Therefore, if such a source is to be used at the transmitter, then an external modulator needs to be used to obtain a reasonable frequency deviation. However, a source that has been stabilized in frequency to this extent, would more appropriately be used as a local oscillator at the receiver. Also, a wide tuning range is a desirable feature for use as a local oscillator because it can be tuned to select different channels in a frequency multiplexed network.

Due to time constraints, this project was necessarily limited in scope. Some suggestions for future work are as follows:

(1) Package and characterize the external cavity laser so that it may be used as a reference source for future work in coherent fiber optics.

(2) Measure the linewidth enhancement factor, α' for the LD and determine its effect on the FM response of the laser and on the behaviour of the laser in an external cavity.

(3) Determine if the source can be continuously tuned as opposed to being tuned from one laser internal cavity mode to the next.

(4) Refine the frequency detection scheme used in this project. It would be more convenient to use a self-homodyne scheme (i.e., eliminate the frequency shift caused by the acousto-optic modulator).

(5) Evaluate the properties of a self-homodyne technique to detect DFSK using a delay line with one bit period delay such that, at the end of the delay line, the two optical fields are still correlated.

REFERENCES

[1] B. Glance, "Densely Spaced Coherent Optical Star Network", **Electronics Letters**, Vol. 23, No. 17, 1987, pp. 875-876.

[2] F. Favre, D. LeGuen, "Effect of Semiconductor Laser Phase Noise on BER Performance in an Optical DPSK Heterodyne Type Experiment", **Electronics Letters**, Vol. 18, No. 22, October 1982, pp. 964-965.

[3] Y. Yamamoto, T. Kimura, "Coherent Optical Fiber Transmission System", **IEEE Journal of Quantum Electronics**, QE-17, June 1981, pp. 919-935.

[4] L.G. Kazovsky, "Coherent Optical Receivers: Performance Analysis and Laser Linewidth Requirements", **Opt. Eng.**, Vol. 25, 1986, pp. 575-579.

[5] S. Murata, I. Mito, K. Kobayshi, "Over 5.8 nm Continuous Wavelength Tuning of 1.5 μm Wavelength Tunable DBR Laser", **Technical Digest**, OFC/100C '87 (Reno, Nevada), January 19-22, 1987, pp. 150.

[6] J. Olesen, S. Saito, T. Mukai, T. Saitoh, O. Mikami, "Solitary Spectral Linewidth and Its Reduction With External Grating Feedback for a 1.55 μm InGaAsP BH Laser", **Japanese Journal of Applied Physics**, Vol. 22, No. 10, 1983, pp. 1664-1666.

[7] R. Wyatt, W.J. Devlin, "10 Khz Linewidth of 15 μm InGaAsP External Cavity Laser with 55 nm Tuning Range", **Electronics Letters**, Vol. 19, No. 3, February 3, 1983, pp. 110-112.

[8] M. Kitmura, M. Yamaguchi, S. Murata, I. Mito, K. Kobayashi, "High-Performance Single-Longitudinal-Mode Operation of InGaAsP/InP DFB-DC-PBH LD's," **IEEE/OSA Journal of Lightwave Technology**, Vol. LT-2, 1984, pp. 363-369.

[9] B. Enning, R.S. Vodhanel, "Adaptive Quantized Feedback Equalization for FSK Heterodyne Transmission at 150 Mbit/sec and 1 Gbit/sec", **Postdeadline Paper**, OFC '88 (New Orleans, Louisiana), January 25-28, 1988, pp. PD23-1-4.

[10] Y. Yamamoto, "Receiver Performance Evaluation of Various Digital Optical Modulation-Demodulation Systems in 0.5-10 μm Wavelength Region", **IEEE Journal of Quantum Electronics**, Vol. QE-16, No. 11, 1980, pp. 1251-1259.

[11] R.W. Tkach, A.R. Chraplyvy, "Regimes of Feedback Effects in 1.5 μm Distributed Feedback Lasers", **Journal of Lightwave Technology**, Vol. LT-4, November 1986, pp. 1655-1661.

[12] T. Saitoh, T. Mukai, O. Mikami, "Theoretical Analysis and Fabrication of Antireflection Coatings on Laser Diode Facets", **Journal of Lightwave Technology**, Vol LT-3, April 1985, pp. 288-293.

[13] H. Kressel, J.K. Butler, "Semiconductor Lasers and Heterojunction LEDs", Academic Press Inc., 1977, pp. 261-275.

[14] G. Eisenstein, L.W. Stulz, "High Quality Anti-Reflection Coatings on Laser Facets by Sputtered Silicon Nitride", **Applied Optics**, Vol 23, 1983, pp. 161.

[15] J.C. Simon, "Polarization Characteristics of Very Low Reflectivity Coatings for Semiconductor Laser Amplifiers",**Technical Digest**, ECOC'86 (Barcelona, Spain) September 22-25, 1986, pp. 249-252.

[16] T. Ikegami, "Reflectivity of Mode at Facet and Oscillation Mode in Double Heterostructure Injection Lasers", **IEEE Journal of Quantum Electronics**, QE-8, No. 6, 1972, pp. 470.

[17] K. Kikuchi, T. Okoshi, "High Resolution Measurement of the Spectrum of Semiconductor Lasers", **Japan Annual Review on Electronics, Computers, Telecommunications, Optical Devices and Fibers**, 1982, published by Ohmsha Ltd., Tokyo, Japan and North Holland Publishing Co., Amsterdam, Netherlands, pp. 51-59.

[18] G.D. Cormack, J.O. Binder, "A Fiber Feedback InGaAsP Laser", Final Report Submitted to the Department of Communications on Completion of Contract OGST.36100-5-0143, University of Alberta, March 1986.

[19] G. W. Stroke, "Diffraction Gratings," **Encyclopedia of Physics**, Vol.29 Editted by S. Flugge, pp. 444-498.

[20] E. Hecht, A. Zajac, **Optics**, Addison-Wesley Publishing Company Inc., Reading, Massachusetts, 1974, pp. 329-395.

[21] A. Yariv, **Optical Electronics**, Holt, Reinhart and Winston, New York, 1985, pp. 28-31.

[22] B. Tromborg, H. Olesen, X. Pan, S. Saito, "Transmission Line Description of Optical Feedback and Injection Locking for Fabry-Perot and DFB Lasers", **IEEE Journal of Quantum Electronics**, Vol. QE-23, No. 11, November 1987, pp. 1875-1889.

[23] M.W. Fleming, A. Mooradian, "Spectral Characteristic of External-Cavity Controlled Semiconductor Lasers", **IEEE Journal of Quantum Electronics**, Vol. QE-17, No. 1, January 1981, pp. 44-59.

[24] E. Patzak, A. Sugimura, S. Saito, T. Mukai, H. Olesen, "Semiconductor Laser Linewidth in Optical Feedback Configurations", **Electronics Letters**, Vol. 19, No. 24, November 24, 1983, pp. 1026-1027.

[25] R. Wyatt, "Spectral Linewidth of External Cavity Semiconductor Lasers with Strong Frequency-Selective Feedback", **Electronics Letters**, Vol. 21, No. 15, July 18, 1985, pp. 658-659.

[26] H. Sato, H. Ohya, "Theory of Spectral Linewidth of External Cavity Semiconductor Lasers", **IEEE Journal of Quantum Electronics**, Vol. QE-22, No. 7, July 1986, pp. 1060-1063.

[27] R.F. Kazarinov, C.H. Henry, "The Relation of Line Narrowing and Chirp Reduction Resulting from the Coupling of a Semiconductor Laser to a Passive Resonator", **IEEE Journal of Quantum Electronics**, Vol. QE-23, No. 9, September 1987, pp. 1401-1409.

[28] M. Osinski, J. Buus, "Linewidth Broadening Factor in Semiconductor Lasers - An Overview", **IEEE Journal of Quantum Electronics**, Vol. QE-23, No. 1, January 1987, pp. 9-29.

[29] C.H. Henry, "Theory of Spontaneous Emission Noise in Open Resonators and its Application to Laser and Optical Amplifiers", **Journal of Lightwave Technology**, Vol. LT-4, No. 3, March 1987, pp. 228-297.

[30] L.E. Richter, H.I. Mandelberg, M.S. Kruger, P.A. McGarth, "Linewidth Determination From Self-Heterodyne Measurements With Subcoherence Delay Times", **IEEE Journal of Quantum Electronics**, Vol. QE-22, No. 11, November 1986, pp. 2070-2074.

[31] J.O. Binder, "Mode-Selection and Tuning in an External Grating Laser," University of Alberta, (Unpublished)

[32] S. Kobayashi, Y. Yamamoto, T. Kimura,"Direct Frequency Modulation in AlGaAs Semiconductor Lasers", **IEEE Journal of Quantum Electronics**, Vol. QE-18, No. 4, 1982, pp. 582-595.

[33] S. Saito, O. Nilsson, Y. Yamamoto, "Oscillation Center Frequency Tuning Quantum FM Noise and Direct Frequency Modulation Characteristics in External Grating Loaded Semiconductor Lasers", **IEEE Journal of Quantum Electronics**, Vol. QE-18, No. 6, June 1982, pp. 961-970.

[34] S. Ryu, S. Yamamoto, "Measurement of Direct Frequency Modulation Characteristics of DFB-LD By Delayed Self-Homodyne Technique", **Electronics Letters**, September 25, 1986, Vol. 22, No. 20, pp. 1052-1054.

[35] B.W. Hakki, T.L. Paoli, "Gain Spectra in GaAs Double-Heterostructure Injection Lasers", **Journal of Applied Physics**, Vol. 46, No. 3, 1975, pp. 1299-1306.

[36] A. Yariv, Quantum Electronics, John Wiley & Sons, Inc., New York, 1975.

[37] Y. Yamamoto, T. Kimura, "Coherent Optical Fiber Transmission Systems", **IEEE Journal of Quantum Electronics**, Vol. QE-17, No. 6, June 1981, pp. 919-935.

[38] R. Lang, K. Kobayashi, "External Optical Feedback Effects on Semiconductor Injection Laser Properties", **IEEE Journal of Quantum Electronics**, Vol. QE-16, March 1980, pp. 347-355.

[39] H. Temkin, N.A. Olsson, J.H. Abeles, R.A. Logan, M.B. Panish, "Reflection Noise in Index-Guided InGaAsP Lasers", **IEEE Journal of Quantum Electronics**, Vol. QE-22, No. 2, February 1986, pp. 286-293.

[40] M.B. Panish, "Heterostructure Injection Lasers", **Proceedings of the IEEE**, Vol 64, No. 10, October 1976, pp. 1512-1542.

[41] E. Patzak, H. Olesen, A. Sugimura, S. Saito, T. Mukai, "Spectral Linewidth Reduction in Semiconductor Lasers by an External Cavity With Weak Optical Feedback", **Electronics Letters**, October 27, 1983, Vol. 19, No. 22, pp. 938-940.

[42] J.C. Simon, "Semiconductor Laser Amplifier for Single Mode Optical Fiber Communications", **Journal of Optical Communications**, Vol, 4, No. 2, 1983, pp. 51-62.

[43] M.R. Matthews, K.H. Cameron, R. Wyatt, W.J. Devlin, "Packaged Frequency - Stable Tunable 20 Khz Linewidth 1.5 μm InGaAsP External Cavity Laser" **Electronics Letters**, January 31, 1985, Vol. 21, No. 3, pp. 113-115.

[44] K. Kikuchi, T. Okoshi, M. Nagamatsu, N. Henmi, "Degradation of Bit-Error Rate in Coherent Optical Communications Due to Spectral Spread of the Transmitter and the Local Oscillator", **IEEE Journal of Lightwave Technology**, Vol. LT-2, No. 6, 1984, pp. 1024-1033.

[45] T. Kimura, Y. Yamamoto, "Review Progress of Coherent Optical Fibre Communication Systems", **Optical and Quantum Electronics**, Vol. 15, 1983, pp. 1-39.

[46] J.M. Osterwalder, B.J. Rickett, "Frequency Modulation of GaAlAs Injection Lasers at Microwave Frequency Rates", **IEEE Journal of Quantum Electronics**, Vo. QE-16, No. 3, 1980, pp. 250-252.

[47] I. Garrett, G. Jacobsen, "Theoretical Analysis of Heterodyne Optical Receivers for Transmission Systems Using (Semiconductor) Lasers with Nonnegligible Linewidth", **Journal of Lightwave Technology**, Vol. LT-4, No. 3, 1986, pp. 323-334.

[48] J. Gowar, "Optical Communication Systems, Prentice Hall International, Inc. London, 1984.

[49] G. Keiser, "Optical Fiber Communications", McGraw-Hill, Inc., New York, 1983.

[50] S. Saito, Y. Yamamoto, T. Kimura, "Optical FSK Heterodyne Detection Experiments Using Semiconductor Laser Transmitter and Local Oscillator", **IEEE Journal of Quantum Electronics**, Vol. QE-17, No. 6, 1981, pp. 935-941.

[51] S. Saito, Y. Yamamoto, T. Kimura, "Optical Heterodyne Detection of Directly Frequency Modulated Semiconductor Laser Signals", **Electronics Letters**, Vol. 16, October 1980, pp. 826-827.

[52] C.H. Henry, R.F. Kazarinov, "Instability of Semiconductor Lasers Due to Optical Feedback From Distant Reflectors", **IEEE Journal of Quantum Electronics**, Vol. QE-22, No. 2, 1986, pp. 294-301.

[53] P. Zorabedian, W.R. Trutna, L.S. Cutler, "Bistability in Grating-Tuned External-Cavity Semiconductor Lasers", **IEEE Journal of Quantum Electronics**, Vol. QE-23, No. 11, 1987, pp. 1855-1860.

[54] N.K. Dutta, N.A. Olsson, K.Y. Liou, "Effect of External Optical Feedback on Properties of External Cavity Semiconductor Lasers", **Electronics Letters**, Vol. 20, No. 14, July 5, 1984.

[55] G.P. Agrawal, "Line Narrowing in a Single-Mode Injection Laser Due to External Optical Feedback", **IEEE Journal of Quantum Electronics**, Vol. QE-20, No. 5, 1984, pp. 468-471.

[56] T.L. Koch, R.A. Linke, "Effect of Nonlinear Gain Reduction on Semiconductor Laser Wavelength Chirping", **Applied Physics Letters**, Vol. 48, No. 10, March 1986, pp. 613-615.

[57] O. Nilsson, Y. Yamamoto, "Small-Signal Response of a Semiconductor Laser With Inhomogeneous Linewidth Enhancement Factor: Possibilities of a Flat Carrier-Induced FM Response", **Applied Physics Letters**, Vol. 46, No. 3, February 1, 1985, pp. 223-225.

[58] C. Harder, K. Vahala, A. Yariv, "Measurement of the Linewidth Enhancement Factor α of Semiconductor Lasers", **Applied Physics Letters**, Vol. 42, No. 4, February 15, 1983, pp. 328-330.

[59] K. Kikuchi, T. Okoshi, "Simple Formula Giving Spectrum-Narrowing Ration of Semiconductor-Laser Output Obtained By Optical Feedback", **Electronics Letters**, Vol. 18, No. 1, January 7, 1982, pp. 10-12.

[60] M. Welch, "Vacuum Evaporation Technology For Optical Thin Films", **Lasers & Optronics**, July 1987, pp. 69-73.

APPENDIX A

DERIVATION OF CONFINEMENT FACTOR FOR TE AND TM MODES

The confinement factor for TE mode, Γ_{TE} is defined as follows:

$$\Gamma_{TE} = \frac{\int_d E_y^2(x)\,dx}{\int_{-\infty}^{\infty} E_y^2(x)\,dx} \qquad (A.1)$$

Considering only the even TE modes, the electric field is given by:

$$E_y^2 = A^2 \cos^2(Kx) \qquad (A.2)$$

inside the active layer, and

$$E_y^2 = A^2 \cos^2(K\,d/2)\, e^{-\gamma(|x|-d/2)} \qquad (A.3)$$

outside the active layer[13].

The symbols K, γ and d are defined as follows:

$$K^2 = n_a^2 K_o^2 - \beta^2 \qquad (A.4)$$

$$\gamma^2 = \beta^2 - n_c^2 k_o^2 \qquad (A.5)$$

where:

d = active layer thickness

n_a = active layer refrative index

n_c = cladding refractive index

$K_o = 2\Pi/\lambda o$

β = the propagation constant

The following equation is obtained for Γ_{TE} by substituting Equation A.2 and A3 into Equation A.1 and performing the integration:

$$\Gamma_{TE} = [\,1 + \frac{2K}{\gamma}\{\frac{\cos^2(Kd/2)}{Kd + \sin Kd}\}]^{-1} \qquad (A.6)$$

In order to determine a numerical value for Γ_{TE}, K and γ must be determined from an eigen value equation obtained by imposing boundary conditions which require E_y and H_z to be continous at $x = \pm d/2$.

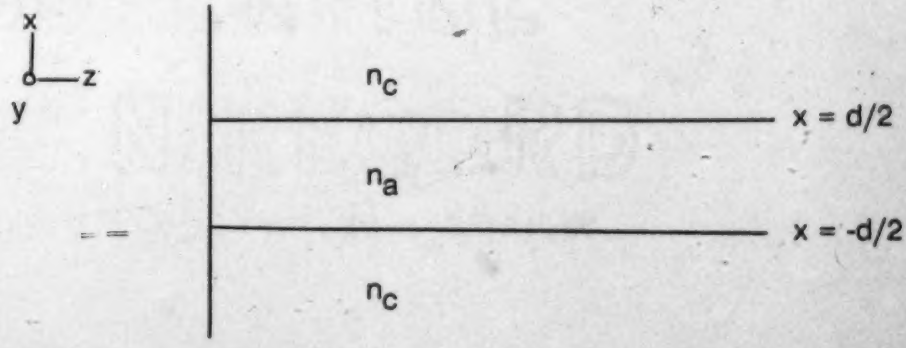

The equation thus obtained is:

$$\tan(Kd/2) = \gamma/K \qquad (A.7)$$

This equation, with equations A.4 and A.5, can be solved numerically for K and γ.

Using the laser parameters listed in Table 3, the following values are obtained for K, γ, and Γ_{TE}

$$K = 5.6\times10^{6}$$

$$\gamma = 3.52\times10^{6}$$

$$\Gamma_{TE} = 0.469 \qquad \text{(A.8)}$$

Γ_{TM} can be found in a similar manner. The following definition is used:

$$\Gamma_{TM} = \frac{\int_{d} E_x^2(x) + E_z^2(x)\,dx}{\int_{-\infty}^{\infty} (E_x^2(x) + E_z^2(x))\,dx} \qquad \text{(A.9)}$$

The electric field for TM polarisation is given as follows [13]:

$$E_x(x) = \frac{\beta\sqrt{(\mu_o)}}{n K_o} H_y(x) \qquad \text{(A.10)}$$

$$\text{and} \quad E_z(x) = \left[\frac{i\sqrt{(\mu_o)}}{n K_o}\right] \frac{\partial H_y(x)}{\partial x} \qquad \text{(A.11)}$$

where $H_y = A\cos(Kx)\, e^{-j\beta z}$, in the active region

and $H_y = A\cos(Kd/2)\, e^{-\gamma(|x|-d/2)}\, e^{-j\beta z}$ outside the active area.

Substituting Equation A.10 and A.11 into A.9 and performing the integration the following equation is obtained for Γ_{TM}:

$$\Gamma_{TM} = \left[\left(1 + 2 \left(\frac{n_a}{n_c}\right)^2 \left(\frac{[(\beta^2 + \gamma^2)(\cos^2(Kd/2))] / \gamma}{\beta \quad (Kd + \sin Kd)/K + K(Kd - \sin Kd)}\right)^{-1}\right)\right] \qquad (A.12)$$

Using the laser parameters listed in Table 3, Γ_{TM} was calculated to be:

$$\Gamma_{TM} = 0.420 \qquad (A.13)$$

Therefore, from Equation A.8 and A.13 the ratio Γ_{TM}/Γ_{TE} is 0.896.

APPENDIX B

CIRCUIT DIAGRAMS

The diagrams of circuits used to control the temperature and the CW bias of the LD are shown here. The thermistor (used to control the current through the Peltier Cooler) temperature calibration is also shown. In Figure B.4, the data for the LD obtained from the manufacturer is given.

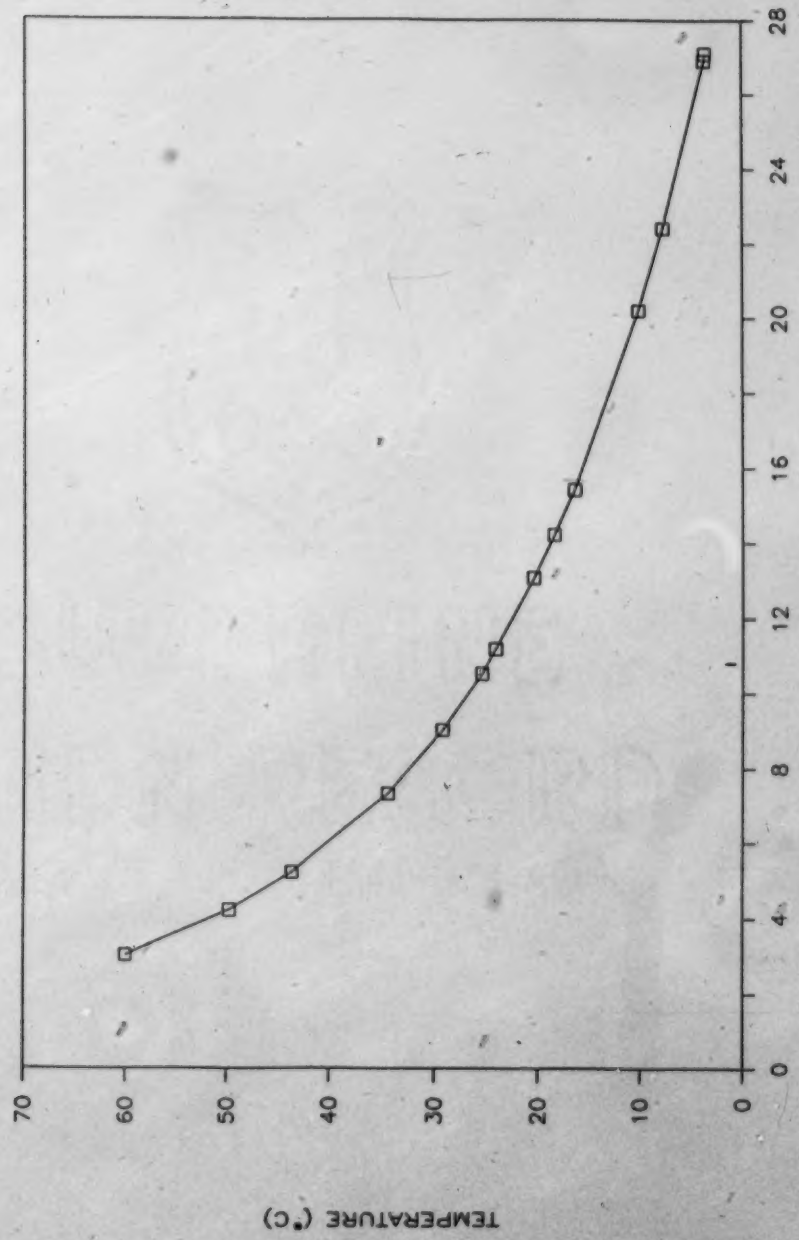

Fig. B.1 Thermistor Temperature Calibration

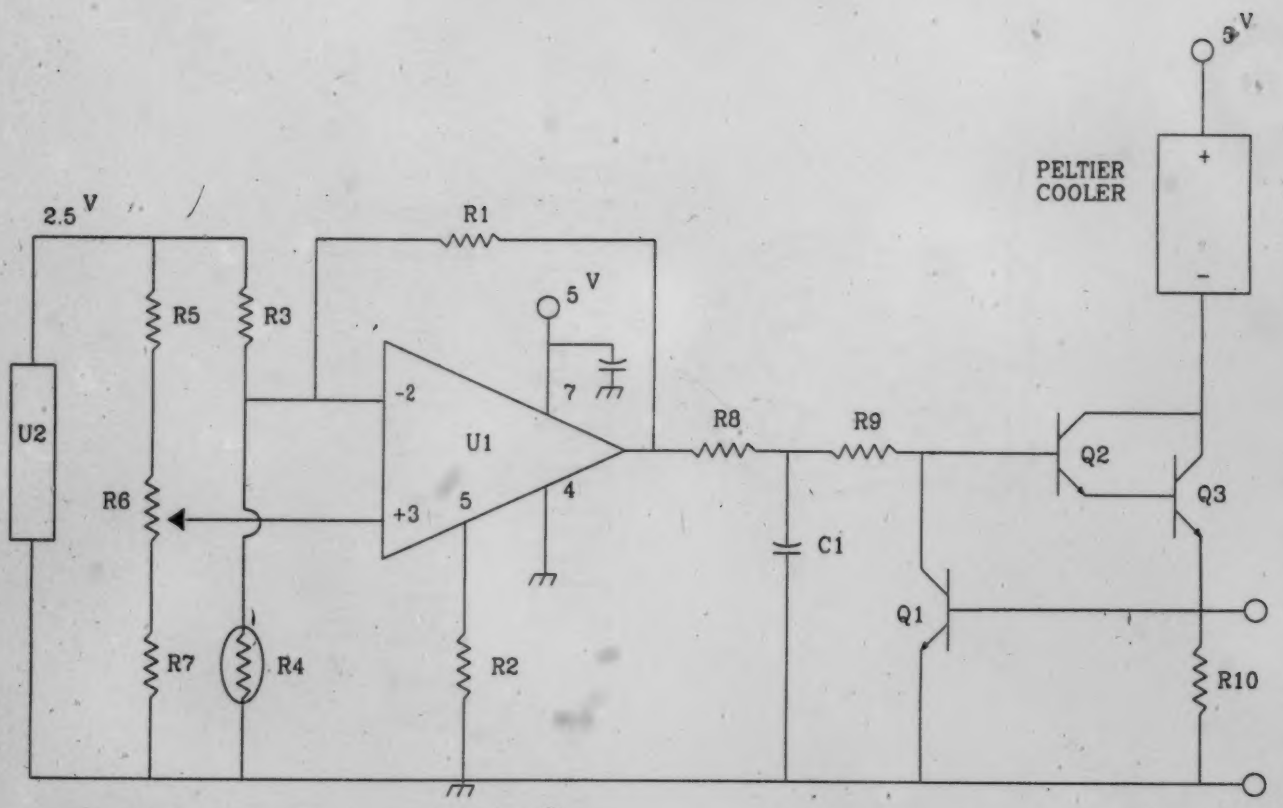

U1 = CA 3130
U2 = CA 1403 (Voltage Regulator 2.5v)
Q1,Q2 = 2N 2222
Q3 = 2N3055
R1 = 100 K Ω
R2 = 30 K

R3 = 10 K Ω
R4 = Thermistor
R5,R7 = 10 K Ω
R8, R9 = 1 K Ω
C1 = 39 uF
R10 = 1 Ω

Fig. B.2 Laser Temperature Control Circuit

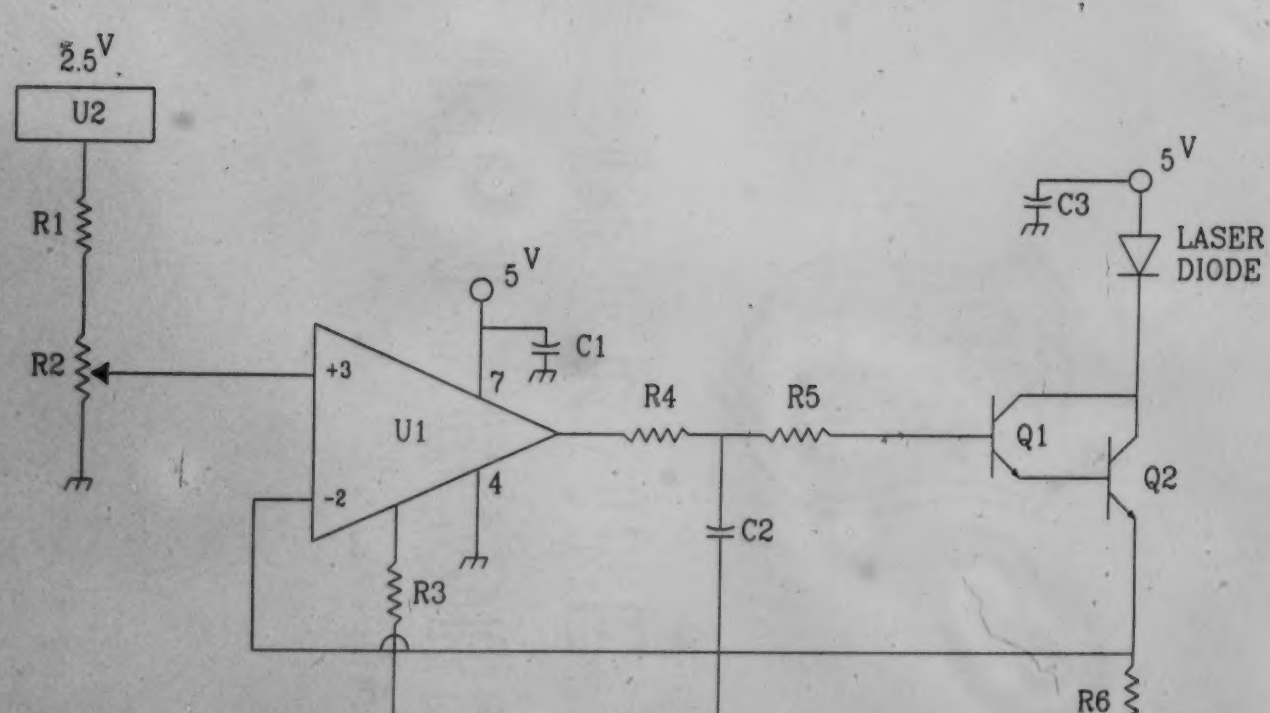

U1 = CA3130
U2 = CA1403
R1 = 430Ω
R2 = 1 KΩ

R3 = 30 KΩ
R4, R5 = 1 KΩ
R6 = 100Ω

C1 = 0.01 uF
C2, C3 = 39 uF

Fig. B.3 Laser CW Bias Circuit

FUJITSU

InGaAsP DOUBLE HETEROSTRUCTURE LASER DIODE

Test Data Sheet (Tc=25°C)

Type : FLD130D45J-A
Sample No. : TH557

Date 1986 . 1 . 18.
Tested by T. Saito
Approved by M. Motoyuya

Optical Output Power vs Current Characteristics

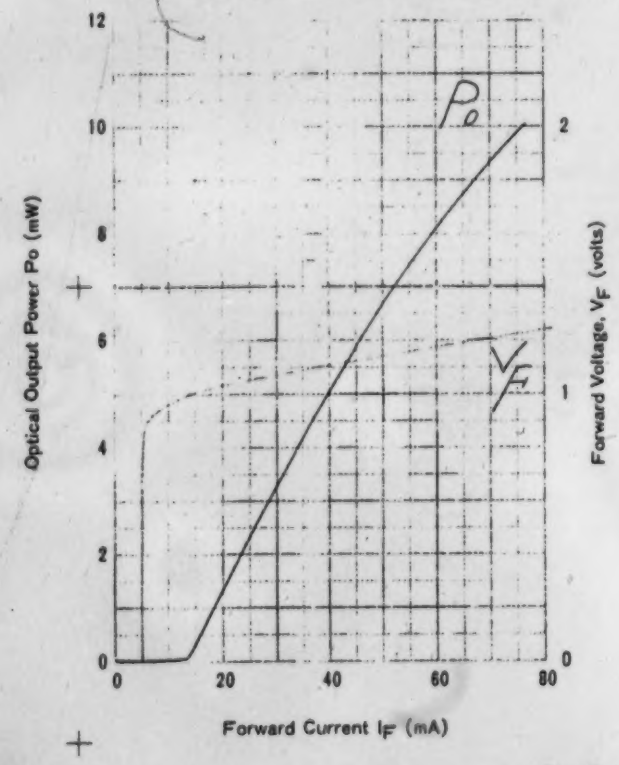

Peak Wavelength (Po = 5 mW)	1315.5 nm
Burn-in Data : R	−0.3 ×10⁻⁴ᵐ

Far-Field Patterns (Po = 5 mW)

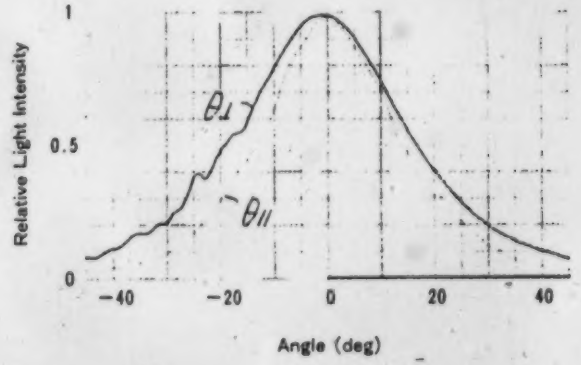

Fig. B.4 Manufacturer's Data Sheet

APPENDIX C

COMPUTER PROGRAM

The computer program used to determine the linewidth of an external cavity laser is given here. In this program it is assumed that the laser operation occurs at the peak of the grating response and therefore the effective reflectivity is considered to be a constant. The effective reflectivity includes all the loss due to lens transmission and coupling into the laser cavity.

```
{$u+}

{PROGRAM TO CALCULATE THE LINEWIDTH OF AN EXTERNAL CAVITY LASER}

var LamdaO,Omega,Tau_Ext,Tau_In,Vg,SigmaL,a,
    theta,OmegaO,DeltaOmega : real;
    Tn : text;
    loop : integer;
    response : char;

{INITIALIZE THE CONSTANTS}

const
      c = 3e8;
      b = 2e-3;
      h = 6.63e-34;
      L = 300e-6;
      R1 = 0.31;
      R2 = 1e-3;
      R3 = 0.2;
      Alpha = -5;
      P =   3.0-3;
      NSP = 4.6;
      DeltaLamda = 0.8e-9;


Function Expl (Parameter : reaL ) : real;

begin
 if Parameter < -70.0
   then Expl := 0.0
   else Expl := exp(Parameter);
end;

Function ArcSin (Parameter : real) : real;

begin
 ArcSin := arctan(Parameter/sqrt(1-sqr(Parameter)));
end;

{THIS PROCEDURE CALCULATES OMEGA FROM THE INPUT WAVELENGTH AND THE
EFFECTIVE REFLECTIVITY.  IT WRITES THE OUTPUT DATA INTO A FILE FOR
EVENTUAL PLOTTING}

Procedure Calculate(Omega : real);
```

```
var Sigma,Gamma,Rho,N_Eff,Nu,T0,T1,RealPart,
    ImaginaryPart,Top,Bottom,F,W,MagnitudeR,
    DeltaNu,EcUpsilon,Phi,A1,B1,C1,D1,E1,
    F1,G1,H1 : real;

begin
   Phi := arcsin(Pi*c/a/Omega);
   N_Eff := 2*b/(a*Cos(Phi));
   Gamma := sqr(N_Eff/4);
   Rho := 2*a*Sin(Phi)/c;
   Nu := Omega/2/Pi;
   T0 := Omega*Tau_Ext;

   A1 := Tau_Ext*sqrt(R3)*cos(T0)*(1-R2);
   B1 := Tau_Ext*sqrt(R3)*sin(T0)*(R2-1);
   C1 := sqrt(R2) + sqrt(R3)*cos(T0)*(1+R2) +
         sqrt(R2)*R3*cos(2*T0);
   D1 := -sin(T0)*sqrt(R3)*(1+R2) - sqrt(R2)*R3*sin(2*T0);

   RealPart := ((A1*C1) + (B1*D1))/(sqr(C1)+sqr(D1));
   ImaginaryPart := ((B1*C1) - (A1*D1))/(sqr(C1) + sqr(D1));

   F := 1/sqr(1 + (RealPart/Tau_In) -
       (Alpha*ImaginaryPart/Tau_In));
   E1 := sqrt(R2)+sqrt(R3)*cos(T0);
   F1 := -sqrt(R3)*sin(T0);
   G1 := 1 + sqrt(R2*R3)*cos(T0);
   H1 := -sqrt(R2*R3)*sin(T0);

   MagnitudeR := sqrt((sqr(E1)+sqr(F1))/(sqr(G1)+sqr(H1)));
   W := Vg*h*Nu/L*ln(1/(sqrt(R1)*MagnitudeR)) /
        (1+(sqrt(R1)/MagnitudeR*(1-sqr(MagnitudeR))/
        (1-R1)));
   EcUpsilon := (SigmaL-ln(sqrt(R1)*MagnitudeR))*Vg*NSP/L;
   DeltaNu := 1/(4*Pi*P)*EcUpsilon*W*F*(1+sqr(Alpha));

   writeln(Tn,Lamda0,DeltaNu);

end;

begin
 assign(Tn,'A2');
 rewrite(Tn);

 Lamda0 := 1.288;
 Vg := 3e8/4;
 SigmaL := 0.51;
 a := 1/1200/1e3;
 Tau_Ext := 19e-2/3e8;
 Tau_In := 300e-6/Vg;

{LOOP FOR THE DETUNING ANGLE}
```

```
 for loop := 1 to 13
  do begin
   Omega0 := 2*Pi*c/Lamda0/1e-6;
   Calculate(Omega0);
   Lamda0 := Lamda0 + 0.002;
  end;
 close(Tn);
end.
```